SURFACE MODIFIED METAL HYDRIDE ALLOYS FOR CARBON DIOXIDE REDUCTION INTO HYDROCARBONS

By

THABANG RONNY SOMO

DISSERTATION

Submitted in fulfilment of the requirements for the degree of

MASTER OF SCIENCE

In

CHEMISTRY

In the

FACULTY OF SCIENCE AND AGRICULTURE

(School of Physical and Mineral Sciences)

At the

UNIVERSITY OF LIMPOPO

SUPERVISOR: DR K.D. MODIBANE

CO-SUPERVISORS: PROF M.J. HATO

DR M.V. LOTOTSKYY (UWC)

2019

DEDICATION

THIS WORK IS DEDICATED TO MY DEAREST DAD AND LATE MOM

RUFUS AND FLORA SOMO

DECLARATION BY CANDIDATE

I …… hereby declare that SURFACE MODIFIED METAL HYDRIDE ALLOYS FOR CARBON DIOXIDE REDUCTION INTO HYDROCARBONS is my own work and effort and that it has not been submitted anywhere for any award. Where other sources of information have been used, they have been acknowledged by means of complete references.

Signature: ……

Date: …….

ACKNOWLEDGEMENTS

Firstly, I would like to thank the Creator of all things, true source of light and wisdom, origin of all being, the God Almighty, for blessing me with the grace to work with constancy, patience and method which carried me throughout the course of my research work.

I would like to express my deep sense of gratitude to my supervisors Dr Kwena Desmond Modibane and Prof. Mpitloane Joseph Hato for the valuable encouragement, inspiration, continued fruitful discussions, advice and critical review of aspects of this study.

To Dr Wafeeq Davids and Dr Mykhaylo Lototskyy, from the HySA/SAIAMC, University of the Western Cape, thanks for hosting me during my six months visit, giving me a platform to learn enormously and introducing me to the field of metal hydrides and hydrogen technology.

My thanks are extended to all my research colleagues and friends in Nanotechnology research group **(**Daphney Makhafola, Suzan Ramaripa, Release Monama, Thabo Pesha, Thabiso Maponya, Kabelo Ramohlola, Gloria Mashao, Nompumelelo Malatji and Daniel Teffu) at University of Limpopo for the discussions we shared and for providing such a wonderful environment, being my family away from home and making Turfloop enjoyable.

Special thanks go to my very good friend Itumeleng Nzimande. Thank you “Itu” for being there for me and encouraging me and always believing in my potentials.

“Blood is thicker than water”, I owe a giant thanks to the Somo family, the people who have brought me thus far in life, thanks for everything you have ever done for me. Thank you to my parents Dorothy and Rufus Somo for instilling the love of learning within me, from a very young age. To two remarkable women my sisters Phuti and Irene Somo, who have always believed that I came for a great purpose in this life, you have always given me motherly sound advice, love and encouragement and I certainly wouldn’t be where I am in life without your love.

Lastly, I would like to acknowledge the financial assistance for my MSc degree from Sasol Inzalo Foundation, National Research Foundation of South Africa (NRF) and NRF Thuthuka grants.

ABSTRACT

Metal alloys are one of few materials that are capable of acting as catalyst precursors in Sabatier reactions, reducing poisonous CO_2 gas into different useful hydrocarbons. However, optimal reduction of CO_2 through these materials takes place at relatively elevated temperatures due to poisoning-intolerance and deterioration of hydrogen absorption/desorption kinetics resulting from the surface chemical action of electrophilic gases at lower or room temperature. This work presents results of the feasibility study focused on improving hydriding kinetics and poisoning-tolerance, which are prerequisites properties that a material should possess to be a suitable catalyst precursor for Sabatier reaction, of the metal hydride (MH) materials. The studies in this work included: (i) element substitution and (ii) surface modification procedure. The substrate alloys investigated had the compositions $LaNi_{4.8-x}Sn_x$ and $TiMn_{1.52}$, where x was 0.2. The activation performances of the materials were estimated by measurement of H_2 absorption kinetics in the absence of vacuum heating, after long-term exposure to air. The presence of oxide layers on the alloy surface resulted in the deterioration of H sorption kinetics for the parent alloys. To overcome impurity effects, surface-modification technique through autocatalytic palladium deposition was employed. The activation performances and kinetics of the surface-modified were found to be superior to that of the unmodified AB_2 and AB_5 alloys. Based on this observation, it was seen that surface-modified MH materials based on the alloy substrate and Pd nanostructured coatings may be utilised as catalysts precursors for CO_2 reduction into hydrocarbons.

RESEARCH OUTPUTS

Publications

- **T. R. Somo**, M. W. Davids, K. D. Modibane, M. J. Hato, M. V. Lototskyy. "Recent developments on hydrogen absorption kinetics of metal hydrides and their catalytic activities in co_2 reduction". *Manuscript in preparation*.
- **T. R. Somo**, M. W. Davids, K. D. Modibane, M. J. Hato, M. V. Lototskyy. "Effect of partial substitution of nickel by tin followed by autocatalytic palladium deposition on the hydrogen absorption kinetics of $lani_5$-type metal hydride alloy". *Manuscript pending submission*.
- **T. R. Somo**, M. W. Davids, K. D. Modibane, M. J. Hato, M. V. Lototskyy. "Improved hydrogenation kinetics of $timn_{1.52}$ alloy coated with palladium through electroless deposition for potential co_2 conversion". *Manuscript pending submission.*
- T. E. Mabokela, T. C. Maponya, **T. R. Somo**, K. D. Modibane, M. J. Hato. "Dynamic Carbon Dioxide Uptake Capacity of Metal organic framework using Thermogravimetrical Evaluation at different CO_2 pressure: Absorption Kinetics, Isotherms and Thermodynamics". *Manuscript pending submission*.
- M. D. Makhafola, **T. R. Somo**, M. J. Hato, K. M. Molapo, E. I. Iwuoha, K. D. Modibane. "Fabrication of graphene oxide/metal organic framework nanocomposites with improved compatibility for hydrogen evolution reaction". *Book Chapter accepted in Intech-Open (Appendix 1).*
- E. I. Iwuoha, M. D. Makhafola, **T. R. Somo**, M. J. Hato, K. M. Molapo, K. D. Modibane. "Graphene oxide/metal organic framework nanocomposite with improved electrocatalytic activity for hydrogen evolution reaction". *Published as a Book Chapter in* Conference *Proceeding in the 3rd International Hydrogen Technologies Congress (IHTEC-2018), March 15-18, 2018, Alanya/Antalya, Turkey (Appendix 2).*
- M. D. Makhafola, **T. R. Somo**, M. J. Hato, K. M. Molapo, E. I. Iwuoha, K. D. Modibane. "Palladium supported graphene oxide based metal organic

framework nanocomposite with improved electrocatalytic efficiency for hydrogen evolution reaction”**.** *Manuscript pending submission.*

Presentations

- **T. R. Somo**, M. W. Davids, K. D. Modibane, M. J. Hato, M. V. Lototskyy. “Effect of partial substitution of nickel by tin followed by autocatalytic palladium deposition on the hydrogen absorption kinetics of $LaNi_5$-type metal hydride alloy”. Poster Presentation. SANI–NanoAfrica 2018 Conference, UKZN, Durban, South Africa on the 22nd-25th April 2018.
- **T. R. Somo**, M. W. Davids, K. D. Modibane, M. J. Hato, M. V. Lototskyy. “Effect of partial substitution of nickel by tin followed by autocatalytic palladium deposition on the hydrogen absorption kinetics of $LaNi_5$-type metal hydride alloy”. Oral Presentation. Faculty of Science and Agriculture Research Day, Fusion Botique, Polokwane, South Africa on the 20th-21st of September 2018.

TABLE OF CONTENTS

DEDICATION ii

DECLARATION BY CANDIDATE iii

ACKNOWLEDGEMENTS iv

ABSTRACT vi

RESEARCH OUTPUTS vii

Publications vii

Presentations viii

LIST OF FIGURES xiii

LIST OF TABLES xv

LIST OF SYMBOLS xv

LIST OF ABBREVIATIONS xviii

CHAPTER 1 1

INTRODUCTION 1

SUMMARY 1

1.1. BACKGROUND ON HYDROGEN TECHNOLOGY 1

1.2. PROBLEM STATEMENT 2

1.2.1. Hydrogen separation and purification 2

1.2.2. Hydrogen storage in hydride-forming alloys 3

1.2.3. Hydrogenation of CO_2 using metal hydrides 4

1.3. RATIONALE OF THE STUDY 5

1.3.1. Aim 6

1.3.2. Objectives 7

1.4. SCIENTIFIC IMPACT 7

1.5. THESIS OUTLINE 8

1.6. REFERENCES 10
CHAPTER 2 15
RECENT DEVELOPMENTS ON HYDROGEN ABSORPTION KINETICS OF METAL HYDRIDES AND THEIR CATALYTIC ACTIVITIES IN Co_2 REDUCTION 15
SUMMARY 16
2.1. INTRODUCTION 17
2.2. HYDROGEN STORAGE IN METAL ALLOYS 18
2.2.1. Types of metal alloys 20
2.2.2. Thermodynamics of metal hydrides 29
2.2.3. Kinetic characteristics of metal hydrides 31
2.2.4. Methods for improving hydriding kinetics of metal hydrides 35
2.3. APPLICATION OF METAL HYDRIDES IN CO_2 CONVERSION USING .. 42
2.4. CONCLUSIONS OF THE REVIEW 47
2.5. REFERENCES 49
CHAPTER 3 62
CHARACTERISATION TECHNIQUES 62
SUMMARY 62
3.1. INTRODUCTION 63
3.2. X-ray diffraction spectroscopy (XRD) 64
3.3. Scanning electron microscopy (SEM) 65
3.4. Energy dispersive spectroscopy (EDS) 67
3.5. Atomic absorption spectroscopy (AAS) 68
3.6. Brunauer, Emmett and Teller (BET) 69
3.7. Volumetric method/Sievert's method 70
3.8. CONCLUSION 72

3.9. REFERENCES 73

CHAPTER 4 75

EFFECT OF PARTIAL SUBSTITUTION OF NICKEL WITH TIN FOLLOWED BY AUTOCATALYTIC PALLADIUM DEPOSITION ON THE HYDROGEN ABSORPTION KINETICS OF $LANI_5$-TYPE METAL HYDRIDE ALLOY 75

SUMMARY 76

4.1. INTRODUCTION 77

4.2. EXPERIMENTAL METHODS 79

4.2.1. Materials 79

4.2.2. Surface modification of alloy 79

4.2.3. Characterisation Techniques 79

4.3. RESULTS AND DISCUSSION 81

4.3.1. Structural Characterisation 81

4.3.2. Morphological and Elemental Characterisations 83

4.3.3. Gas absorption studies 88

4.4. CONCLUSIONS 94

4.5. REFERENCES 95

CHAPTER 5 99

IMPROVED HYDROGENATION KINETICS OF $TiMn_{1.52}$ ALLOY COATED WITH PALLADIUM THROUGH ELECTROLESS DEPOSITION FOR POTENTIAL CO_2 CONVERSION 99

SUMMARY 100

5.1. INTRODUCTION 101

5.2. EXPERIMENTAL METHODS 102

5.2.1. Materials 102

5.2.2. Surface modification of alloy 103

5.2.3. Characterisation techniques 103
5.3. RESULTS AND DISCUSSION 104
5.3.1. Structural characterisation 104
5.3.2. Morphological and elemental characterisations 105
5.3.3. Hydrogen absorption kinetics 108
5.4. CONCLUSIONS 111
5.5. REFERENCES 112
CHAPTER 6 115
GENERAL DISCUSSION, CONCLUSIONS AND RECOMMENDATIONS 115
6.1. CONCLUSIONS 115
6.2. RECOMMENDATIONS 119
APPENDIX 1 121
APPENDIX 2 122

LIST OF FIGURES

Figure 2.1: Different ways to store hydrogen. 18
Figure 2.2: Hydride family tree of alloys and complexes, TM = transition metal. 21
Figure 2.3: Contour maps of electronic densities for TiFe-type alloy. 23
Figure 2.4: Schematic illustration of (a) simple hydride and (b) TiFe hydride. 23
Figure 2.5: Crystal structures of (a) C14 and (b) C15 Laves phase. 25
Figure 2.6: Crystal structure of AB_5-type alloys..... 27
Figure 2.7: Structure of MgH_2. 28
Figure 2.8: Schematic PCT-diagram and van't Hoff plot, taken from Dornheim.. 29
Figure 2. 9: Presure-composition-temperature diamgram..... 31
Figure 2.10: Index of power, n, which can be determined from Equation 2.6. 33
Figure 2.11: The autocatalytic palladium deposition on hydride-forming alloy material. 41
Figure 2.12: Different mechanisms of hydrogen dissociation on the surface of Pd-treated alloy material..... 41
Figure 2.13: Representation of methane formation from CO_2 reduction on the surface of $ZrCoH_x$. 44
Figure 2. 14: Effects of the CO_2/H_2 feed ratio on CO_2 conversion (XCO2), H_2 conversion (XH2) and selectivity to CO (SCO) and methanol (SMeOH) in CO_2 hydrogenation over the $Cu/ZnO/Al_2O_3$ catalyst. Reaction conditions: T = 260 ˚C, P = 36 MPa. GHSV = 10,471 h^{-1}..... 46
Figure 4.1: X-ray diffractogram of a) $LaNi_5$, b) $LaNi_{4.8}Sn_{0.2}$, c) Pd-$LaNi_5$ and d) Pd-$LaNi_{4.8}Sn_{0.2}$..... 82
Figure 4.2: SEM micrographs of (a, b) $LaNi_5$ and (c, d) $LaNi_{4.8}Sn_{0.2}$ and their particle size distribtuion histograms ((c) Pd-$LaNi_5$ and (f) Pd-$LaNi_{4.8}Sn_{0.2}$) 85
Figure 4.3: EDS plots of a) $LaNi_5$, b) $LaNi_{4.8}Sn_{0.2}$, c) Pd-$LaNi_5$ and d) Pd-$LaNi_{4.8}Sn_{0.2}$ 86
Figure 4.4: SEM micrographs of (a, b) Pd-$LaNi_5$ and (c, d) Pd-$LaNi_{4.8}Sn_{0.2}$ samples and their particle size distribution histograms ((c) Pd-$LaNi_5$ and (f) Pd-$LaNi_{4.8}Sn_{0.2}$). 87

Figure 4.5: Adsorption-desorption isotherm of BET for a) $LaNi_5$, b) $LaNi_{4.8}Sn_{0.2}$, c) Pd-$LaNi_5$ and d) Pd-$LaNi_{4.8}Sn_{0.2}$.....89
Figure 4.6: Dynamics of hydrogen absorption (T = 20 ˚C, P_{H2} = 30 bar) by uncoated and Pd-coated AB_5 alloys after pre-exposure to air and no preliminary activation (vacuum heating). 91
Figure 4.7: Dynamics of hydrogen absorption (T = 20 ˚C, P_{H2} = 30 bar) by uncoated and Pd-coated AB_5 alloys after preliminary activation (vacuum heating at 300 ˚C).....93
Figure 5.1: X-ray diffractograms of $TiMn_{1.52}$ and Pd-$TiMn_{1.52}$……...105
Figure 5.2: SEM micrographs of (a, b) $TiMn_{1.52}$ and (d, e) Pd-$TiMn_{1.52}$ and their particle size distribution histograms ((c) $TiMn_{1.52}$ and (f) Pd-$TiMn_{1.52}$).....107
Figure 5.3: EDS plots of (a) $TiMn_{1.52}$ and (b) $TiMn_{1.52}$. 108
Figure 5.4: Dynamics of hydrogen absorption (T = 20 ˚C, P_{H2} = 30 bar) by uncoated and Pd-coated AB_2 alloys after pre-exposure to air and without preliminary activation (vacuum heating).....109
Figure 5.5: Dynamics of hydrogen absorption (T = 20 ˚C, P_{H2} = 30 bar) by uncoated and Pd-coated AB_2 alloys after preliminary activation (vacuum heating). 110

LIST OF TABLES

Table 2.1: Lattice parameter, a, of different types of alloys before and after hydrogenation and their hydrogen storage capacities.....20
Table 2.2: Lattice parameters, a, of AB-type alloys before and after hydrogenation and their plateau width. 22
Table 2.3: Lattice parameter, a, of AB_2-type alloys before and after hydrogenation and their plateau width. 24
Table 2.4: Lattice parameter, a, of AB_5-type alloys before and after hydrogenation and their plateau width. 26
Table 2. 5: Thermodynamic data of some selected alloys. 30
Table 2. 6: Kinetic parameters and hydrogen absorption capacities of different types of alloy. 38
Table 2.7: Comparison of rare constants of different alloys before and after surface modification. 40
Table 2.8: Comparison of CO_2 conversion and CO selectivity by different catalyst precursors. 45
Table 4.1: Results of refinement of XRD patterns of AB_5-type alloys……83

Table 4. 2: Elemetal composition data of $LaNi_5$ and $LaNi_{4.8}Sn_{0.2}$ alloy. 84
Table 4.3: Physical properties of uncoated and Pd-coated alloys. 90
Table 4.4: Fit of the experimental data for hydrogen absorption by non-activated and activated materials using the Avrami-Erofeev equation 92
Table 5.1: Table 1: Elemental composition data of $TiMn_{1.52}$ alloy……106

Table 5.2: Fit of the experimental data for hydrogen absorption by non-activated and activated materials using the Avrami-Erofeev equation. 111

LIST OF SYMBOLS

α:	Reacted fraction
β:	full width at half-maximum (FWHM) (radians)
λ:	Wavelength (=0.154 nm for Cu-Kα)
τ:	Crystallite size (nm)
d:	Distance between atomic layers in a crystal
ΔG_f:	Gibbs free energy change (kJ mol^{-1})
ΔH:	Enthalpy change (kJ/mol H_2)
H/M:	Actual hydrogen concentration
H/M_{max}:	Maximum hydrogen concentration
k:	Rate constant
n:	Avrami exponent
N_0:	Number of available nucleation sites per unit volume
P_{H2}:	Equilibrium hydrogen pressure
P°:	Standard pressure
R:	Radius of a particle

ΔS:	Entropy of formation (J/mol K H_2)
U:	Interface velocity

LIST OF ABBREVIATIONS

AAS: Atomic absorption spectroscopy

ABS/DES: Absorption/desorption

BET: Brunauer-Emmett-Teller

C_H: Hydrogen concentration

CV: Contracting volume model

EDS: Energy dispersive spectroscopy

FESEM: Field-emission scanning electron microscopy

HySA: Hydrogen South Africa

IMC: Intermetallic compound

JMA: Johnson-Mehl-Avrami

MH: Metal hydride

MHs: Metal hydrides

MS: Mass spectroscopy

P: Pressure

PCI: Pressure composition isotherm

PCT: Pressure composition temperature

PGM:	Platinum group metals
PSA:	Pressure swing adsorption
SAIAMC:	South African Institute for Advanced Materials Chemistry
SC:	Surface control
SEM:	Scanning electron microscopy
T:	Temperature
TSA:	Temperature swings absorption
UL:	University of Limpopo
UWC:	University of the Western Cape
XRD:	X-ray diffractometry

CHAPTER 1

INTRODUCTION OF METAL HYDRIDES

SUMMARY

Hydrogen processing (production, separation, purification and storage) in metal alloy materials is the key step in unlocking many possible applications such as catalytic use of metal hydrides for conversion of CO_2 into hydrocarbons. Hence, this chapter introduces some challenges that function as stumbling blocks for a successful hydrogen technology. These challenges include problems associated with technologies in hydrogen separation and purification, solid-state materials in hydrogen storage and conversion of CO_2 using metal hydrides. Furthermore, the chapter discusses the rationale of this study and elaborates further on the choice of the type of metal alloy. The aim and objectives of the study are also elaborated together with scientific impact, where economic and scientific importance of a successful investigation on the chosen materials for this study is also discussed.

1.1. BACKGROUND ON HYDROGEN TECHNOLOGY

Consumption of South African energy, which relies mostly on non-renewable fossil fuels, is expected to increase intensely within the next years due to globalisation and growing population. The increase in demand means that more secure and diversified energy sources need to be exploited and employed. Moreover, depletion of fossil fuels is becoming a serious issue and their combustion results in increase of atmospheric greenhouse gases as well as climate change and global warming [1]. The impact of global warming is serious in many different aspects, including rapid rising sea level, ice melting at the Earth's pole, and increasing precipitation across the world [2]. An innovative and promising alternative energy strategy is to build a pollution-free hydrogen-based energy infrastructure, which has high energy security due to high abundance of hydrogen. If generation of energy is based on hydrogen,

economic growth may be maintained. Currently, hydrogen is obtained through several technologies including natural gas reforming, coal gasification, partial oxidation of light alcohols, auto-thermal reforming, electrolysis and fossil fuel processing [3]. Nevertheless, the purity of hydrogen produced through these technologies is poor and machineries responsible for hydrogen purification are expensive and thus economically unfeasible [4]. Implementation of hydrogen technology and use of hydrogen as a non-greenhouse emitter energy carrier requires efficient machineries that are responsible for generation of high purity of hydrogen gas from industrial streams, hydrogen purification from gaseous mixtures, safe and secure storage, and ease distribution of hydrogen for use. Currently, materials responsible for separating hydrogen from other gases and store it in a compact way are accountable for successful operation of hydrogen economy [5].

1.2. PROBLEM STATEMENT

1.2.1. Hydrogen separation and purification

According to Zuttel [6], the following characteristics should be possessed by a hydrogen absorber to be considered an appropriate material in hydrogen absorption/desorption (i.e. separation, purification, storage and delivery): (1) the media should operate at temperatures less than 100 ˚C, (2) efficient mechanical strength by hydrogen absorber, (3) the media must exhibit low heat losses possess moderate operational pressures and (4) it should also exhibit good poisoning-resistance in the presence of gas impurities such as sulphur, carbon dioxide and carbon monoxide. Several methods including membrane filtration, adsorption and absorption have recently been exploited for hydrogen separation from gaseous mixtures [7-9]. Utilisation of these conventional separation techniques requires destructive environments, high pressure and temperature as well as expensive chemical processes [8]. Currently, large-scale hydrogen is separated from gas streams through a well-known pressure-swing adsorption (PSA) method [10]. PSA involves the separation of a specific gas from a gaseous mixture under pressure

based on its molecular characteristics and its affinity for an adsorbent bed [11]. For hydrogen separation, this technique is limited by several industrial processes including economical inadequacies; low hydrogen specificity of adsorbent beds; low mechanical stability of adsorbent beds; large size of PSA reactors resulting in inadequate rapid gas transfer; high operational costs due to compression and cooling of gases [8]. Another technology that is capable of separating and generating high-purity hydrogen is palladium membrane technology [12]. Unfortunately, these membranes suffer from poor thermo-mechanical stabilities at high temperature, are costly, suffer from hydrogen embrittlement after repeated thermal cycling in hydrogen and are easily poisoned by aggressive surface adsorbates (e.g. H_2S, CO, CO_2, O_2, H_2O) over extended operation [12]. Moreover, this technology involves very long heating periods [13]. An attractive technology in the separation and purification of hydrogen from poisonous gas mixture is absorption technique [14]. This technique involves an interaction between a hydrogen absorber and hydrogen atoms through physical-chemical processes. Hydride-forming alloys such as binary systems (e.g. Pd, Mg) [15] and ternary systems (e.g. $LaNi_5$, $TiMn_{1.52}$) [16] are of particular interest and intensive research on these materials is currently underway. These materials are characterised by their interactions with atomic hydrogen; minimal energy expenditure; and simplicity in operation [17-18]. For these reasons alternative separation/purification media, based on absorptive materials, are sought to effectively separate and purify hydrogen from hydrogenous product gas mixtures containing aggressive components.

1.2.2. Hydrogen storage in hydride-forming alloys

Due to low density of hydrogen (0.08988 g/L at 1 atm), it is important to subsequently store hydrogen after its separation and purification from poisonous gas mixture [19]. The storage media should possess several characteristics which include maintaining the high purity of hydrogen, allowing fast adsorption and desorption rates, allowing efficient transport of hydrogen, and does not require large amounts of energy in its operation [19-20]. So far, three technologies are well-known for hydrogen storage: compressed; liquefied; and solid-state hydrogen storage [21].

With compressed hydrogen storage hydrogen is compacted at high pressure (approximate maximum operating pressure is 20 MPa) and stored in high strength stainless steel cylinders. Such heavy cylinders are not recommended for mobile applications and their safety is still a concern while more energy associated with hydrogen compression is not economically favoured [22]. Due to a critical temperature of -241 ˚C linked to hydrogen, about 15 kWh/kg of energy is necessary to liquefy hydrogen to be stored in high-efficiency cryogenic containers [23].

On the other hand, solid-state storage, in which the hydrogen is absorbed into a solid material, has attracted much attention, although no completely satisfactory material has yet been identified [6]. In solid-state storage, hydrogen gas interacts with metal hydride-forming materials, chemically binding materials, and high-surface area nanostructured materials. An attractive feature of solid-state storage is that the absorption of hydrogen using many of these materials is reversible, thereby reducing operational costs [24]. The material requirements for effective solid-state hydrogen storage include the following: (1) appropriate thermodynamics; (2) fast kinetics (quick uptake and release); (3) high storage capacity (specific capacity to be determined by usage); (4) effective heat transfer; (5) high gravimetric and volumetric densities (lightweight and space efficient); (6) long cycle lifetime for hydrogen sorption; (7) high mechanical strength and durability; (8) safety under normal use and (9) acceptable risk under abnormal conditions [6]. In comparison with other known solid-state materials such as carbon nanotubes and metal organic frameworks, metal hydride forming materials have the potential for reversible on-board hydrogen storage and release at low temperatures and pressures [25]. However, low hydrogen capacity, poor poisoning-resistance and slow hydrogenation kinetics serve as the main hindrances toward a metal hydride-based use of hydrogen, and thus further research needs to be conducted [26, 27].

1.2.3. Hydrogenation of CO_2 using metal hydrides

Catalytic hydrogenation of CO_2 into useful hydrocarbons such as methanol and CO is of particular interest in order to minimise CO_2 atmospheric concentrations [28], [29]. However, catalysts which are responsible for this reaction surfer from surface

poisoning by impurities and they operate at very high temperature (above 250 ˚C) while their selectivity towards hydrocarbons is poor [30]. Metal oxides are frequently used as catalyst precursors due to their ability to bind and activate CO_2 largely depends on their basicity and reducibility while reduced oxides have also been reported to have a strong tendency to react with CO_2 [31]. The major problem related to metal oxides precursors is that they decompose upon hydrogenation of CO_2 due to poor cyclic stability [31]. Several metal hydrides have been reported to be active towards conversion of CO_2 [32, 33]. An example is $LaNi_5$, which was reported to have a CO_2 conversion capacity of 89% at 500 ˚C by Kustov and Tarasov [34]. However, its selectivity towards CO was under 15% as it gave a mixture of CO, methane and water. To enhance the catalytic activity of metal hydrides at optimal conditions and favourable temperature, a poisoning-resistant metal hydride with fast and large hydrogen capacity is of particular interest. Hence, this work focuses on building such an ideal metal hydride to be suited for CO_2 conversion into hydrocarbons.

1.3. RATIONALE OF THE STUDY

As was previously established, the use of metal alloys for hydrogen storage is limited by several factors including hydriding/hydrogenation rate and low hydrogen uptake capacity which is caused by difficulty in initial activation and poor poisoning-resistance in the presence of impurities. Several mechanisms and methods including spark plasma sintering, mechanical alloying, melt spinning, adding catalytic dopants, adding catalysts, GPa hydrogen pressure method, hydriding combustion synthesis, and alloying with other elements have been widely studied in an attempt to enhance hydriding kinetics of different metal hydrides, however much work is still need to be done as the effect of these attempts is insignificant for real-life application [15, 35]. Of these mechanisms, addition of catalytic dopants on the surface of a metal alloy material has shown great potential [36, 37]. For instance, a bulk alloy material could be designated due to its excellent kinetic or thermodynamic properties and a dopant could be preferred due to its outstanding poisoning-tolerance and high affinity for

hydrogen. Examples of dopants used as surface catalytic materials include deposition of platinum group metals (PGMs) on the surface of an alloy material prior to hydrogen storage [7]. If PGMs are deposited on the surface of an alloy a swift movement of hydrogen atoms into and out of a bulk alloy material is usually observed, but the PGMs do not play any role for hydrogen storage in this instance [38]. The abundance of coal and PGM resources in South Africa countenance the PGM-based research to be simplified, and as such a local hydrogen technology based on these materials can be developed. Another important factor to look at is the choice of a type of metal alloy material and currently AB_5-type ($LaNi_5$) and Ti-Mn-based AB_2-type alloys have shown great hydrogen performance due to their reasonable plateau pressure and better activation property, respectively, but poor initial activation, hydrogen storage capacity and hydriding kinetics are still the burning issues [39, 40]. Poor initial activation possessed by $LaNi_5$ alloy can be addressed by partial substitution of Ni with elements containing bigger active sites [39]. These elements alter the particle size of bulk alloy to finer size, creating more fresh surfaces to allow faster contact with hydrogen [41]. Furthermore, the inclusion of these elements also minimise the oxide coating on the ally surface and decrease the absorption plateau pressure. Hence, an effect of combination of partial substitution of Ni with Sn, which has bigger active sites than Ni, in $LaNi_5$ alloy and surface modification through autocatalytic deposition of palladium on poisoning-resistance and hydriding kinetics, is studied using Sieverts-type apparatus. On the other hand, hydriding kinetics of Pd-coated and uncoated Ti-Mn-based alloy $TiMn_{1.52}$ are also compared. The results of these two studies can help in realisation of suitable alloy material to meet requirements for catalytic application in carbon dioxide conversion into hydrocarbons.

1.3.1. Aim

The aim of this study is to investigate the effect of autocatalytic deposition of palladium on the hydrogenation kinetics of AB_5 type alloys ($LaNi_5$ and $LaNi_{4.8}Sn_{0.2}$

alloys) and AB_2 type alloy ($TiMn_{1.52}$ alloy) as potential surface modified alloys for conversion of carbon dioxide into hydrocarbons.

1.3.2. Objectives

The objectives of this study were to:

i. modify $LaNi_5$, $LaNi_{4.8}Sn_{0.2}$ and $TiMn_{1.52}$ alloys through autocatalytic palladium deposition,
ii. characterise unmodified and surface-modified alloys by scanning electron microscopy (SEM) with energy dispersive spectroscopy (EDS), X-ray diffraction spectroscopy (XRD), atomic absorption spectroscopy and Brunauer-Emmett-Teller (BET),
iii. investigate the effect of palladium deposition on the hydrogenation kinetics of AB_5 and AB_2 type alloys by a comparison of hydrogen absorption before (after pre-exposure to air) and after activation by evacuation and heating at 300 ^{0}C using Sieverts-type apparatus.

1.4. SCIENTIFIC IMPACT

South Africa is suddenly the focus of the world as the research and development efforts towards clean energy are intensifying due to availability of mineral resources. Platinum group metals (PGMs) are of key importance in the development of fuel cells and other clean energy economy technologies. South Africa is the world's main source of these metals, accounting, for example, for 76% of the global PGMs supply. This work is in line with the objectives of the national program launched by South Africa as a reply to the global energy and environment challenges. This project is aimed at addressing challenging problems of safe and efficient CO_2 reduction and hydrocarbons production. The work contributes to the novel technology for development of surface modified MH based CO_2 reduction and hydrocarbons production in the integrated system by using South African minerals particularly PGMs. This will make South Africa to benefit from diversification of Pd containing materials and developed capabilities in the emerging clean energy economy. Owing

to the high demand for South African industries to use a clean technology in order to overcome challenging problems of carbon emission from utilisation of local fossil fuels, it is of paramount importance that in the present work, the focus is on the problem of CO_2 reduction and hydrocarbons production on the basis of surface modified MH materials.

1.5. THESIS OUTLINE

This study attempts to tune the catalytic properties of metal hydride systems for reduction of carbon dioxide to produce hydrocarbons. The Outline of the remaining chapters in this study:

- **Chapter one** introduces us to metal alloy as hydrogen storage materials. This chapter also looks at problems associated with formation of metal hydrides from metal alloys and molecular hydrogen as well as difficulties in catalytic activity of metal hydrides in carbon dioxide conversion. Lastly, we also discuss the importance and rationale of the current study on the hydrogenation kinetics and in catalytic hydrogenation of CO_2.
- **Chapter two** focuses on the literature review of energy, different types of metal hydrides, hydrogenation kinetics of metal hydrides and the application of metal hydrides as catalyst precursors in CO_2 conversion to form hydrocarbons.
- **Chapter three** fundamentally serves as a continuation of the literature review, but with more emphasis placed on the characterisation techniques employed in the study. It also gives and outline of the different materials that were used in the study.
- **Chapter four** concentrates on the effect of partial substitution of nickel by tin followed by autocatalytic palladium deposition on the hydrogen absorption kinetics of $LaNi_5$-type metal hydride alloy.

- **Chapter five** focuses on improved hydrogenation kinetics of $TiMn_{1.52}$ alloy coated with palladium through electroless deposition for potential co_2 conversion
- In **Chapter six** the study is concluded with a concise discussion of the objectives achieved pertaining to the study of kinetic properties of fabricated AB_5 and AB_2 type alloys. Recommendations are made, anomalies noted, and the greater relevance and implications of the study are discussed.

1.6. REFERENCES

[1] R. N. Rosa, “The Role of Synthetic Fuels for a Carbon Neutral Economy,” *J. carbon Res.*, vol. 3, p. 11, 2017.

[2] N. A. Ghani, “Modification of Activated Carbon from Biomass Nypa and Amine Functional Groups as Carbon Dioxide Adsorbent,” *J. Phys. Sci.*, vol. 28, pp. 227–240, 2017.

[3] P. Nikoleishvili, G. Gorelishvili, and G. Tsurtsumia, “Hydrogen Generation by Reforming of Sodium Hypophosphite on Cobalt-Boron Oxides Containing Catalyst,” *green Sustain. Chem.*, vol. 7, pp. 85–93, 2017.

[4] D. Symes, A. Dhir, and M. Lees, “Design for on-site hydrogen production for hydrogen fuel cell vehicle refueling station at University of Birmingham, U.K.,” *Energy procedia*, vol. 29, pp. 606–615, 2012.

[5] D. Dunikov, V. Borzenko, and C. Chu, “Biohydrogen purification using metal hydride technologies,” *Int. J. Hydrogen Energy*, vol. 41, pp. 21787–21794, 2016.

[6] A. Züttel, “Materials for hydrogen storage,” *Mater. Today*, vol. 6, pp. 24–33, 2003.

[7] J. Ren, M. Williams, and M. V Lototskyy, “Improved tolerance of Pd/Cu-treated metal hydride alloys towards air impurities,” *Int. J. Hydrogen Energy*, vol. 35, pp. 8626–8630, 2013.

[8] S. Miura, A. Fujisawa, and N. Hanada, “A hydrogen purification and storage system using CO adsorbent and metal hydride,” *J. Alloys Compd.*, vol. 580, pp. S414–S417, 2013.

[9] S. Miura, A. Fujisawa, and M. Ishida, “A hydrogen purification and storage system using metal hydride,” *Int. J. Hydrogen Energy*, vol. 37, pp. 2794–2799, 2011.

[10] G. Barkhordarian, T. Klassen, and R. Bormann, “kinetic investigation of the effect of milling time on the hydrogen sorption reaction of magnesium catalyzed with different Nb_2O_5 contents,” *J. Alloys Compd.*, vol. 407, pp. 249–255, 2006.

[11] C. Yu, C. Huang, and C. Tan, “A Review of CO_2 Capture by Absorption and Adsorption,” *Aerosol Air Qual. Res.*, vol. 12, pp. 745–769, 2012.

[12] S. Yun and S. T. Oyama, “Correlations in palladium membraines for hydrogen separation: a review,” *J. Memb. Sci.*, vol. 375, pp. 28–45, 2011.

[13] Y. H. Ma, “Palladium membranes for hydrogen separation,” *Membr. energy Convers.*, vol. 2, pp. 245–261, 2007.

[14] D. F. Wong, K. Young, and K. Y. S. Ng, “First-principles study of structure, initial lattice expansion, and pressure-composition-temperature hysteresis for substituted $LaNi_5$ and $TiMn_2$ alloys,” *Model. Simul. Mater. Sci. Eng.*, vol. 24, p. 085007, 2016.

[15] J. Liu, X. P. Song, and G. L. Chen, “Hydrogen storage performance of Mg-based composites prepared by spark plasma sintering,” *J. Alloys Compd.*, vol. 486, pp. 338–342, 2009.

[16] X. Shan, J. H. Payer, and W. D. Jennings, “Mechanism of increased performance and durability of Pd-treated metal hydriding alloys,” *Int. J. Hydrogen Energy*, vol. 34, pp. 363–369, 2009.

[17] K. Young and J. Nei, “The Current Status of Hydrogen Storage Alloy Development for Electrochemical Applications,” *Materials (Basel).*, vol. 6, pp. 4574–4608, 2013.

[18] Y. Bouhadda, A. Rabehi, and N. Fenineche, “Hydrogen solid storage: First-principles study of $ZrNiH_3$,” *Int. J. Hydrogen Energy*, vol. 34, pp. 4997–5002, 2009.

[19] A. Zuttel, “Materials for hydrogen storage,” *Mater. Today*, vol. 6, pp. 24–33, 2003.

[20] L. Schlapbach and A. Züttel, “Hydrogen-storage materials for mobile applications,” *Nature*, vol. 414, pp. 353–358, 2001.

[21] V. A. Yartys and M. V. Lototskyy, “An overview of hydrogen storage methods,” *Hydrog. Mater. Sci. Chem. Carbon Nanomater.*, pp. 75–104, 2004.

[22] B. Sakintuna, F. Lamari-darkrim, and M. Hirscher, “Metal hydride materials for solid hydrogen storage: A review,” *Int. J. Hydrogen Energy*, vol. 32, pp. 1121–1140, 2007.

[23] D. O. Northwood and G. G. Ivey, “Review Storing energy in metal hydrides: a review of the physical metallurgy,” *J. Mater. Sci.*, vol. 18, pp. 321–347, 1983.

[24] M. Ceramics, V. V Skorokhod, and V. P. Klimenko, “Reversable hydriding of $LaNi_{5-x}Al_x$−Pd composite in the presence of carbon monoxide,” *Powder Metall. Met. Ceram.*, vol. 39, pp. 575–583, 2001.

[25] S. Kumar, G. P. Tiwari, and N. Krishnamurthy, “High performance FeTi-3.1 mass% V alloy for on board hydrogen storage solution,” *Energy*, vol. 75, pp. 520–524, 2014.

[26] R. Andreas, “Hydrogen storage methods,” *Naturwissenschaften*, vol. 91, pp. 157–172, 2004.

[27] W. Luo, “($LiNH_2$-MgH_2): a viable hydrogen storage system,” *J. Alloys Compd.*, vol. 381, pp. 284–287, 2004.

[28] L. Li, D. Mao, and J. Yu, “Highly selective hydrogenation of CO_2 to methanol over CuO-ZnO-ZrO_2 catalysts prepared by a surfactant-assisted coprecipitation method,” *J. Power Sources*, vol. 279, pp. 394–404, 2015.

[29] X. Su, J. Xu, and Y. Huang, “Catalytic carbon dioxide hydrogenation to methane: A review of recent studies,” *J. Energy Chem.*, vol. 25, pp. 553–565, 2016.

[30] S. Kato, A. Borgschulte, and A. Züttel, “CO_2 hydrogenation on a metal hydride surface,” *Phys. Chem. Chem. Phys.*, vol. 14, pp. 5518–5526, 2012.

[31] J. A. Rodriguez, P. Liu, and J. G. Chen, “Hydrogenation of CO_2 to Methanol : Importance of Metal−Oxide and Metal−Carbide Interfaces in the Activation of CO_2,” *ACS Catal.*, vol. 5, pp. 6696–6706, 2015.

[32] P. Adeniyi, A. Abbas, and W. Daud, “Insight into catalytic reduction of CO_2: Catalysis and reactor design,” *J. Clean. Prod.*, vol. 140, pp. 1298–1312, 2017.

[33] S. Kato, S. K. Matam, and M. Rohwerder, “The Origin of the Catalytic Activity of a Metal Hydride in CO_2 Reduction,” *Angew. Chemie Int. Ed.*, vol. 55, pp. 1–6, 2016.

[34] L. M. Kustov and A. L. Tarasov, “Hydrogenation of carbon dioxide: a comparison of different types of active catalysts,” *Ital. Oral Surg.*, vol. 24, pp. 349–350, 2014.

[35] M. Zhu, Y. Lu, and H. Wang, “Thermodynamic Tuning of Mg-Based Hydrogen Storage Alloys: A Review,” *Materials (Basel).*, vol. 6, pp. 4654–4674, 2013.

[36] S. Suda *et al.*, “Fluorinated Metal Hydrides for the Catalytic Hydrolysis of Metal-Hydrogen Complexes,” *Met. Mater. Int.*, vol. 7, pp. 73–75, 2001.

[37] R. V Denys, M. V. Lototskyy, V. M. Linkov, and M. Williams, “Palladium mixed-metal surface-modified AB_5-type intermetallides enhance hydrogen sorption kinetics,” *S. Afr. J. Sci.*, vol. 106, pp. 1–6, 2010.

[38] W. Davids, M. V Lototskyy, and V. Linkov, “Chemical surface modification for the improvement of the hydrogenation kinetics and poisoning resistance of TiFe,” *J. Alloys Compd.*, vol. 509S, pp. S770– S774, 2011.

[39] S. K. Pandey, A. Srivastava, and O. N. Srivastava, “Improvement in hydrogen storage capacity in $LaNi_5$ through substitution of Ni by Fe,” *Int. J. Hydrogen Energy*, vol. 32, pp. 2461–2465, 2007.

[40] T. Erika, C. Sebastian, and Z. Fernando, “Temperature performance of AB_5 hydrogen storage alloy for Ni-MH batteries,” *Int. J. Hydrogen Energy*, vol. 41, pp. 19684–19690, 2016.

[41] S. Li, H. Cheng, and K. Yang, “Investigation of hydrogen absorption/desorption properties of $ZrMn_{0.85-x}Fe_{1+x}$ alloys,” *J. Alloys Compd.*, vol. 460, pp. 186–190, 2008.

CHAPTER 2

RECENT DEVELOPMENTS ON HYDROGEN ABSORPTION KINETICS OF METAL HYDRIDES AND THEIR CATALYTIC ACTIVITIES IN Co_2 REDUCTION

T. R. Somo[a], K. D. Modibane[a*], M. W. Davids[b], M. J. Hato[a], M. V. Lototskyy[b]

[a]Department of Chemistry, School of Physical and Mineral Sciences, University of Limpopo (Turfloop), Polokwane, Sovenga 0727, South Africa.

[b]HySA System, South African Institute for Advanced Material Chemistry, University of the Western Cape, Bellville 7535, Cape Town, South Africa

*Corresponding Author.

E-mail address: kwenamodibane@ul.ac.za

SUMMARY

Hydride-forming alloys are currently rated number one by most researchers as the best hydrogen storage materials because of their relatively high volumetric densities and reversible H_2 absorption/desorption kinetics with high storage capacity. Nonetheless, their practical use is obstructed by several factors including heavy weight and slow hydrogen absorption/desorption kinetics. Lately, common strategies such as spark plasma sintering, mechanical alloying, melt spinning, high hydrogen pressure method, hydriding combustion synthesis, surface modification and alloying with other elements have been exploited as to try to overcome slow kinetic challenge. Through these methods, improvement in hydriding kinetics has been achieved to some extent, but it is still far from that required for practical application. In this review, we provide a critical overview of various metal hydrides (MHs) ranging from binary hydrides (CaH_2, MgH_2, etc) to ternary hydrides (examples being Ti-Mn-N and Ca-La-Mg-based systems) that are used in solid hydrogen storage as well as alternative catalysts in carbon dioxide conversion. The reaction mechanism, surface modification techniques and hydrogen storage properties of these various MHs were discussed in detail. We also discussed the remaining challenges and proposed some suggestions to the emerging research of MHs.

Keywords: Hydrogen storage, Metal hydrides, Kinetics, Surface medication. CO_2 conversion

2.1. INTRODUCTION

The use of fossil fuels (Coal, oil and natural gas) for energy generation can lead to serious environmental concerns including increased amounts of greenhouse gases. Amongst the numerous alternative energy approaches, building an energy infrastructure that involves the use of hydrogen as the primary energy carrier may enable a non-polluting energy security in the future. Hydrogen fuel cell involves chemical reaction between hydrogen and oxygen to produce water vapour and electricity at an efficiency of 40-65% [1]. The electric current produced is sufficient to power an electric engine. When compared with the common fuels, hydrogen is relatively non-polluting and only water is exhausted when hydrogen is in use [2]. Approximately 4.5 litre of gasoline would be required to produce an energy that can be provided by just one kilogramme of hydrogen [3]. Moreover, hydrogen is abundant worldwide and thus its use can inhibit the depletion of fossil fuel reserves. Hydrogen in a form of gas is 14 times lighter than air and four times lighter than helium [4]. This allows hydrogen to easily disperse into the air in the event of an accident, eliminating the possibility of explosion. However, hydrogen cannot be used as a gas because it has a very low density of 0.08988 g/L at 1 atm; and therefore a lot of space is needed for portable and mobile applications [5]. In order to avoid this, hydrogen can be physically stored either on high pressure gas cylinders or as liquid hydrogen. Nevertheless, hydrogen storage through these methods is limited by high pressures required for compression of the hydrogen gas for High-pressure storage and a large amount of energy that is required for achieving liquefaction when storing hydrogen as a liquid [6].

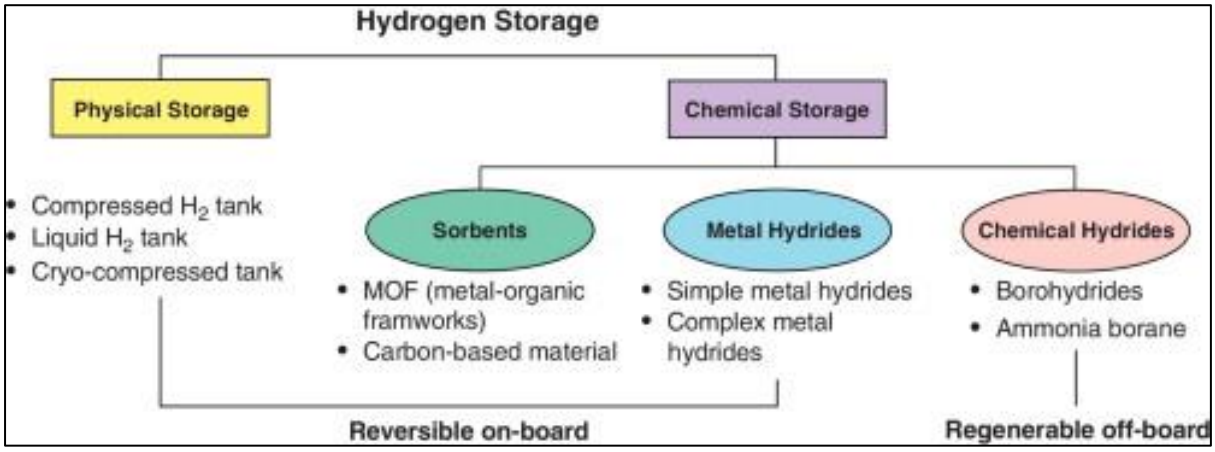

Figure 2.1: Different ways to store hydrogen [7]**.**

A convenient way to store hydrogen is through the absorption of hydrogen onto solid nanostructured materials such as different types of metal alloys, chemical sorbents (such as MOFs and carbon-based materials) or chemical hydrides (Figure 1) [7]. Of the above mentioned chemical storage materials, metal hydrides offer a safe, volume-efficient technology aimed at hydrogen storage for reversible on-board applications due to their higher hydrogen-storage gravimetric density (7.6 wt.% by Mg-tytpe alloys) [8], which is close to the long-term target published by the US Department of Energy (DOE) [5]. There are excellent reviews regarding MHs used for hydrogen storage application that have been published [5, 9, 10]. In this review, we consider the overview to provide an up-to-date of the recent developments on MHs and also highlight their limitations. We further demonstrated application of MHs in catalysis. This review consists of two sections mainly on hydrogen storage in metal alloys and metal hydrides as catalysts in CO_2 conversion. We anticipate that this work can provide an inspiring perspective for further research on MHs with good hydrogen storage properties.

2.2. HYDROGEN STORAGE IN METAL ALLOYS

In the late 1960s, scientists discovered that there are some intermetallic compounds that undergo direct, reversible reactions with gaseous hydrogen. Such intermetallic

alloys include Mg_2Ni, $LaNi_5$, $TiMn_2$ and TiFe among many others [11]. It is well documented that metallic hydrides are chemically formed from the reaction of hydrogen gas with metal or alloy according to Equation 2.1 [6]:

$$\text{Metal (M)} + H_2\,(g) \rightarrow \text{metal hydride (MH)} \qquad 2.1$$

The formation of metal hydride undergoes six distinct states of hydrogen absorption in metals: hydrogen to metal; physisorption which involves physical attachment of hydrogen to a metal through van der Waals interaction; chemisorption, the chemical attachment of hydrogen to metal by forming a chemical bond; subsurface hydrogen; solid solution (α-phase) and hydride (β-phase) [12]. The formation of α- and β-phases may be described by Equations 2.2 and 2.3, respectively [13]. A α-phase is formed when small amount of hydrogen occupies the interstitial sites of the host metal M, producing an H-poor solid solution while β-phase involves saturation of the solid solution to generate a second phase.

$$M + \frac{1}{2}yH_2 \leftrightarrow MHy \qquad 2.2$$

$$MHy + {\sim}\frac{1}{2}(x - y)\,H_2 \leftrightarrow MHx \qquad 2.3$$

During the formation of β-phase, the equilibrium pressure is fixed at any given temperature. This is because according to Gibbs' phase rule (F=C–P+2) the number of degrees of freedom F is one during the interaction of M and H atoms since three phases P (two solid and one gaseous) and two components C (H and M) are available [13]. The constant pressure level is referred to as the plateau pressure. During the formation, the metal atoms stretch apart to accommodate the hydrogen atoms and the physical structure of the metal atoms may also change to form a metal hydride. For example, Table 2.1 shows different types of metal alloys ranging from AB to AB_5, demonstrating that hydrogenation of metal is accompanied by increase in lattice parameters of the parent alloy. The A_2B alloys were reported to possess higher hydrogen storage capacity of 3.75 and 3.04 wt.% for P6222 and Fddd phase, respectively. On the other hand, AB_5 showed to have low absorption capacity of 1.43 wt.%. Moreover, peaks from X-ray diffractogram may broaden and shift towards smaller 2θ values as a result of larger lattice parameters [14].

Table 2.1: Lattice parameter, a, of different types of alloys before and after hydrogenation and their hydrogen storage capacities

Type of alloy	Structure	Alloy lattice parameter, a, Å	Hydride lattice parameter, a, Å	Storage capacity Wt%	References
AB	BCC	2.976	7.029	1.75	[15]
AB_2	C14	4.866	4.902	1.70	[16]
	C15	6.939	7.158	2.01	[17]
AB_5	$CaCu_5$	5.003	5.395	1.43	[18]
A_2B	(P6222)	5.205	5.463	3.75	[17]
	(Fddd)	5.284	5.411	3.04	[17]

Conversely, metal hydrides release H_2 gas when heat is applied on the hydride, this process is called desorption. Hydrogen atoms (H) move out from the metal to the surface of the metal hydride, combine into hydrogen molecules (H_2) and flow away as hydrogen gas. The metal atoms contract to form its original metal crystal structure [19].

2.2.1. Types of metal alloys

AB, A_2B, AB_2, AB_5 (A represents one or more strongly hydride-forming elements while B represents one or more weakly hydride-forming elements, B usually helps to dissociate the H_2 molecule) and Mg-based alloys are classes of alloys that can absorb hydrogen in order to form hydrides. Some metals such as Fe, Mn, Ca and Cu are capable of forming hydrides directly [20]. However, such complexes are either too unstable or too stable for gaseous applications. For binary hydrides that are too unstable, the pressures at which they absorb and release hydrogen are too high at practical temperatures and their enthalpies are too high. For binary hydrides that are

too stable, the pressures at which they absorb and release hydrogen are too low at practical temperatures and their enthalpies are too low [20].

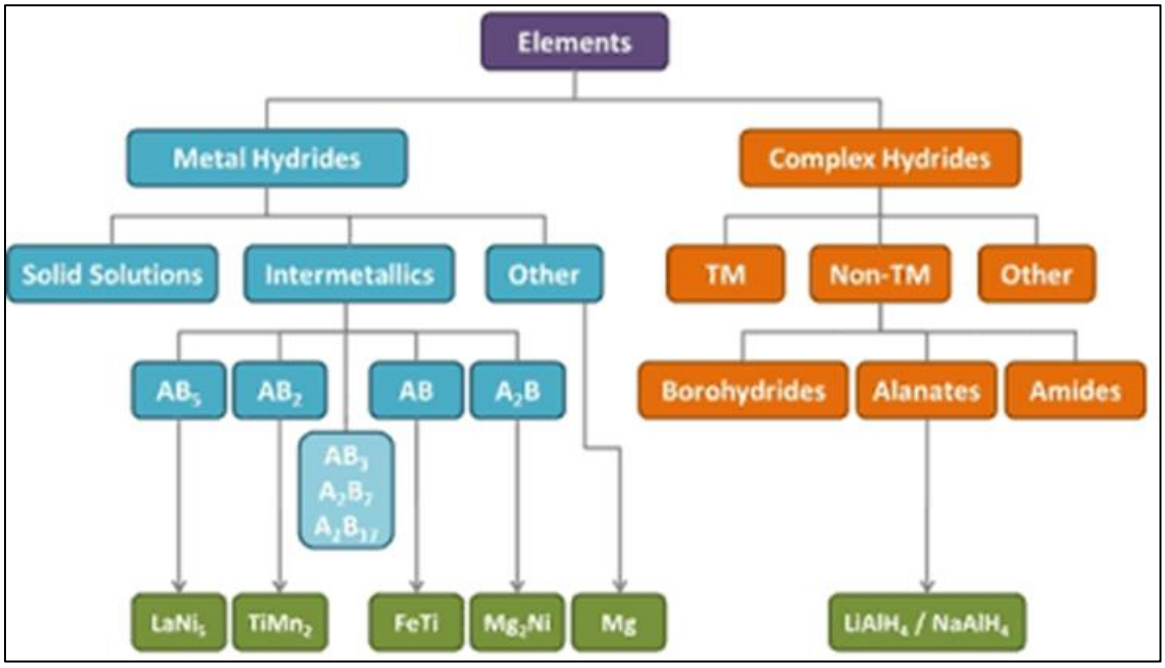

Figure 2.2: Hydride family tree of alloys and complexes, TM = transition metal [21].

In addition to binary alloys, multi-component systems (examples include $(Ti_{0.85}Zr_{0.15})_{1.05}Mn_{1.2}Cr_{0.6}V_{0.1}M_{0.1}$ (M=Ni, Fe, Cu)) do exist [22]. Another alloy type that is capable of forming metal hydride is solid solution alloy. Solid solution alloys are formed by dissolving a hydrogen-absorbing metal in another. Unlike the binary alloys and multi-component systems, the solution alloys do not have stoichiometric compositions [23]. However, the high temperature needed for desorption of solid solution hydride forming materials rules out these storage methods for practical purposes [21]. The A_aB_b-type alloys showed to react reversibly with hydrogen gas to form an intermediate strength hydride $A_aB_bH_x$ at ambient temperature and pressure [24]. These types of alloys are further reviewed in detail in this chapter.

2.2.1.1. AB alloys

ZrNi and TiFe alloys were the first AB compounds to successfully demonstrate reversible hydrogen absorption [25]. Unfortunately, the use of $ZrNiH_3$ for practical purposes was condemned due to several limitations including high desorption temperature of approximately 300 °C [26]. Other AB-type alloys include TiCo and ZrCo and their characteristics are summarised in Table 2.2.

Table 2.2: Lattice parameters, a, of AB-type alloys before and after hydrogenation and their plateau width.

Type	Alloy	Structure	Alloy lattice parameter, a, Å	Hydride composition	Plateau width Δ(H/M)	References
AB	TiCo	B2(CsCl)	2.994	$TiCoH_{1.4}$	1.30	[25]
	TiFe	B2(CsCl)	2.970	$TiFeH_2$	1.86	[27]
	ZrCo	B2(CsCl)	3.213	$ZrCoH_2$	2.70	[17]
	ZrNi	(CrB)	3.272	$ZrNiH_3$	1.43	[17]

The most successful AB alloy with favourable operational conditions is the TiFe alloy and its substitution alterations as well as surface modifications with the aim to enhance its hydrogen performances are still under study [28]. The crystal structure of TiFe-based AB alloys is an ordered body-centred cubic structure with CsCl as prototype [29]. In the CsCl-type structure, hydrogen atom occupies a central position of the octahedron is forever occupied by hydrogen atom while the six vertices are occupied by four Ti and two Fe atoms as depicted by Figure 2.3, thus referred to as the Ti_4Fe_2H octahedron. According to this crystal geometry, hydrogen absorption capacity in TiFe is expected to be H/M=1.5, however, a smaller amount (H/M=1.0) is usually observed [29, 30].

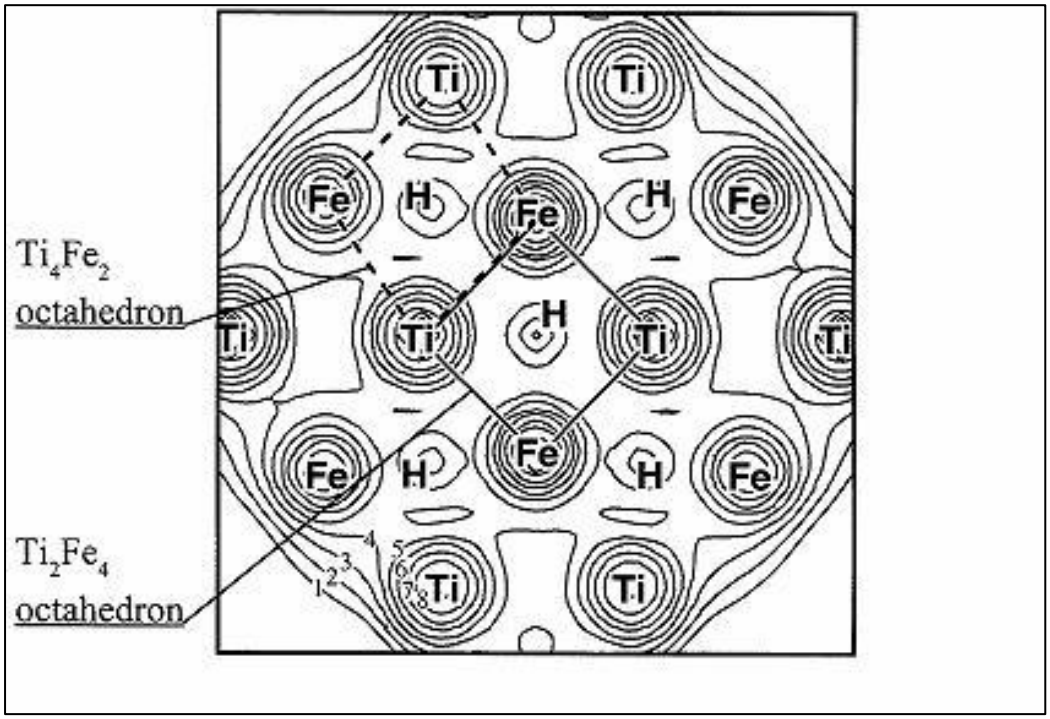

Figure 2.3: Contour maps of electronic densities for TiFe-type alloy [29].

This observation is caused by a formation of another octahedron with the four vertices now being occupied by Fe atoms and Ti atoms occupying only two, forming Ti_2Fe_4H octahedron as shown in Figure 2.3. Once the active sites on Ti_2Fe_4 octahedral are occupied by hydrogen atoms, it is not possible for hydrogen atoms to occupy the nearest Ti_4Fe_2 octahedral sites [29, 31]. This is illustrated in Figure 2.4. Ti atoms functions as H_2 absorbing atoms and since there is lesser number of them in Ti_2Fe_4 octahedral structure, the hydrogen absorption capacity is reduced from H/M=1.5 to H/M=1.0 [30].

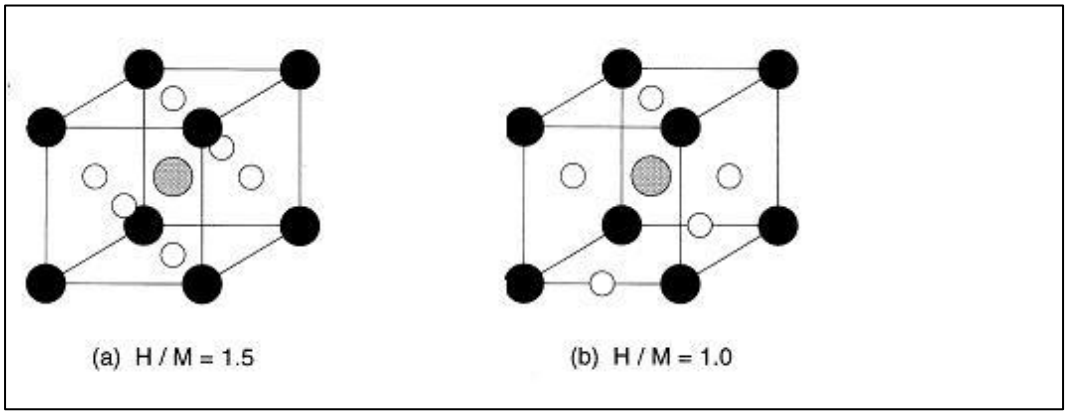

Figure 2.4: Schematic illustration of (a) simple hydride and (b) TiFe hydride [29].

Generally, pressure-compoition-temperature diagram of TiFe compounds usually consists of two plateaus, where the equilibrium pressure of γ-hydride is lower than that of β-hydride at ambient temperature [30]. Activation is a major problem in TiFe-type alloys because activation process involves time-consuming steps, which must be repeated several times [32]. The steps involve grounding of FeTi particles to ≤100 mesh followed by heating at temperature range of 573-773 K in vacuum [32]. Such limitations have prevented real-life application of the AB alloys.

2.2.1.2. AB_2 Laves phase alloys

Table 2.3: Lattice parameter, a, of AB_2-type alloys before and after hydrogenation and their plateau width.

Type	Alloy	Structure	Alloy lattice parameter, a, Å	Hydride composition	Plateau width Δ(H/M)	References
AB_2	$TiCr_{1.8}$	C15	6.939	$TiCr_{1.8}H_{2.6}$	1.54	[17]
		C14	4.927	$TiCr_{1.8}H_{2.6}$	2.43	
	$TiMn_{1.5}$	C14	4.862	$TiMn_{1.5}H_{2.5}$	1.86	[33]
	$ZrCr_2$	C15	7.220	$ZrCr_2H_{3.8}$	0.42	[17]
		C14	5.097	$ZrCr_2H_3$	0.98	
	$ZrMn_2$	C14	5.035	$ZrMn_2H_3$	1.77	[34]
	ZrV_2	C15	7.440	$ZrV_2H_{4.9}$	1.00	[35]

In the AB_2 Laves phase alloy, metal A is usually Ti or Zr, and metal B is another transition metal including V, Cr or Mn. These alloys crystallize in Lave phase structures. Three types of laves phases; namely: hexagonal C14 phase ($MgZn_2$), hexagonal C36 phase ($MgNi_2$) and cubic C15 phase ($MgCu_2$) represent AB_2- type alloys (Table 2.3) [36]. Hydrogenation performance of hexagonal C36 phase has been reported to be poor [37]. C15 and C14 phases (corresponding to atomic ratio of

R_A/R_B=1.225) have shown better performance as hydrogen absorbers [37]. Figure 5 show that the number of interstitial tetrahedral sites for hydrogen occupation is the same in both C14 and C15 structures with environments A_2B_2, AB_3 and B_4. Large amount of hydrogen is absorbed on the A_2B_2 sites due to their high coordination with A-type elements, which have stronger affinity to hydrogen compared to B-type elements. The structural stability of AB_2 alloys depends on the atomic ratio, electronegativity and valence of the elements used [38], [39]. It has been found and reported that hexagonal C14 $ZrCr_2$ Laves phases are more stable compared to cubic C15 [40].

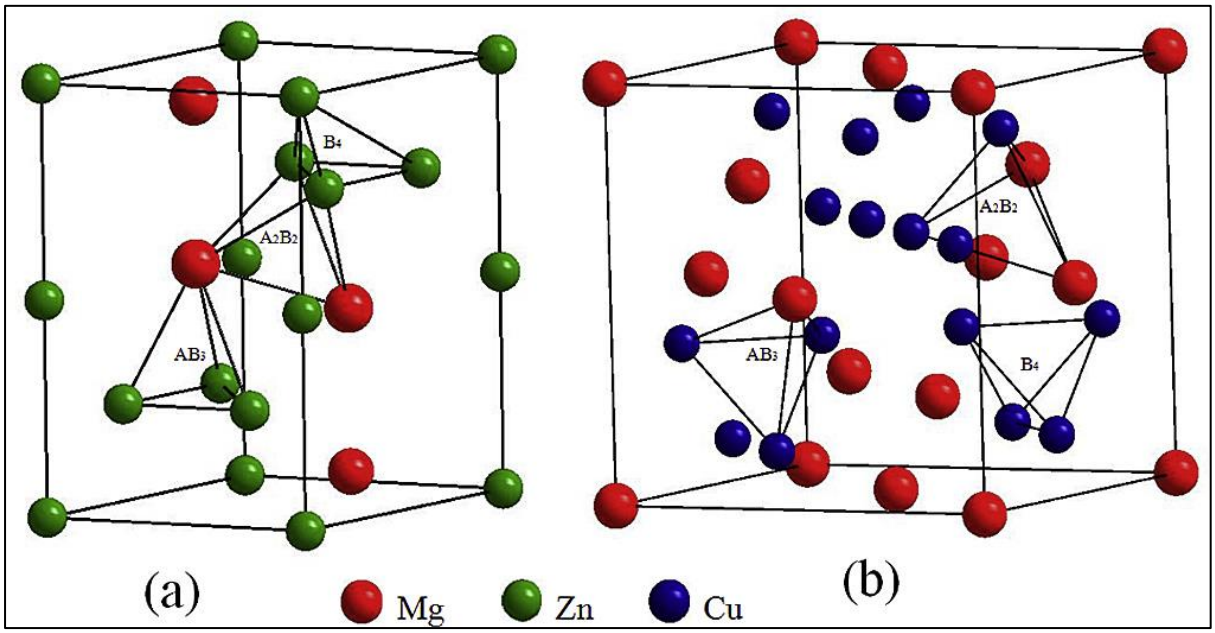

Figure 2.5: Crystal structures of (a) C14 and (b) C15 Laves phases [37].

The reported hydrogen storage of AB_2-type alloys is nearly 2 wt. %, with low hysteresis [39]. But binary AB_2-type alloys suffer from poor surface activity and poisoning intolerance [22]. Therefore, modification of the A/B stoichiometry and substitution of A, B or both A and B are exploited to improve performance of AB_2 alloys for hydrogen storage [41].

2.2.1.3. AB_5 alloys

With AB_5-type alloys, the A site is usually occupied by La, Ca or rare earth element while Ni, Cu, Co, Pt or Fe fill the B site [42]. These metal hydride alloys are typified by $LaNi_5$ and they can be easily activated for hydrogen absorption [43]. A reaction between these alloys and hydrogen at a room temperature and a pressure above equilibrium plateau pressure results in a ternary metal hydride [43]. It is notable that the hysteresis effect in AB_5-type alloy is relatively small as compared to other low temperature systems with a large and distinct miscibility gap [42].

Table 2.4: Lattice parameter, a, of AB_5-type alloys before and after hydrogenation and their plateau width.

Type	Alloy	Structure	Alloy lattice parameter, a, Å	Hydride composition	Plateau width, Δ(H/M)	References
AB_5	$LaNi_5$	($CaCu_5$)	5.017	$LaNi_5H_6$	2.48	[42]
	$MnNi_5$	($CaCu_5$)	4.912	$MnNi_5H_6$	1.75	[17]
	$CaNi_5$	($CaCu_5$)	4.943	$CaNi_5H_6$	2.70	[17]

The AB_5 alloys are known to have a $CuCa_5$-type hexagonal crystal structure and the crystal structure normally belongs to space group P6/mmm (#191) [44, 45]. The A-type atoms of AB_5 alloys in hexagonal structure are in the 1a positions and B-type atoms in both the 2c and the 3g positions, as shown in Figure 2.6 [37]. The position of these atoms is affected by their size. Large B-elements prefer to occupy the 3g sites, which has bigger space compared to 2c, however, substitution B-elements with a size similar to nickel have a random distribution on the 2c and the 3g sites [37, 44].

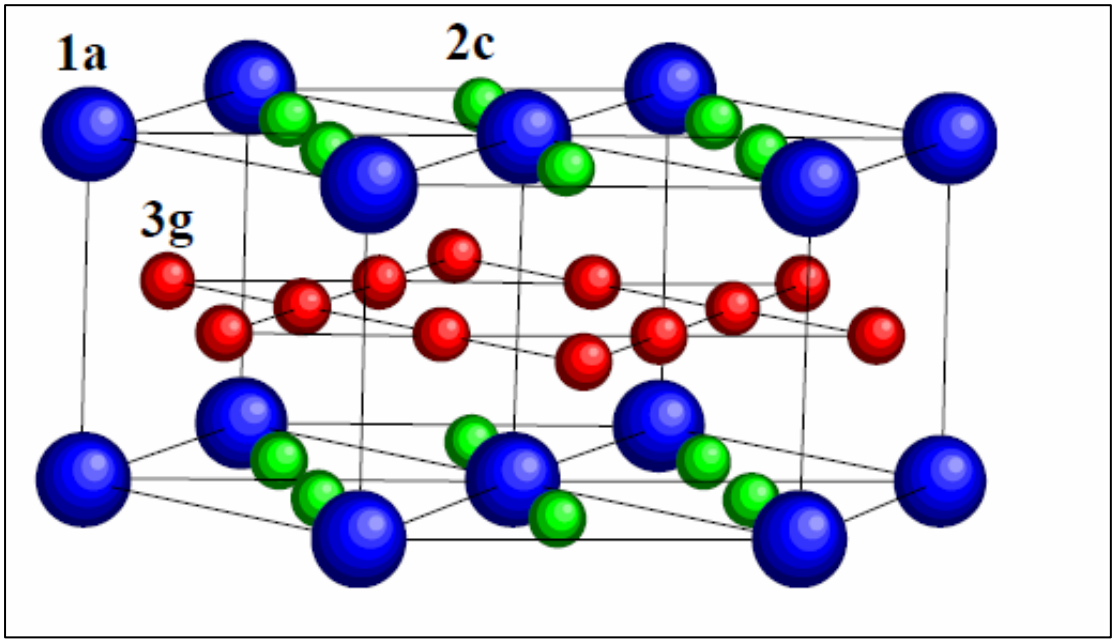

Figure 2.6: Crystal structure of AB_5-type alloys [37].

AB_5-type hydrides possess long recyclability (hundreds of cycles) when compared to other intermetallic hydrides (AB, A_2B, AB_2 and A_2B_2) [46]. These alloys retain better hydrogenation behaviour at moderate temperatures due to their low hysteresis, adaptability, relatively favourable plateau pressures, fast activation and better selectivity for hydrogen [47]. The common disadvantage of $LaNi_5$ alloy is that it is prone to surface reaction with poisonous gases such as CO, CO_2 and sulphur, forming an oxide layer which causes slow hydrogen sorption kinetics [48]. The PCT-curve of $LaNi_5$ usually depicts an equilibrium pressure of 1.8 bar which extends up to a concentration of 6.48 hydrogen atoms per formula unit (H/M=1.08) at ambient temperature [18]. This equilibrium absorption/desorption pressure can also be reduced by the introduction of substitutions in the AB_5 materials [18, 49].

2.2.1.4. Mg-based alloys

In Mg-based alloys, A is Mg while B is a transition metal. These alloys were reported to possess energy density of 9 MJ/kg and the highest maximum hydrogen storage capacity (7.6 and 3.6 wt% for MgH_2 and Mg_2NiH_4, respectively) compared to all

hydride-forming materials [50]. Furthermore, Mg is very cheap and accessible element due to its abundance [51]. Crystal structure of a metallic Mg is hexagonal with lattice parameters a= 3.2094 Å and c=5.2108 Å as well as a space group of P63/mmc [52]. Once the Mg metal is hydrogenated, the crystal structure changes to tetragonal structure as shown by Figure 2.7 while the lattice parameters changes from a= 3.2094 Å to a =4.517 Å and from c=5.2108 Å to c=3.0205 Å [53].

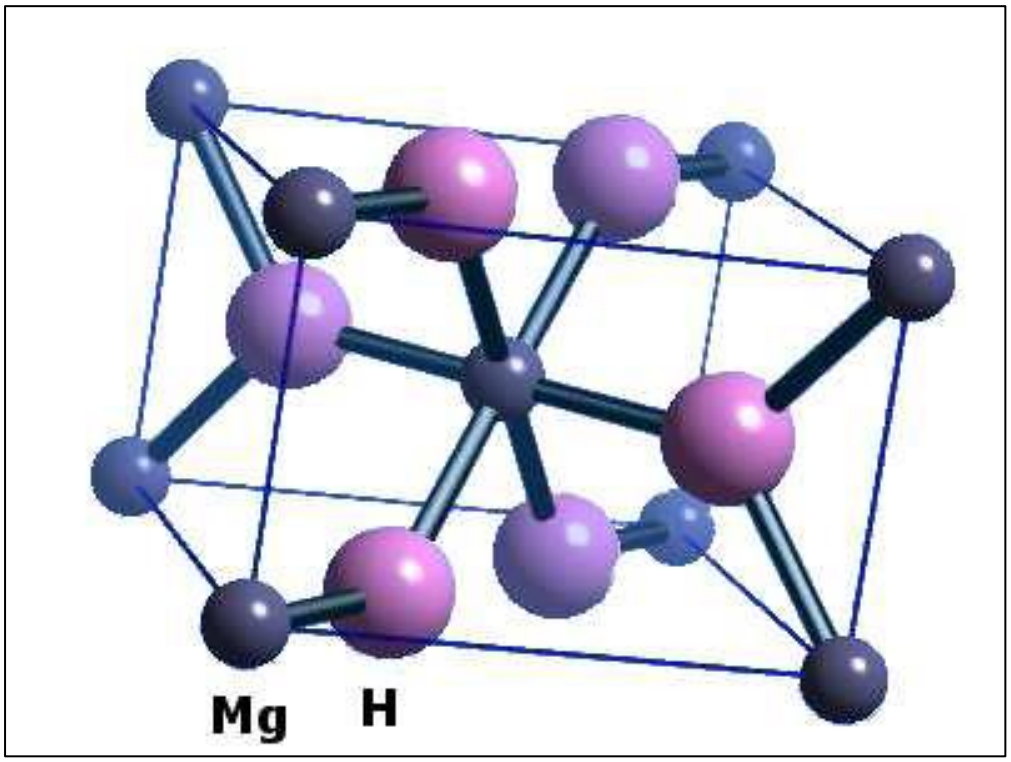

Figure 2.7: Structure of MgH_2 [53].

The hydride stability of this alloy is very high and therefore high dissociation temperature of around 561 K is required to transform MgH_2 hydride into Mg and H_2 gas [54]. Also, the hydriding kinetics of MgH_2 hydride is relatively slow because the dissociation of molecular hydrogen into hydrogen atoms is difficult on the surface of Mg metal [55].

2.2.2. Thermodynamics of metal hydrides

The thermodynamics of any metal hydride formation can be traced by studying PCT isotherms. A PCT diagram (Figure 8) supplies information on the pressure change during a reaction between hydrogen and hydrogen storage material at different temperatures [56]. Different stages passed by hydrogen phase during metal hydride formation can also be assessed by the PCT isotherm. The stages include α-hydride phase, (α+β)-hydride phase as well as the β-hydride phase as shown in Figure 2.8 [57]. A plot of logarithm of the pressure against reciprocal of temperature (1/T) gives a linear curve known as Van't Hoff plot.

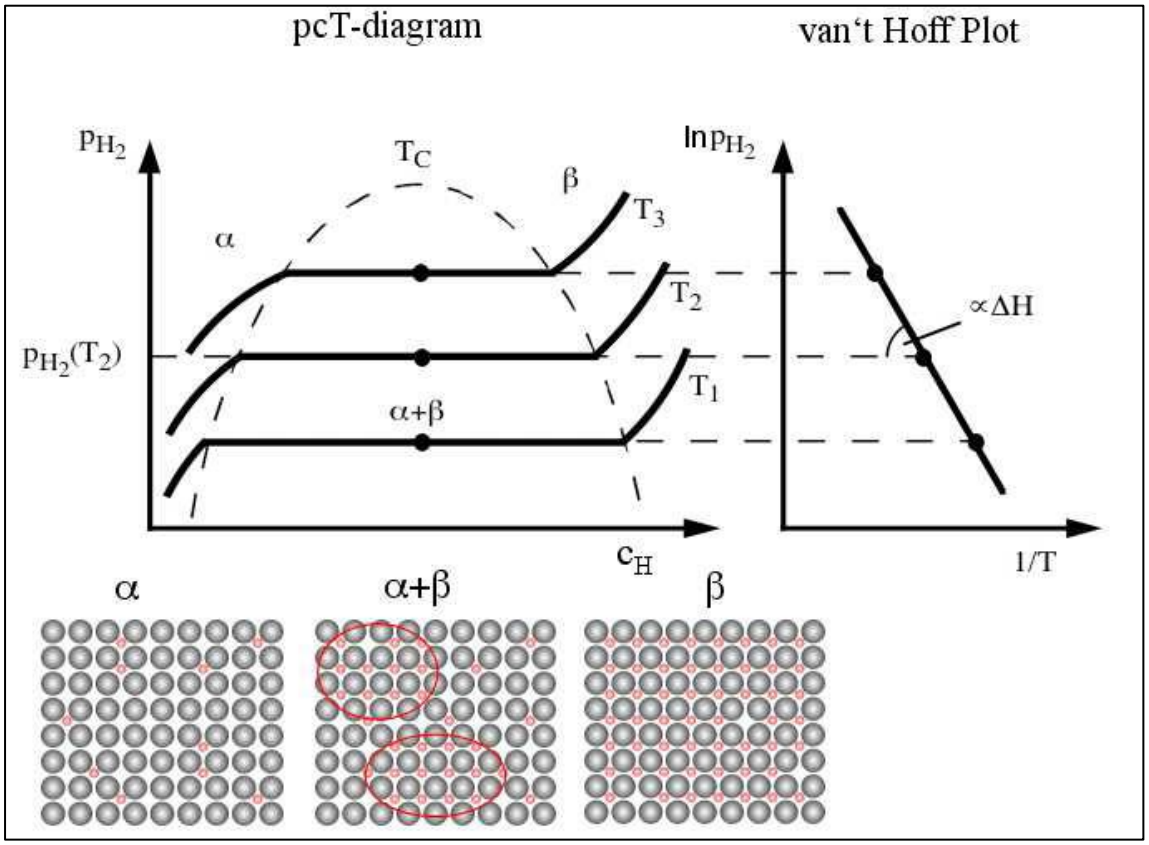

Figure 2.8: Schematic PCT-diagram and van't Hoff plot, taken from Dornheim [57].

From this plot other thermodynamic properties such as the enthalpy change (ΔH) and entropy change (ΔS) of hydride formation can be obtained using Van't Hoff equation [57]:

$$ln\left[\frac{P_{H_2}}{P^{\circ}}\right] = \frac{\Delta \mathrm{H}}{RT} - \frac{\Delta \mathrm{S}}{R} \quad 2.4$$

Where P_{H2} is the equilibrium hydrogen pressure upon transition of α-hydride to β-hydride phase, P° is the standard pressure, R is the gas constant, and T is the temperature. Subsequently, Gibb's free energy change can also be calculated as follows:

$$\Delta G = \Delta \mathrm{H} - \mathrm{T}\Delta S \quad 2.5$$

Table 2. 5: Thermodynamic data of some selected alloys.

Type	Alloy	Desorption pressure (atm) @ 298 K	Desorption temperature (K) @ 1 atm	Entropy, ΔS˚ (kj/mol.K)	Enthalpy, ΔH˚ (kj/mol)	References
AB	TiFe	4.1	265	0.106	28.1	[30]
AB_2	$TiCr_{1.8}$	182	182	0.111	20.1	[58]
	$TiMn_{1.5}$	8.4	252	0.114	28.7	[30]
	$ZrFe_2$	86	235	0.121	21.3	[59]
	$ZrMn_2$	0.0001	440	0.121	53.2	[59]
AB_5	$LaNi_5$	1.8	285	0.18	30.8	[5]
	$MnNi_5$	23	217	0.097	21.1	[17]
	$CaNi_5$	0.5	316	0.101	31.9	[17]
A_2B	Mg_2Ni	0.00001	528	0.14	43.2	[17]

Another important parameter in understanding the thermodynamics of metal hydrides is the P–C isotherm hysteresis of metal hydride alloy, which is depicted by Figure 2.9. The line of the upper pressure represents the hydride formation; the lower line of the lower pressure represents the hydride decomposition while the flat part of both lines is called Plateau [60]. And the difference in equilibrium pressures between the absorption and desorption reactions is called Hysteresis. The equilibrium pressure for hydride formation is higher than that of hydride

decomposition and this is related to extra energy needed to overcome the constraints related to the lattice expansion during hydride formation [56].

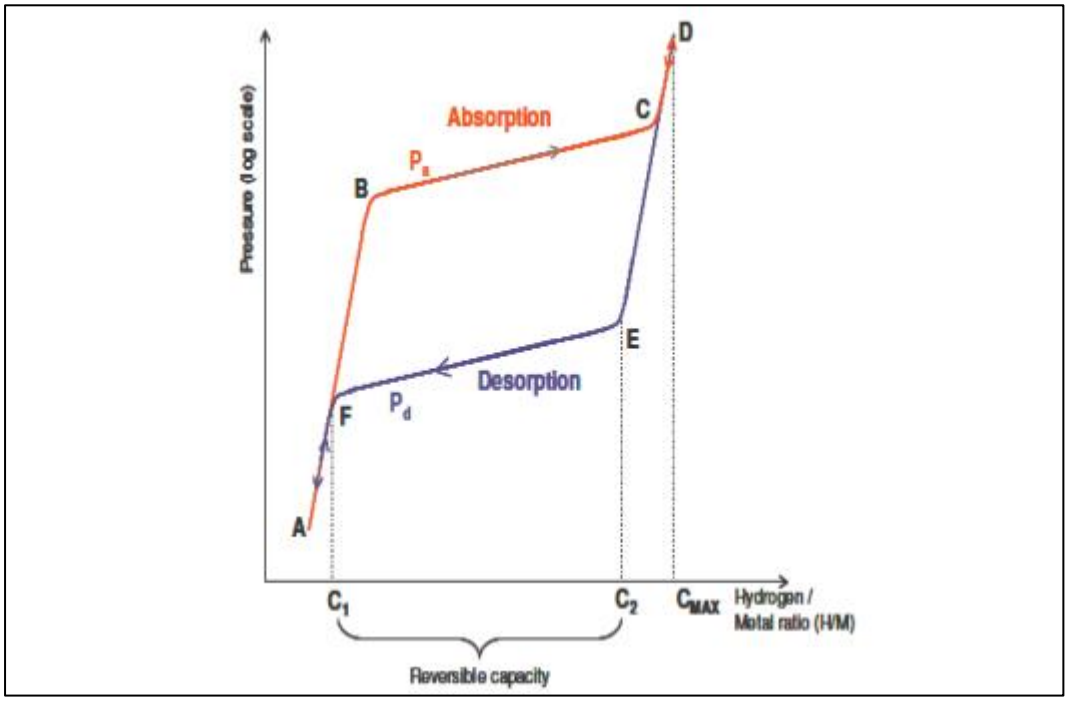

Figure 2. 9: Presure-composition-temperature diamgram [60].

2.2.3. Kinetic characteristics of metal hydrides

The hydrogenation behaviour of a hydrogen storage material depends mostly on the kinetic parameters (rate and time of desorption/absorption process) [19]. Almost all metal hydrides have been reported to exhibit poor hydrogen absorption/desorption kinetics [34]. Previous work have shown that poor hydrogen absorption kinetics is mainly attributed to the formation of an oxide layer on the surface of a metal or metal alloy making it difficult for splitting of molecular H_2 into atomic H and diffusion of atomic H into the bulk alloy [61]. Poor hydrogen desorption kinetics is mainly attributed to strong metal-hydrogen bond; nucleation of metal on the surface of hydride (nucleation requires a lot of energy); low diffusion rate of H in a metal hydride and formation of molecular H_2 from the desorbed atomic H [62]. The kinetics can be improved through the determination of the rate-determining mechanisms

during desorption/absorption of hydrogen. At least four models can be employed to identify rate-determining mechanisms and they are discussed here:

2.2.3.1. Surface controlled process (SC)

Surface controlled model presumes that chemisorption, which can be splitting of molecular H_2 during hydrogen absorption or formation of molecular H_2 from the desorbed atomic H during hydrogen desorption, is the slowest and thus the rate-determining step [63]. This assumption suggests that the number of atomic H is contant and therefore their diffusion into the main bulk alloy is relatively fast. Surface controlled model use Equation 2.6 [64]:

$$\alpha_{SC}(t) = k_{SC}t \qquad 2.6$$

Where α_{SC} is a fraction reacted, t is time and k_{SC} is a reaction constant. According to surface controlled mechanism cracking the surface passivation layer may increase the number of active sites responsible for hydrogen diffusion and subsequently enhance chemisorption process, and thus the kinetics as well [63].

2.2.3.2. Avrami-Erofeev model

Avrami together with Erofeev developed a kinetic equation (Equation 2.7) that describes the kinetics involved during nucleus growth due to gas adsorption [62]. They hypothesised that the kinetic parameter, rate of reaction, can be decelerated by ingestion and coalescence [62]. Ingestion occurs when development of a potential nucleation site is disturbed by growth of nucleus that already exists, while coalescence occurs when two growing nuclei merge, blocking possibility of new sites. The general equation corresponding to this model is:

$$-\ln(1-\alpha_{AE}) = (k_{AE}t)^n \qquad 2.7$$

Where n = 2, 3 or 4. Avrami-Erofeev model has been used to explain the hydrogenation kinetics of metal hydrides (MHs) according to the equation below [65]:

$$\left(\frac{H}{M}\right) = \left(\frac{H}{M}\right)_{\max} - \left\{1 - \exp\left(-\left(\frac{t}{t_0}\right)^n\right)\right\} \quad 2.8$$

Where (H/M) is the actual hydrogen concentration in the alloy; $(H/M)_{max}$ is the maximum hydrogen concentration in the alloy; t is time; t_0 is the characteristic time of hydrogen absorption (reciprocal rate constant k) while n is the index of power and it is interpreted as a value indirectly connected to the reaction mechanism (Figure 2.10). According to the figure, when n ≤ 1, the rate-determining mechanism is the diffusion control and when n > 1 then nucleation is the rate-determining step.

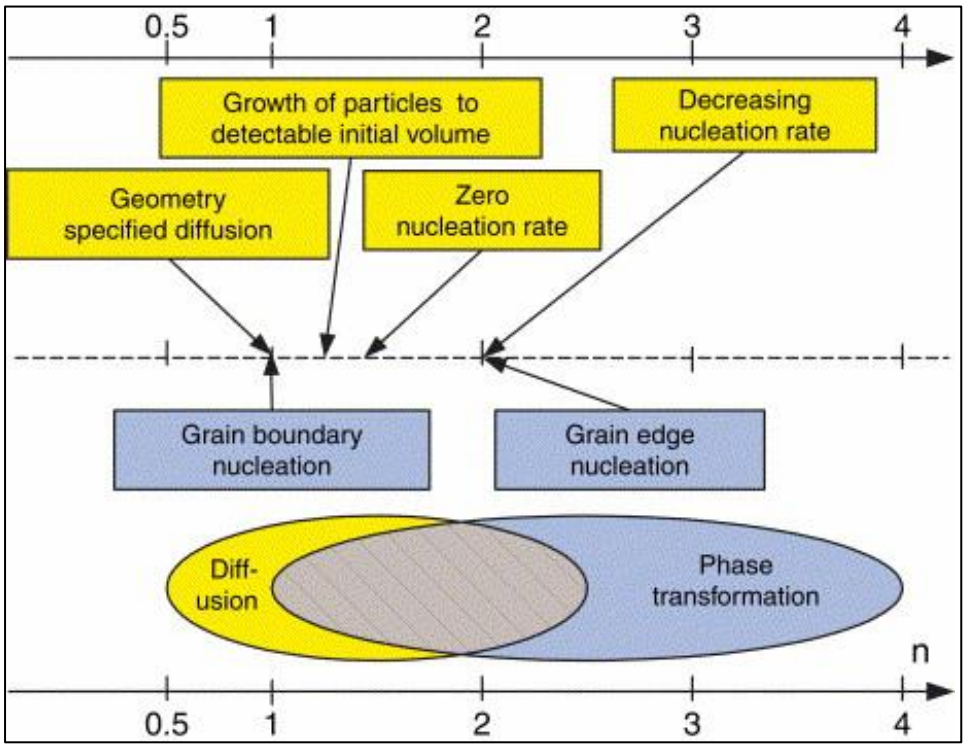

Figure 2.10: Index of power, n, which can be determined from Equation 2.6 [66].

2.2.3.3. Contracting volume model (CV)

Contracting volume model assumes that nucleation occurs on the surface of a particle while growth starts on the surface going into the bulk. It further postulates

that nucleation mechanism is fast compared to growth mechanism because the nucleation region is thin [63]. The interface velocity at which a new phase grows is constant but only when diffusion of atomic H is not the rate determining step [63]. The model is described by the equation below:

$$\alpha_{CV}(t) = 1 - (1 - k_{CV}t)^n \quad 2.9$$

Where n is 3 if the growth is three-dimensional and 2 if the growth is two-dimensional. k_{cv} can be obtained from Equation 2.10:

$$k_{CV} = \frac{U}{R} \quad 2.10$$

And U represents the interface velocity while R is the radius of the particle. In case of contracting volume model, the best way to improve the reaction kinetics is to reduce the particle sizes of the bulk material [63].

2.2.3.4. Johnson-Mehl-Avrami model (JMA)

The Johnson-Mehl-Avrami model is applicable in cases where there is no starting point for both nucleation and growth mechanisms; implying that the mechanisms can start either at the surface or within the bulk material [67]. Similarly to the contracting volume model, the constant interface velocity is the rate determining step with the exception that nucleation can start in the bulk in the case of JMA model. Equation 2.11 is applied for this model [67]:

$$(-\ln(1 - \alpha))^{1/n} = k_{JMA}t \quad 2.11$$

Just like in CV model, n is 3 if the growth is three-dimensional and 2 if the growth is two-dimensional. K_{JMA} can be calculated as follows [63]:

$$k_{JMA} = k_g N_0 U^n \quad 2.12$$

Assuming that the shape of the growing phase is spherical, k_g is given by $\frac{4}{3}\pi$; N_0 is the number of available nucleation sites per unit volume and U is the interface velocity of a growing phase.

2.2.4. Methods for improving hydriding kinetics of metal hydrides

There are several techniques that can be employed to improve the kinetics of hydride-forming materials and this section discusses them. These materials are also under research for carbon dioxide reduction. It is postulated that the hydrogen sorption kinetics possessed by a certain alloy plays a role in CO_2 reduction into hydrocarbons. Hence this section will be followed by a critical review on catalytic activity of hydride-forming alloys in CO_2 reduction/conversion.

2.2.4.1. Mechanical alloying

Mechanical alloying (MA) method is usually applied when synthesising highly immiscible alloys in a non-equilibrium state [68]. MA provides various advantages including smaller restrictions with respect to composition and it works much better when applied to A_2B alloys [69]. Through the use of this method, nanocrystalline alloys are obtained, starting either with a pre-prepared alloy or with a mixture of pure elemental metals [70]. Nano-crystalline alloys that are prepared through mechanical alloying technique possess better activation compared to their polycrystalline counterparts [70]. For example, Polycrystalline FeTi is activated by heating up to temperatures above 400 ˚C followed by annealing at 7 bar pressure and its hydrogenation requires a high pressure of 40-70 bar [71]. But with a mechanically alloyed nanocrystalline FeTi alloy, a single vacuum heating at 400 ˚C for 30 minutes is sufficient to obtain full hydrogen absorption cycles [71].

2.2.4.2. Melt-spinning technique

Zhang and co-workers reported that the hydriding/dehydriding kinetics of many hydride-forming alloys, including AB_5-type materials, are strongly affected by their structures, with nanocrystalline and amorphous alloys reported to be absorbing

hydrogen at an improved rate [72]. Melt-spinning technique is a useful method that is used to change structures of alloys to amorphous and nanocrystalline structure. This method improves the amorphous nature of materials by reducing their grain size [73]. The only problem related with this method is the poor cycle stability of the melt-spun alloys due to the disappearing of the metastable structures generated by melt-spinning [72].

2.2.4.3. Spark plasma sintering

Another technique that has attracted much attention is spark plasma sintering (SPS) due to its ability to easily synthesise metal powders with different melting temperatures within just 5-10 minutes [74]. This technique involves generation of spark plasma through direct pulse current and working concurrently with a uniaxial pressure. Sintering takes place at low temperatures in a small period of time and this makes the alloys to have low porosity [75]. Although this technique produces alloys with high purity surfaces, Liu *at al.* [74] reported that the hydriding kinetics of composites prepared by SPS is greatly improved only when hydrogen absorption is conducted at high temperatures (573 k).

2.2.4.4. Element alloying and partial substitution of A- or B-type elements

Element alloying involves formation of alloy composite by combining a pre-synthesised alloy with a metal of interest through evacuation to a suitable pressure, forming a second phase. Some examples include Mg-$Mg_2Ni_{0.75}Fe_{0.25}$, TiFe-8wt%Zr and Mg-$LaNi_5$ [76]. Hu *et al*. [33] reported that the formation of a second phase results in reduction of dissociation energy for hydrogen molecules, allowing them to easily dissociate into hydrogen atoms. Another way to enhance the hydriding kinetics is through partial substitution of alloy elements. Li *et al*. [77] reported that partial substitution of A elements, B elements or both A and B elements with elements having advanced electron attractive power and bigger active sites can enhance the

rate of hydrogen absorption/desorption process. For example, $La_{0.75}Mg_{0.25}Ni_{3.25}Co_{0.2}Al_{0.05}$ alloy possess better hydriding kinetics with a rate constant of 1.49 min^{-1} compared to non-substituted $LaNi_5$ alloy which exhibit a rate constant of 0.23 min^{-1} [78]. Table 2.6 shows a compilation of selected non-substituted and their substituted alloys and some few alloyed composites. 90% saturation time is the time it takes an alloy to saturate 90% of its maximum hydrogen capacity. The kinetic parameters (rate constant and 90% saturation time) of substituted alloys are superior to their non-substituted counterparts. This observation can be attributed to the fact that with the increase of elements containing bigger active sites, the particle size of the alloys changes to finer size, creating more fresh surfaces to allow faster contact with hydrogen [77]. Furthermore, the inclusion of these elements also minimise the oxide coating, which usually slows down the entry of hydrogen. One more reason can be the decrease in the absorption plateau pressure, hence the hydriding kinetics accelerates [58]. Nevertheless, this technique does not solve some drawbacks such as poisoning tolerance and as such, the hydriding kinetics is not significantly improved. Therefore, a co-modification technique (combination of this technique with any another surface modification technique) is recommended.

Table 2. 6: Kinetic parameters and hydrogen absorption capacities of different types of alloy.

Non-substituted alloy				Substituted/alloyed alloy				References
Alloy name	90% saturation time, (min)	Rate constant, (min^{-1})	Hydrogen absorption capacity, (wt%)	Alloy name	90% saturation time, (min)	Rate constant, (min^{-1})	Hydrogen absorption capacity, (wt%)	
$LaNi_5$	4.3 (est. from kinetic curve)	0.23	1.42	$La_{0.75}Mg_{0.25}Ni_{3.25}Co_{0.2}Al_{0.05}$	0.67 (est. from kinetic curve)	1.49	1.39	[78]
$ZrNi_2$	1.88 (est. from kinetic curve)	0.53	0.80	$ZrMn_{1.5}Ni_{0.5}$	1.33 (est. from kinetic curve)	0.75	3.62	[79]
TiFe	18.9 (est. from kinetic curve)	0.05	1.19	TiFe+8wt%Zr	0.45 (est. from kinetic curve)	2.22	1.74	[76]
TiFe	18.95	0.05	1.19	TiFe+4wt.%V	6.13	0.16	1.10	[71]
$TiMn_{1.5}$	2.15	0.47	1.74	Mg–30wt%$TiMn_{1.5}$	1.86	0.54	1.52	[33]
$TiZrMnCr_{0.8}Fe_{0.2}$	4.02 (est. from kinetic curve)	0.25	1.45	$(Ti_{0.65}Zr_{0.35})_{1.05}MnCr_{0.8}Fe_{0.2}$	0.92 (est. from kinetic curve)	1.09	2.19	[80]
$ZrMn_2$	1.80	0.56	0.98	$ZrMn_{0.45}Fe_{1.4}$	0.43	2.33	0.90	[77]
$TiCr_2$	2.40 (est. from kinetic curve)	0.42	2.10	$TiCr_{1.1}V_{0.45}Nb_{0.45}$	1.00 (est. from kinetic curve)	1.00	1.89	[58]
Mg_6Ag	10.22	0.10	4.23	$Mg_{5.7}In_{0.3}Ag$	4.58	0.22	3.33	[81]

2.2.4.5. Surface modification of metal hydride alloys

Shortcomings that are faced by metal hydrides for gaseous applications are well known as impurity interactions, which include poisoning of the metal by impure gases such as carbon monoxide, sulphur and carbon dioxide, disproportionation during absorption/desorption cycling, retardation, innocuous and difficulty of initial activation [82]. These shortcomings result in rapid loss of hydrogen capacity with cycling, caused by impurities strongly or irreversibly adsorbed on the surface active sites, reduction in adsorption/desorption kinetics without significant loss in the ultimate capacity, caused by impurities reversibly adsorbed on the surface active sites, bulk corrosion leading to irreversible reaction capacity loss and Loss in adsorption kinetics due to surface blanketing [83]. To overcome the above-mentioned problem, nanostructuring of the materials and surface modification technology can be employed before hydrogen sorption can take place [84]. The most common surface modification technologies include fluorination, potassium borohydride, Ni-weak acid, ion implantation, hydrochloric (HCl) acid, platinum group metals (PGMs) decomposition and Y_3O_2 deposition. Table 2.7 depicts the effect of some selected surface modification technologies on the hydriding kinetics of different alloys. A similar trend on the rate constant observed in Table 6 is also observed for surface modified alloys. Yeung *et al*. [85] reported that of the surface modification techniques described, PGMs deposition is the most attractive due to its ability to simultaneously prevent deactivation by guarding the catalytically active sites on the surface of bulk material against and enhance the hydriding kinetics during hydrogen absorption.

Table 2.7: Comparison of rare constants of different alloys before and after surface modification.

Surface modified alloy	Surface modification technology	Rate constant before modification, min^{-1}	Rate constant after modification, min^{-1}	References
$LaNi_{4.25}Al_{0.75}$	Pd deposition	4.8×10^{-1}	1.33	[86]
$La_{0.9}Pr_{0.05}Nd_{0.05}Al_{0.3}Mn_{0.4}Co_{0.65}Ni_{3.5}$	Pd deposition	2.4×10^{-3}	2.2×10^{-2}	[87]
$LaNi_4Al$	Pd deposition	9.3×10^{-3}	1.7×10^{-2}	[88]
$La_{0.40}Ce_{0.48}(Nd,Pr)_{0.16}Ni_{3.34}Co_{0.64}Al_{0.63}Mn_{0.58}$	Pd deposition	1.6×10^{-4}	6.2×10^{-4}	[89]
TiFe	Pd deposition	1.1×10^{-3}	4.2×10^{-2}	[15]
$MgLa_{0.3}Ni_{0.7}$	Fluorination	5×10^{-3}	1.3×10^{-2}	[90]
$LaNi_{4.7}Al_{0.3}$	Fluorination	4.8×10^{-1}	0.48	[91]
$La_{0.9}Pr_{0.05}Nd_{0.05}Al_{0.3}Mn_{0.4}Co_{0.65}Ni_{3.5}$	Pt deposition	2.4×10^{-3}	4.5×10^{-2}	[87]
$La_{0.9}Pr_{0.05}Nd_{0.05}Al_{0.3}Mn_{0.4}Co_{0.65}Ni_{3.5}$	Ru deposition	2.4×10^{-3}	3.3×10^{-2}	[87]
$La_{0.40}Ce_{0.48}(Nd,Pr)_{0.16}Ni_{3.34}Co_{0.64}Al_{0.63}Mn_{0.58}$	Pd-Ni co-deposition	1.6×10^{-4}	1.1×10^{-3}	[89]
$La_{0.9}Pr_{0.05}Nd_{0.05}Al_{0.3}Mn_{0.4}Co_{0.65}Ni_{3.5}$	Pt-Ru co-deposition	2.4×10^{-3}	2.9×10^{-2}	[87]

Moreover, this technique does not only enhance the hydriding rate but also the absorption capacity of the alloys. In particular, palladium is capable of catalysing hydrogen sorption reactions, promoting easy activation, and improving poisoning tolerance. It has high hydrogen affinity and it is impermeable to larger molecules such as CO_2 and sulphur.

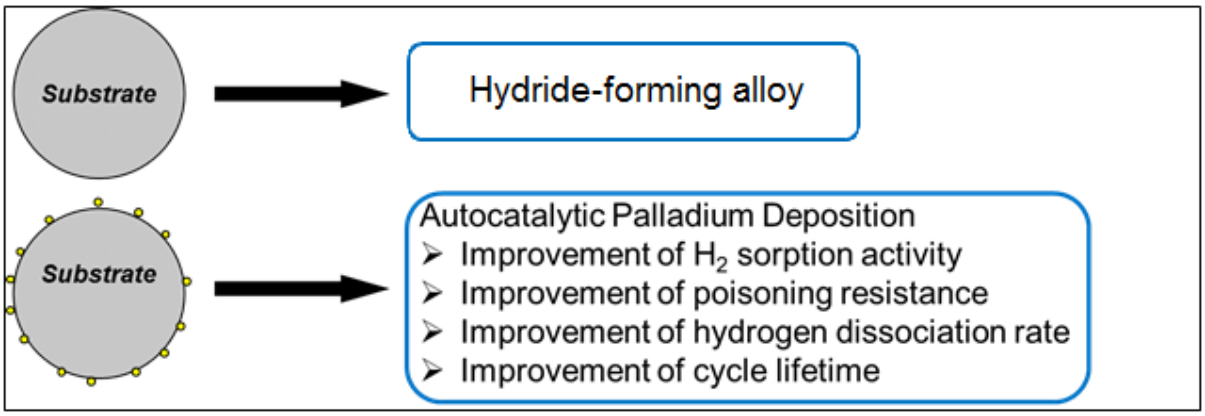

Figure 2.11: The autocatalytic palladium deposition on hydride-forming alloy material.

Figure 2.12 shows different mechanisms of hydrogen dissociation on the surface of Pd-treated AB_5-type alloys. During the hydrogen spillover mechanism hydrogen molecules are dissociated into hydrogen atoms on the surface of palladium which then spillover to the active sites of the bulk alloy [92]. Pd thin film on the surface of AB_5 alloy dissociates hydrogen molecules and allows the resulting hydrogen atoms to pass through the film as they diffuse into the bulk alloy. However, this technique is costly because lots of Pd is loaded [93].

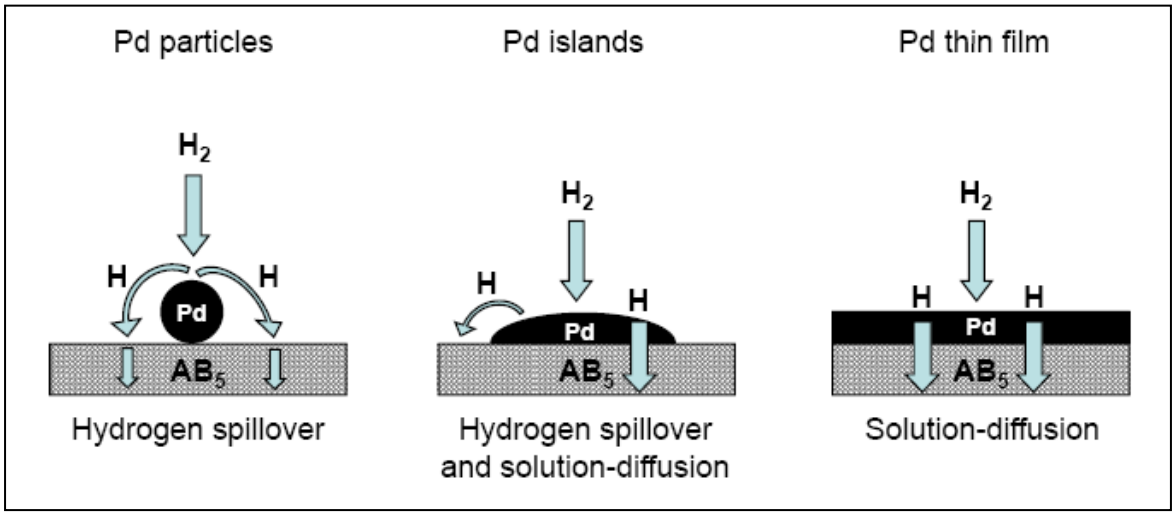

Figure 2.12: Different mechanisms of hydrogen dissociation on the surface of Pd-treated alloy material.

Palladium-treated materials also exhibit the power to absorb hydrogen at low temperature, without activation step prior to absorption, and enhanced kinetics of hydrogen sorption processes [89]. Moreover, this method is extremely active towards

dissociative hydrogen chemisorption and permeable for hydrogen atoms; enabling hydrogen to rapidly absorb into the bulk material while still maintaining the hydrogenation activity even after exposure to the impurities inhibiting hydrogen sorption [94]. The properties being improved include surface catalytic activity, specific surface area layer, activation characteristics as well as protective nature of the complexes against poisoning materials such as sulphur, water vapour and carbon oxides [90].

2.3. APPLICATION OF METAL HYDRIDES IN CO_2 CONVERSION USING

The increase in total energy consumption due to an increase in population growth and industrialization can lead to elevated atmospheric carbon dioxide concentrations as well as global temperature, causing global warming and climate change [95]. Additionally, the world reserve of natural gas is estimated to be roughly 1020 m^3 [96]. When looking at the current rate of use, this amount of natural gas can only last for 60 years, hence a need to convert carbon dioxide into hydrocarbons is very crucial. The best approach to mitigate the effect of CO_2 emission is through carbon dioxide reduction, leading to production of hydrocarbons [97]. The CO_2 conversion into hydrocarbons has been investigated for some years and several virtuous reviews and papers examining the reaction mechanisms have been published [96, 98]. Much work has been focusing on different techniques that can be utilised to effectively reduce CO_2 and different products that can be formed from different techniques [99]. Carbon dioxide can be reduced to hydrocarbons as part of waste management into profit through electrochemical, photochemical or catalytic reduction processes [99]. However, the catalysts that are utilised for photochemical reduction process suffer from low extinction coefficients in the visible region [100], and electrochemical reduction method is limited by the requirement of high overpotentials to reduce CO_2 and poor selectivity of the product [101]. Moreover, converting CO_2 to industrially important chemicals is a challenging concept because CO_2 is a very stable molecule [101]. It is also impossible to capture all the atmospheric carbon dioxide and thermodynamically, it is possible but difficult to reduce CO_2 to CO_2^- because a lot of energy is required for structural rearrangement from linear CO_2 to bent CO_2^- and this

also requires a large overpotential as well (0.1 to 0.6 V) [98]. CO_2 reduction can take place through the Sabatier reaction (Equation 13) [102].

$$CO_2 + 4\ H_2 = CH_4 + 2\ H_2O \quad H\ (298.15\ K) = -164.747\ kJ\ /mol \qquad 2.13$$

However, the above-mentioned reaction is affected by the high kinetic barriers of the eight-electron reduction process and this led to investigations in the look for thermally stable catalysts with high activities at low temperatures [103]. Among the available catalysts for Sabatier process, Ni-based catalysts have been fully studied for industrial purposes due to their high affinity for hydrogen, low cost and ease of availability. However, Ni catalyst may be deactivated even at low temperature due to the sintering of Ni particles, formation of mobile nickel sub-carbonyls, or formation of carbon deposits [104]. To enhance the stability and catalytic activity of the Ni-based catalysts, rare earth elements are often added to nickel catalysts [105]. $LaNi_5$ alloy, which is AB_5-type hydride-forming alloy, has been reported as a good rare earth/d transition metal alloy for catalytic conversion of CO_2 into hydrocarbons due to its ability to operate at elevated temperature and pressure conditions, high volumetric densities, reversible H_2 absorption/desorption kinetics and fast kinetic reactions [106]. For example, the rate of the hydrogenation of ethene was increased on a hydrogen-absorbing intermetallic compound, $LaNi_5Hx$ [107], for the synthesis of ammonia and the conversion of synthesis gas. Kaneko *et al*. [108] reported that atomic hydrogen on the surface of a metal hydride with high hydrogen adsorption is of particular interest for the hydrogenation of carbon dioxide. In a mixture of hydrogen and carbon dioxide, hydrocarbons will be produced on the metal hydride alloy in the course of the hydrogen desorption. An example is given in Figure 2.13, which depicts that at initial stage, the surface of ZrCoHx is covered with surface carbon dioxide molecules to form formate. When the temperature is increased hydrogen atoms diffuse from the active sites of ZrCo and react with formate precursors to form methane and water [107].

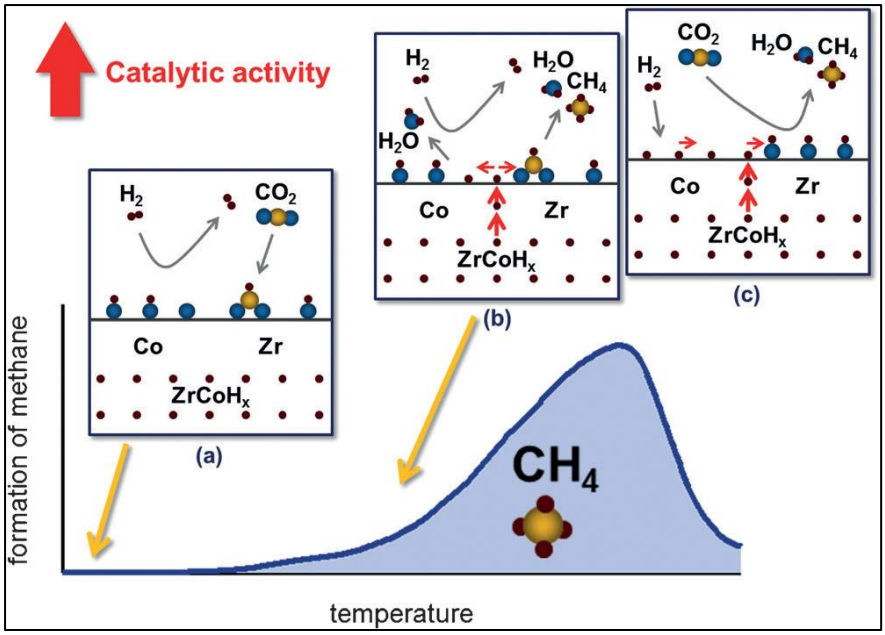

Figure 2.13: Representation of methane formation from CO_2 reduction on the surface of $ZrCoH_x$ [107].

Metal hydride alloys offer two advantages for CO_2 reduction, namely; high volumetric density and reversible absorption/desorption carried out at low pressure and temperatures [109]. These materials have been reported by Ren et al. [110] as active materials for CO_2 reduction. Other hydrides-forming materials that are capable of reducing CO_2 include transition metal borohydrides [111]. Formate and methoxy products are usually the major products of the reaction between CO_2 and borohydrides materials [111]. However, the life cycle of these type of hydrides is very low and as such their application is limited [112]. Hydride-forming semiconductors have previously been studied for homogenous reduction of CO_2 to form CO, where in a liquid-form a hydride is terminated from a semiconductor and readily react with CO_2 [113]. An example is a hydride functionalized silicon nanocrystals (silyl dihydrides), which has been extremely studied due to large surface areas, lack of toxicity and tuneable chemical and physical properties of silicon [114]. The stability of silyl dihydrides is usually balanced by the incorporation of transition metals such as copper, but such incorporation does not prevent the disadvantages discovered for silyl dihydrides, including regeneration of catalysts from the liquid-phase mixture for reuse, solubility and diffusion of CO_2 [114]. Alexander *et al*. [115] previously reported that the activity of transition metals towards CO_2 reduction can be enhanced by introducing borane additives. Moreover, the borane must be of appropriate Lewis

acidity: weaker acids possess poor transfer of hydride; stronger acids can effectively tranfer hydride without CO_2 reduction, while moderate acids such as trialkylborane were reported to be active for both hydride transfer and CO_2 reduction [115]. Generally, the major limitations associated with reduction of CO2 using metal hydrides are (1) selectivity of the resulting product (usually a mixture of hydrocarbons is formed) [116]; (2) decomposition of the catalysts upon CO_2 conversion [105]; (3) difficulty in regeneration [114]; (4) low life cycle and poisoning of the hydride-forming alloys in the presence of impurities such as CO_2 and CO gases [82] as well as (6) low conversion of CO_2 due to poor hydride desorption at ambient conditions [107]. Table 2.8 shows that optimal hydrogenation of CO2 by metal hydrides and metal oxides is achievable at very high temperature (500 ˚C for catalysts in Table 2.8). Furthermore, $LaNi_5$ shows significant potential as 89 % of CO_2 is converted over this catalyst at 500 ˚C and 1 atm but its selectivity is still poor. On the other hand, Fe_2O_3–K_2O oxide precursor has better selectivity towards CO, however, only its CO_2 hydrogenation capacity is relatively poor. Kustov and Tarasov [117] advised that poor catalytic hydrogenation and selectivity are caused by poisoning intolerance of catalyst precursors.

Table 2.8: Comparison of CO_2 conversion and CO selectivity by different catalyst precursors.

Catalyst	CO_2 Conversion (%)	CO selectivity (%)	Conditions	References
$LaNi_5$	89	09	T=500 ˚C, P= 1 atm	[117]
Fe_2O_3–K_2O	38	95	T=500 ˚C, P= 1 atm	[117]
2% Au/SO_4–ZrO_2	30	87	T=500 ˚C, P= 1 atm	[117]
5% Rh/ZnO–CuO	12	72	T=500 ˚C, P= 1atm	[117]
Ni/Y_2O_3	81	2.5	T=350 ˚C, P= 1 atm	[118]

The catalytic activity of metal hydrides towards CO_2 reduction and consequent hydrocarbons production is affected by several important parameters including the H_2/CO_2 ratio, dehydridng/hydriding rate, temperature and presure of a reaction [119]. These parameters further give the insight on the possible amount of CO_2 that can be converted as well as the selectivity of resulting hydrocarbons. In general terms, Kim and co-workers observed that the rate at which CO_2 conversion takes place and the amount that can be converted increase as the H_2/CO_2 ratio increases up to 3 [120]. When the ratio is above 3 the selectivity of hydrocarbons is uncontrollable, resulting in a mixture of products such as CO, CH_4 and parafin. Interestingly, other findings have shown that at pressures above 36 MPa, the unwanted hydrocarbons are not produced even at H_2/CO_2 ratios above 3 [121] (Figure 2.13).

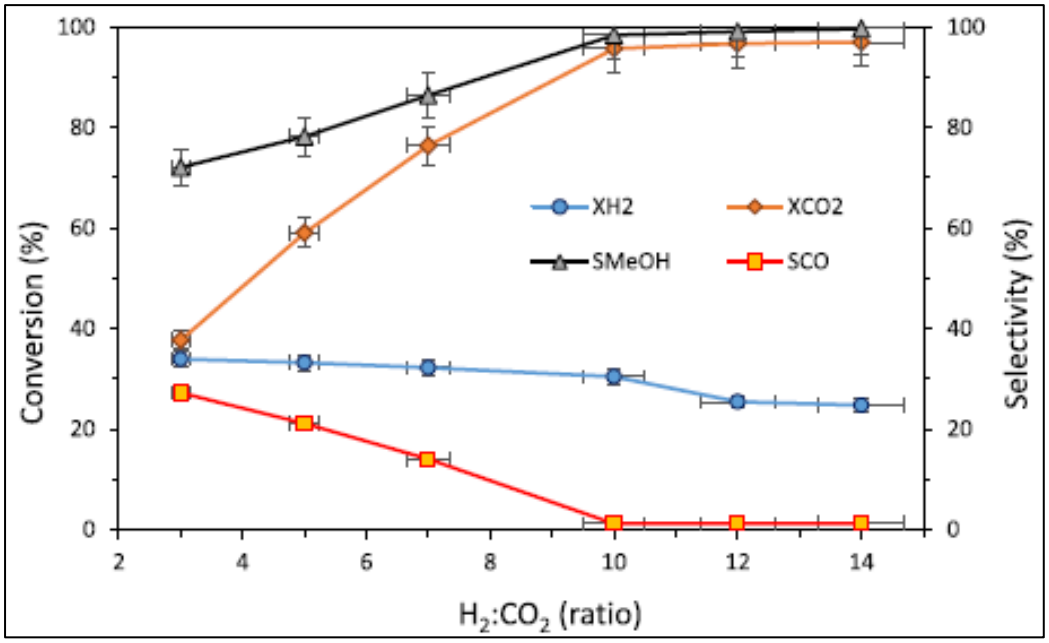

Figure 2. 14: Effects of the CO_2/H_2 feed ratio on CO_2 conversion (XCO2), H_2 conversion (XH2) and selectivity to CO (SCO) and methanol (SMeOH) in CO_2 hydrogenation over the $Cu/ZnO/Al_2O_3$ catalyst. Reaction conditions: T = 260 ˚C, P = 36 MPa. GHSV = 10,471 h^{-1} [121].

Generally, Increase in temperature and pressure causes the rate of a reaction to increase by increasing the concentration of the reactants and the collision speed of the particles. Li *et al.* [122] reported that production of hydrocarbons from CO_2 reduction is favored by an increase in temperature until the system reaches its thermodynamic limit. Moreover, Brook *et al*. [123] reported that an increase in gas

and wall temperature at constant H_2:CO_2 ratio results in creased CO_2 conversion and CH_4 production while the residence time decreases.

2.4. POISONING-TOLERANCE OF Pd-COATED METAL HYDRIDES

The sorption performance of metal hydride alloys in contaminated hydrogen streams can be enhanced by surface encapsulation using metallic coatings which exhibit good mechanical stability and high poisoning tolerance without negatively affecting the hydrogenation and kinetic properties. Platinum group metals (PGM's) have been identified as possessing the ability to dissociate hydrogen molecules with no or very little activation energy required [123]. Also, these metals are attractive in the surface modification of metal hydride-forming alloys since thermochemical data suggests that the oxides of these metals can be reduced in H_2 at room temperature, making these metals promising in the enhancement of hydrogen absorption kinetics of metal hydride-forming alloys [124]. It is also known that the surface deposition of Pd, Ni, or Cu layers result in improvements in the activation of the grains of hydride-forming metal alloys [119].

2.5. CONCLUSIONS OF THE REVIEW

Hydrogenation kinetics and storage in solid state materials is a major concern in developing a successful hydrogen technology and economy. The US DOE requires a hydrogen absorber with hydrogen capacity of 6.5 wt.% at room temperature and desorption temperature between 60 and 120 ˚C with high cycle life. Hydride-forming alloys are a promising class of hydrogen absorbers capable of storing 7.6 wt.% of hydrogen through MgH_2-based binary system. However, the large hydrogen capacity demonstrated by MgH_2 is accompanied by several drawbacks such as high hydrogen desorption temperature (approximately 387.4 ˚C), slow sorption kinetics and poor poisoning-tolerence toward air and oxygen. Ternary-based systems such as AB, AB_2, AB_5 and A_2B alloys have also shown potential towards hydrogen absorption, but slow sorption kinetics and poor poisoning-tolerence are still the key issues for these kinds of alloy systems. The present article reviews some challenges regarding the hydride-forming alloys, particularly their hydriding kinetics. In this

regard, several techniques to enhance hydriding kinetics of metal alloys are reviewed. The work is carried out in an attempt to facilitate suitable material choice for application in carbon dioxide conversion, which can be achieved by addressing and finding solutions to hydrogenation kinetics and storage of metal alloys. Althogh much attention has been given to the techniques that are discussed in this paper with the aim to minimise dehydrogenation temperature, enhance the kinetics and poisoning-tolerence of different alloys, further research is needed. The collected data represented in Table 6 and 7 reveal encouraging improvements in terms of hydriding kinetics through metal alloying/substitution and surface modification technologies, respectively. In the light of the achievements, we recommend that through the combination of metal alloying/substitution and surface modification techniques there is high potential in developing better metal hydride materials with high hydriding kinetics and strong tolerence toward poisonouos gases. Development of an efficient hydrogen-based economy through solid state storage is of great importance as some applications such as catalytic use of metal hydrides in CO_2 conversion awaits for suitable materials. This is because poisoning-tolerence, fast hydriding/dehydriding kinetics, and large hydrogen storage capacity of a catalyst precursor are the prerequisites for CO_2 conversion.

2.5. REFERENCES

[1] M. V Lototskyy, I. Tolj, and L. Pickering, “Materials International The use of metal hydrides in fuel cell applications,” *Prog. Nat. Sci. Mater. Int.*, vol. 27, pp. 3–20, 2017.

[2] K. Young and J. Nei, “The Current Status of Hydrogen Storage Alloy Development for Electrochemical Applications,” *Materials (Basel).*, vol. 6, pp. 4574–4608, 2013.

[3] P. Nikoleishvili, G. Gorelishvili, and G. Tsurtsumia, “Hydrogen Generation by Reforming of Sodium Hypophosphite on Cobalt-Boron Oxides Containing Catalyst,” *green Sustain. Chem.*, vol. 7, pp. 85–93, 2017.

[4] A. Rodionov and P. Moretto, “Risk assessment of hydrogen explosion for private car with hydrogen-driven engine,” *Int. J. Hydrogen Energy*, vol. 36, pp. 2398–2406, 2011.

[5] B. Sakintuna, F. Lamari-darkrim, and M. Hirscher, “Metal hydride materials for solid hydrogen storage: A review,” *Int. J. Hydrogen Energy*, vol. 32, pp. 1121–1140, 2007.

[6] R. Andreas, “Hydrogen storage methods,” *Naturwissenschaften*, vol. 91, pp. 157–172, 2004.

[7] L. Schlapbach and A. Züttel, “Hydrogen-storage materials for mobile applications,” *Nature*, vol. 414, pp. 353–358, 2001.

[8] L. E. A. Berlouis, E. Cabrera, and P. J. Hall, “Thermal analysis investigation of hydriding properties of nanocrystalline Mg–Ni- and Mg–Fe-based alloys prepared by high-energy ball milling,” *J. Alloys Compd.*, vol. 305, pp. 82–89, 2000.

[9] J. C. Crivello, B. Dam, and V. A. Yartys, “Review of magnesium hydride-based materials: development and optimisation,” *Appl. Phys. A Mater. Sci. Process.*, vol. 122, pp. 1–20, 2016.

[10] B. Sakintunaa, F. Lamari-Darkrimb, and M. Hirscher, “Metal hydride materials

for solid hydrogen storage: A review," *Int. J. Hydrogen Energy*, vol. 32, pp. 1121–1140, 2007.

[11] X. Qu, P. Li, and F. Zhai, "The development of metal hydrides using as concentrating solar thermal storage materials," *Front. Mater. Sci.*, vol. 9, pp. 317–331, 2015.

[12] V. A. Yartys and M. V. Lototskyy, "An overview of hydrogen storage methods," *Hydrog. Mater. Sci. Chem. Carbon Nanomater.*, pp. 75–104, 2004.

[13] S. A. Willems, "Metal hydride electrodes stability of $LaNi_5$-related compounds," *Zeitschrift für Phys. Chemie*, vol. 147, p. 231, 1984.

[14] S. K. Pandey, A. Srivastava, and O. N. Srivastava, "Improvement in hydrogen storage capacity in $LaNi_5$ through substitution of Ni by Fe," *Int. J. Hydrogen Energy*, vol. 32, pp. 2461–2465, 2007.

[15] W. Davids, M. V Lototskyy, and V. Linkov, "Chemical surface modification for the improvement of the hydrogenation kinetics and poisoning resistance of TiFe," *J. Alloys Compd.*, vol. 509S, pp. S770– S774, 2011.

[16] S. Semboshi, N. Masahashi, and S. Hanada, "Degradation of hydrogen absorbing capacity in cyclically hydrogenated $TiMn_2$," *Acta Metall. Sin.*, vol. 49, pp. 927–935, 2001.

[17] H. Takeda, T. Kabutomori, and K. Ohnishi, "Metal hydride air-conditioning," *Encycl. Life Support Syst.*, vol. 2, pp. 249–263, 2009.

[18] A. N. Kazakov, D. O. Dunikov, and S. V Mitrokhin, "AB_5-type intermetallic compounds for biohydrogen purification and storage," *Int. J. Hydrogen Energy*, vol. 41, pp. 21774–21779, 2016.

[19] A. Andreasen, *Predicting formation enthalpies of metal hydrides*, vol. 1484. 2004.

[20] X. Q. Chen, R. Podloucky, and P. Rogl, "Computational and experimental study of phase stability, cohesive properties, magnetism and electronic structure of $TiMn_2$," *Acta Mater.*, vol. 51, pp. 1239–1247, 2003.

[21] R. Bowman and G. Sandrock, “Metal Hydrides for Energy Storage and Conversion Applications,” *J. Alloys Compd.*, vol. 9, pp. 25–27, 2015.

[22] P. Liu, X. Xie, and T. Liu, “Hydrogen storage properties of $(Ti_{0.85}Zr_{0.15})_{1.05}Mn_{1.2}Cr_{0.6}V_{0.1}M_{0.1}$ (M=Ni, Fe, Cu) alloys easily activated at room temperature,” *Prog. Nat. Sci. Mater. Int.*, vol. 27, pp. 652–657, 2017.

[23] X. Xu and M. D. Sumption, “A model for the compositions of non-stoichiometric intermediate phases formed by diffusion reactions, and its application to Nb_3Sn superconductors,” *Sci. Rep.*, vol. 6, p. 19096, 2016.

[24] H. M. Systems, H. M. Systems, and H. F. Alloys, “Metal Hydrides : Transition Metal Hydride Complexes,” *Encycl. Mater. Sci. Technol.*, vol. 6, pp. 1–9, 2004.

[25] N. Acharya, B. Fatima, and S. P. Sanyal, “Theoretical study of B_2 type technetium AB (A=Tc, B=Ti, V, Nb and Ta) intermetallic compounds,” *J. Phys. Chem. Solids*, vol. 99, pp. 25–33, 2016.

[26] Y. Bouhadda, A. Rabehi, and N. Fenineche, “Hydrogen solid storage: First-principles study of $ZrNiH_3$,” *Int. J. Hydrogen Energy*, vol. 34, pp. 4997–5002, 2009.

[27] M. W. Davids and M. Lototskyy, “Influence of oxygen introduced in TiFe-based hydride forming alloy on its morphology, structural and hydrogen sorption properties,” *Int. J. Hydrogen Energy*, vol. 37, pp. 18155–18162, 2012.

[28] W. Davids, M. V. Lototskyy, and M. Williams, “Surface modification of TiFe hydrogen storage alloy by metal-organic chemical vapour deposition of palladium,” *Int. J. Hydrogen Energy*, vol. 36, pp. 9743–9750, 2011.

[29] T. Nambu, H. Ezaki, and M. Morinaga, “Electronic structure and hydriding property of titanium compounds with CsCl-type structure,” *J. Alloys Compd.*, vol. 295, pp. 213–216, 1999.

[30] T. Tsuchiya, N. Okinaka, and T. Akiyama, “Combustion synthesis of TiFe-based hydrogen storage alloy from titanium oxide and iron,” *Int. J. Hydrogen Energy*, vol. 38, pp. 6681–6686, 2013.

[31] S. Kato, A. Borgschulte, and A. Züttel, “CO_2 hydrogenation on a metal hydride

surface," *Phys. Chem. Chem. Phys.*, vol. 14, pp. 5518–5526, 2012.

[32] V. Y. Zadorozhnyy, G. S. Milovzorov, and S. D. Kaloshkin, "Preparation and hydrogen storage properties of nanocrystalline TiFe synthesized by mechanical alloying," *Prog. Nat. Sci. Mater. Int.*, vol. 27, pp. 149–155, 2017.

[33] Y. Q. Hu, H. F. Zhang, and Z. Q. Hu, "Preparation and hydriding/dehydriding properties of mechanically milled Mg–30 wt% $TiMn_{1.5}$ composite," *J. Alloys Compd.*, vol. 354, pp. 296–302, 2003.

[34] V. Kumar, D. Pukazhselvan, and S. K. Singh, "Hydrogen absorption/desorption characteristics of room temperature $ZrMn_{2-x}Ni_x$ system (x = 1.25–1.50)," *Bull. Mater. Sci.*, vol. 37, pp. 655–660, 2014.

[35] J. Radakovic, M. Iordoc, and K. Batalovic, "Influence of Ta and Nb on the hydrogen absorption kinetics in Zr-based alloys," *Int. J. Hydrogen Energy*, vol. 40, pp. 5677–5682, 2015.

[36] E. D. Koultoukis, C. N. Christodoulou, and D. Fruchart, "High-Temperature Activated AB_2 Nanopowders for Metal Hydride Hydrogen Compression," *Int. J. energy Res.*, vol. 38, pp. 477–486, 2014.

[37] L. Ouyang, J. Huang, and M. Zhu, "Progress of hydrogen storage alloys for Ni-MH rechargeable power batteries in electric vehicles: A review," *Mater. Chem. Phys.*, vol. 200, pp. 164–178, 2017.

[38] F. Stein, M. Palm, and G. Sauthoff, "Structure and stability of Laves phases . Part I. Critical assessment of factors controlling Laves phase stability," *intermetallics*, vol. 12, pp. 713–720, 2004.

[39] T. Hammerschmidt, A. N. Ladines, and R. Drautz, "Crystal-Structure Analysis with Moments of the Density-of-States: Application to Intermetallic Topologically Close-Packed Phases," *crystals*, vol. 6, pp. 1–12, 2016.

[40] A. Ioannidou, S. Makridis, and E. S. Kikkinides, "Structural and Hydrogenation Properties of $Zr_{0.9}Ti_{0.1}Cr_{1.2-x}V_{0.8}Ni_x$ (x=0, 0.4) Compounds," *Mater. Sci. forum*, vol. 636, pp. 26–31, 2010.

[41] J. Park, H. Jang, and J. Lee, "Hydrogen storage properties of $TiMn_2$-based

alloys for metal hydride heat pump," *Mater. Sci. Eng.*, vol. 331, pp. 351–355, 2002.

[42] T. Erika, C. Sebastian, and Z. Fernando, "Temperature performance of AB_5 hydrogen storage alloy for Ni-MH batteries," *Int. J. Hydrogen Energy*, vol. 41, pp. 19684–19690, 2016.

[43] Y. Chen, C. A. C. Sequeira, X. Song, R. Neto, and Q. Wang, "Polytypism of La–Ni phases in multicomponent AB_5 type hydride electrode alloys," *Int. J. Hydrogen Energy*, vol. 27, pp. 63–68, 2002.

[44] H. Hayakawa, E. Akiba, and T. Kohno, "Crystal Structures of La–Mg–Ni_x (x = 3-4) System Hydrogen Storage Alloys," *Mater. Trans.*, vol. 46, pp. 1393–1401, 2005.

[45] M. F. J. Boeije, E. K. Delczeg-czirjak, and E. Brück, "On the phase stability of $CaCu_5$-type compounds," *J. Alloys Compd.*, vol. 722, pp. 549–554, 2017.

[46] D. B. Willey, I. R. Harris, and A. S. Pratt, "The improvement of the hydrogenation properties of nickel-metal hydride battery alloy by surface modification with platinum group metals (PGMs)," *J. Alloys Compd.*, vol. 295, pp. 613–620, 1999.

[47] D. Dunikov, V. Borzenko, and C. Chu, "Biohydrogen purification using metal hydride technologies," *Int. J. Hydrogen Energy*, vol. 41, pp. 21787–21794, 2016.

[48] S. Miura, A. Fujisawa, and N. Hanada, "A hydrogen purification and storage system using CO adsorbent and metal hydride," *J. Alloys Compd.*, vol. 580, pp. S414–S417, 2013.

[49] S. P. Malyshenko, S. V Mitrokhin, and I. A. Romanov, "Effects of scaling in metal hydride materials for hydrogen storage and compression," *J. Alloys Compd.*, vol. 645, pp. S84–S88, 2015.

[50] H. X. Huang, K. L. Huang, and S. Q. Liu, "Microstructures and electrochemical properties of $Mg_{0.9}Ti_{0.1}Ni_{1-x}M_x$ (M = Co, Mn; x = 0, 0.1, 0.2) hydrogen storage alloys," *Powder Technol.*, vol. 198, pp. 144–148, 2010.

[51] P. Vermeulen, R. A. H. Niessen, and P. H. L. Notten, “Hydrogen storage in metastable $Mg_yTi_{(1-y)}$ thin films,” *Electrochem. commun.*, vol. 8, pp. 27–32, 2006.

[52] W. Li, C. Li, and J. Chen, “Magnesium nanowires: enhanced kinetics for hydrogen absorption and desorption,” *J. Am. Chem. Soc.*, vol. 129, pp. 6710–6711, 2007.

[53] F. C. Gennari, F. J. Castro, and J. Gamboa, “Synthesis of Mg_2FeH_6 by reactive mechanical alloying: formation and decomposition properties,” *J. Alloys Compd.*, vol. 339, pp. 261–267, 2002.

[54] W. Luo, “($LiNH_2$-MgH_2): a viable hydrogen storage system,” *J. Alloys Compd.*, vol. 381, pp. 284–287, 2004.

[55] F. J. Castro, V. Fuster, and G. Urretavizcaya, “Hydrogen sorption properties of a MgH_2-10wt.% graphite mixture,” *J. Alloys Compd.*, vol. 509, pp. S595–S598, 2011.

[56] M. Tliha, C. Khaldi, and N. E. Fenineche, “Kinetic and thermodynamic studies of hydrogen storage alloys as negative electrode materials for Ni/MH batteries: A review,” *J. solid state Electrochem.*, vol. 18, pp. 577–593, 2014.

[57] M. Tliha, C. Khaldi, and S. Boussami, “Kinetic and thermodynamic studies of hydrogen storage alloys as negative electrode materials for Ni/MH batteries: A review,” *J. solid state Electrochem.*, vol. 18, pp. 577–593, 2014.

[58] A. Martínez and D. S. Santos, “Influence of the substitution of V by Nb in the structure and properties of hydrogen absorption/desorption of $TiCr_{1.1}V_{0.9}$ alloy,” *J. Alloys Compd.*, vol. 536, pp. S231–S235, 2012.

[59] V. N. Verbetsky, S. V Mitrokhin, and E. A. Movlaev, “Intermetallic hydrides with high dissociation pressure,” *Mater. matters*, vol. 2, p. 9, 2007.

[60] P. Dantzer, “Properties of intermetallic compounds suitable for hydrogen storage applications,” *Mater. Sci. Eng.*, vol. 329, pp. 313–320, 2002.

[61] M. Zhu, Y. Lu, and H. Wang, “Thermodynamic Tuning of Mg-Based Hydrogen Storage Alloys: A Review,” *Materials (Basel).*, vol. 6, pp. 4654–4674, 2013.

[62] P. Vajeeston, A. Kjekshus, and M. Hanfland, “Structural stability and pressure-induced phase transitions in MgH_2,” *Phys. Rev.*, vol. 73, pp. 1–8, 2006.

[63] G. Barkhordarian, T. Klassen, and R. Bormann, “Kinetic investigation of the effect of milling time on the hydrogen sorption reaction of magnesium catalyzed with different Nb_2O_5 contents,” *J. Alloys Compd.*, vol. 407, pp. 249–255, 2006.

[64] “Hydriding kinetics of ball-milled nanocrystalline MgH_2 powders,” *J. Mater. Res.*, vol. 22, pp. 3144–3151, 2007.

[65] K. D. Modibane, M. Lototskyy, M. W. Davids, M. Williams, M. J. Hato, and K. M. Molapo, “Influence of co-milling with palladium black on hydrogen sorption performance and poisoning tolerance of surface modified AB5-type hydrogen storage alloy,” *J. Alloys Compd.*, vol. 750, pp. 523–529, 2018.

[66] T. Forde, J. P. Maehlen, V. A. Yartys, M. V Lototsky, and H. Uchida, “Influence of intrinsic hydrogenation/dehydrogenation kinetics on the dynamic behaviour of metal hydrides: A semi-empirical model and its verification,” *Int. J. Hydrogen Energy*, vol. 32, pp. 1041–1049, 2007.

[67] M. Avrami, “Kinetics of phase change,” *J. Chem. Phys.*, vol. 7, pp. 1103–1112, 1939.

[68] L. Guevara, R. Welsh, and M. A. Atwater, “Parametric Effects of Mechanical Alloying on Carbon Nanofiber Catalyst Production in the Ni-Cu System,” *Metals (Basel).*, vol. 8, p. 286, 2018.

[69] J. L. Iturbe-garcía, M. R. García-núñez, and B. E. López-muñoz, “Synthesis of the Mg_2Ni Alloy Prepared by Mechanical Alloying Using a High Energy Ball Mill,” *J. Mex. Chem. Soc.*, vol. 54, pp. 46–50, 2010.

[70] L. Zaluski, A. Zaluska, J. O. Strrm-olsen, and R. Schulz, “Catalytic effect of Pd on hydrogen absorption in mechanically alloyed Mg_2Ni , $LaNi_5$ and FeTi,” *J. Alloys Compd.*, vol. 217, pp. 295–300, 1995.

[71] S. Kumar, G. P. Tiwari, and N. Krishnamurthy, “High performance FeTi-3.1 mass% V alloy for on board hydrogen storage solution,” *Energy*, vol. 75, pp.

520–524, 2014.

[72] Y. Zhang, S. Xu, and D. Zhao, “Hydrogen storage kinetics of nanocrystalline and amorphous Cu−Nd-added Mg_2Ni-type alloys,” *Trans. Nonferrous Met. Soc. China*, vol. 24, pp. 3524–3533, 2014.

[73] Y. Zhang, W. Zhang, J. G. Z. Yuan, and W. B. Y. Qi, “A Comparison Study of Hydrogen Storage Thermodynamics and Kinetics of $YMg_{11}Ni$ Alloy Prepared by Melt Spinning and Ball Milling,” *Acta Metall. Sin.*, vol. 30, pp. 1040–1048, 2017.

[74] J. Liu, X. P. Song, and G. L. Chen, “Hydrogen storage performance of Mg-based composites prepared by spark plasma sintering,” *J. Alloys Compd.*, vol. 486, pp. 338–342, 2009.

[75] H. Becker, “Processing of bulk Al_70_{75} alloy by spark plasma sintering,” *Mater. Sci. Eng.*, vol. 179, p. 2050, 2017.

[76] C. Gosselin, D. S. Santos, and J. Huot, “First hydrogenation enhancement in TiFe alloys for hydrogen storage,” *J. Phys. D. Appl. Phys.*, vol. 50, p. 375303, 2017.

[77] S. Li, H. Cheng, and K. Yang, “Investigation of hydrogen absorption/desorption properties of $ZrMn_{0.85-x}Fe_{1+x}$ alloys,” *J. Alloys Compd.*, vol. 460, pp. 186–190, 2008.

[78] P. Muthukumar, A. Satheesh, and M. Groll, “Studies on hydriding kinetics of some La-based metal hydride alloys,” *Int. J. Hydrogen Energy*, vol. 34, pp. 7253–7262, 2009.

[79] V. Kumar, D. Pukazhselvan, and S. K. Singh, “Effect of Ni concentration on the stuctural and hydrogen storage characteristics of Zr-Mn based laves phase system,” *Mater. Renewables Sustain. Energy*, no. 02, p. 12, 2013.

[80] K. Manickam, D. M. Grant, and G. S. Walker, “Optimazation of AB_2 type alloy composition with superior hydrogen storage properties for stationary applications,” *Int. J. Hydrogen Energy*, vol. 40, pp. 16288–16296, 2015.

[81] T. Si, Y. Cao, and M. Zhu, “Enhanced hydrogen storage properties of a Mg-Ag

alloy with solid dissolution of indium: A comparative study," *J. Mater. Chem.*, vol. 3, pp. 8581–8589, 2015.

[82] K. D. Modibane, M. Williams, and M. Lototskyy, "Poisoning-tolerant metal hydride materials and their application for hydrogen separation from CO_2/CO containing gas mixtures," *Int. J. Hydrogen Energy*, vol. 38, pp. 9800–9810, 2013.

[83] K. F. Aguey-Zinsou, J. R. Ares Fernandez, and T. Klassen, "Effect of Nb_2O_5 on MgH_2 properties during mechanical milling," *Int. J. Hydrogen Energy*, vol. 32, pp. 221–233, 2007.

[84] M. Williams, A. N. Nechaev, and M. V. Lototskyy, "Influence of aminosilane surface functionalization of rare earth hydride-forming alloys on palladium treatment by electroless deposition and hydrogen sorption kinetics of composite materials," *Mater. Chem. Phys.*, vol. 115, pp. 136–141, 2009.

[85] K. L. Yeung, S. C. Christiansen, and A. Varma, "Palladium composite membranes by electroless plating technique Relationships between plating kinetics, film microstructure and membrane performance," *J. Memb. Sci.*, vol. 159, pp. 107–122, 1999.

[86] M. Ceramics, V. V Skorokhod, and V. P. Klimenko, "Reversable hydriding of $LaNi_{5-x}Al_x$−Pd composite in the presence of carbon monoxide," *Powder Metall. Met. Ceram.*, vol. 39, pp. 575–583, 2001.

[87] D. B. Willey, D. Pederzolli, and I. R. Harris, "Low temperature hydrogenation properties of platinum group metal treated, nickel metal hydride electrode alloy," *J. Alloys Compd.*, vol. 332, pp. 806–809, 2002.

[88] X. Shan, J. H. Payer, and W. D. Jennings, "Mechanism of increased performance and durability of Pd-treated metal hydriding alloys," *Int. J. Hydrogen Energy*, vol. 34, pp. 363–369, 2009.

[89] R. V Denys, M. V. Lototskyy, V. M. Linkov, and M. Williams, "Palladium mixed-metal surface-modified AB_5-type intermetallides enhance hydrogen sorption kinetics," *S. Afr. J. Sci.*, vol. 106, pp. 1–6, 2010.

[90] F.-J. Liu, “F-treatment effect on the initial activation characteristics of Mg-La-Ni amorphous alloys,” *J. Alloys Compd.*, vol. 231, pp. 696–701, 1995.

[91] B. Zhao, L. Liu, and P. Zhang, “Enhanced hydrogen capacity and absorption rate of $LaNi_{4.25}Al_{0.75}$ alloy in impure hydrogen by a combined approach of fluorination and palladium deposition,” *Int. J. Hydrogen Energy*, vol. 41, pp. 3465–3469, 2016.

[92] V. B. Parambhath, R. Nagar, and S. Ramaprabhu, “Effect of Nitrogen Doping on Hydrogen Storage Capacity of Palladium Decorated Graphene,” *Langmuir*, vol. 28, p. 7826−7833, 2012.

[93] M. Charbonnier, M. Romand, and Y. Goepfert, “Palladium reduction: A key step for the electroless Ni metallization of insulating substrates by a tin-free process,” *Thin Solid Films*, vol. 515, pp. 1623–1633, 2006.

[94] M. V Lototskyy, M. Williams, and V. A. Yartys, “Surface-modified advanced hydrogen storage alloys for hydrogen separation and purification,” *J. Alloys Compd.*, vol. 509, pp. 555–561, 2011.

[95] D. McCollum, N. Bauer, and K. Calvin, “Fossil resource and energy security dynamics in conventional and carbon-constrained worlds,” *Clim. Chang.*, vol. 123, pp. 413–426, 2014.

[96] A. B. Robinson, N. E. Robinson, and W. Soon, “Environmental Effects of Increased Atmospheric Carbon Dioxide,” *J. Am. physicians Surg.*, vol. 12, pp. 79–90, 2007.

[97] C. Dong, M. Ji, and H. Chen, “Reaction Mechanisms of CO_2 Reduction to Formaldehyde Catalyzed by Hourglass Ru, Fe, and Os Complexes: A Density Functional Theory Study,” *Catalysts*, vol. 7, p. 5, 2016.

[98] W. Lin, K. M. Stocker, and G. C. Schatz, “Reducing CO_2 to CO and H_2O on Ni(110): The In fluence of Subsurface Hydrogen,” *J. Phys. Chem.*, vol. 120, pp. 23061–23068, 2016.

[99] J. Bonin, A. Maurin, and M. Robert, “Molecular catalysis of the electrochemical and photochemical reduction of CO_2 with Fe and Co metal based complexes .

Recent advances," *Coord. Chem. Rev.*, vol. 334, pp. 184–198, 2017.

[100] F. Laurencelle, Z. Dehouche, and J. Goyette, "Hydrogen sorption cycling performance of $LaNi_{4.8}Sn_{0.2}$," *J. Alloys Compd.*, vol. 424, pp. 266–271, 2006.

[101] D. A. Lote, "Literature Survey on Electrochemical Reduction of CO_2," *Int. J. Electron. Electr. Eng.*, vol. 7, pp. 341–346, 2014.

[102] K. P. Brooks, J. Hu, and H. Zhu, "Methanation of carbon dioxide by hydrogen reduction using the Sabatier process in microchannel reactors," *Chem. Eng. Sci.*, vol. 62, pp. 1161–1170, 2007.

[103] Y. Zhao, Z. Zhang, and X. Qian, "Absorption of carbon dioxide by hydrogen donor under atmospheric pressure," *Renew. Sustain. Energy Rev.*, vol. 64, pp. 84–90, 2016.

[104] X. Su, J. Xu, and Y. Huang, "Catalytic carbon dioxide hydrogenation to methane: A review of recent studies," *J. Energy Chem.*, vol. 25, pp. 553–565, 2016.

[105] H. Ando, M. Fujiwara, and M. Tanaka, "Catalytic hydrogenation of carbon dioxide over $LaNi_5$ activated during the reaction," *J. Mol. Catal. A*, vol. 144, pp. 117–122, 1999.

[106] T. Shima and Z. Hou, "Rare Earth/d-Transition Metal Heteromultimetallic Polyhydride Complexes Based on Half-Sandwich Rare Earth Moieties," *Organometallics*, vol. 28, pp. 2244–2252, 2009.

[107] S. Kato, S. K. Matam, and M. Rohwerder, "The Origin of the Catalytic Activity of a Metal Hydride in CO_2 Reduction," *Angew. Chemie Int. Ed.*, vol. 55, pp. 1–6, 2016.

[108] T. Kaneko, F. Derbyshire, and E. Makino, "Partial oxidation of methane by pulsed corona discharges," *Encycl. Ind. Chem.*, vol. 7, pp. 688–692, 2005.

[109] X. Su, J. Xu, and Y. Huang, "Catalytic carbon dioxide hydrogenation to methane : A review of recent studies," *J. Energy Chem.*, vol. 25, pp. 553–565, 2016.

[110] J. Ren, M. Williams, and M. V Lototskyy, “Improved tolerance of Pd/Cu-treated metal hydride alloys towards air impurities,” *Int. J. Hydrogen Energy*, vol. 35, pp. 8626–8630, 2013.

[111] C. V Picasso, D. A. Safin, and Y. Filibcuk, “Reduction of CO_2 with KBH_4 in solvent-free conditions,” *Int. J. Hydrogen Energy*, vol. 41, pp. 14377–14386, 2016.

[112] Y. Zhao and Z. Zhang, “Thermodynamic properties of CO_2 conversion by sodium borohydride,” *Chem. Eng. Technol.*, vol. 38, pp. 110–116, 2015.

[113] M. Khandelwal and R. J. Wehmschulte, “Deoxygenative reduction of carbon dioxide to methane, toluene, and diphenylmethane with $[Et_2Al]+$ as catalys,” *Angew. Chemie Int. Ed.*, vol. 51, pp. 7323–7326, 2012.

[114] W. Sun, C. Qian, and L. He, “Heterogeneous reduction of carbon dioxide by hydride-terminated silicon nanocrystals,” *Nat. Commun.*, vol. 7, p. 12553, 2016.

[115] A. J. M. Miller, J. A. Labinger, and J. E. Bercaw, “Trialkylborane-Assisted CO_2 Reduction by Late Transition Metal Hydrides,” *Organometallics*, vol. 30, pp. 4308–4314, 2011.

[116] J. L. Inglis, B. J. MacLean, and M. T. Pryce, “Electrocatalytic pathways towards sustainable fuel production from water and CO_2,” *Coord. Chem. Rev.*, vol. 256, pp. 2571–2600, 2012.

[117] L. M. Kustov and A. L. Tarasov, “Hydrogenation of carbon dioxide: a comparison of different types of active catalysts,” *Ital. Oral Surg.*, vol. 24, pp. 349–350, 2014.

[118] H. Muroyama, Y. Tsuda, and T. Matsui, “Carbon dioxide methanation over Ni catalysts supported on various metal oxides,” *J. Catal.*, vol. 343, pp. 178–184, 2016.

[119] P. Adeniyi, A. Abbas, and W. Daud, “Insight into catalytic reduction of CO_2: Catalysis and reactor design,” *J. Clean. Prod.*, vol. 140, pp. 1298–1312, 2017.

[120] J. S. Kim, H. K. Kim, and S. B. Lee, “Characteristics of carbon dioxide

hydrogenation in a fluidized bed reactor," *Korean J. Chem. Eng.*, vol. 18, pp. 463–467, 2001.

[121] "Towards full one-pass conversion of carbon dioxide to methanol and methanol-derived products," *J. Catal.*, vol. 309, pp. 66–70, 2015.

[122] L. Li, D. Mao, and J. Yu, "Highly selective hydrogenation of CO_2 to methanol over CuO-ZnO-ZrO_2 catalysts prepared by a surfactant-assisted coprecipitation method," *J. Power Sources*, vol. 279, pp. 394–404, 2015.

[123] K. P. Brooks, J. Hu, and H. Zhu, "Methanation of carbon dioxide by hydrogen reduction using the Sabatier process in microchannel reactors," *Chem. Eng. Sci.*, vol. 62, pp. 1161–1170, 2007.

CHAPTER 3

CHARACTERISATION TECHNIQUES

SUMMARY

Any scientific investigation should be monitored by suitable and adequate characterisation techniques that are able to detect any alternation and addition of new materials. As such, different characterisation techniques were used in this study and Chapter 3 discusses in detail their literature review. Moreover, the chapter outlines how the techniques operate and the operation conditions used in this particular study are also discussed. In summary, techniques that are discussed herein include:

- X-ray diffraction spectroscopy (XRD) technique, which is used in this study for phase identification of unmodified metal alloys and to monitor the effect of Pd deposition on the structure of parent alloy materials.
- Scanning electron microscopy (SEM), for alloy particle size/shape; alloy particle size distribution; Pd particle dispersion on the surface of alloy particles; Pd particle size/shape; and Pd particle size distribution.
- Energy dispersive spectroscopy (EDS) and Atomic absorption spectroscopy (AAS) techniques for qualitative and quantitative determination of elemental composition of the substrate materials along with determination of the total elemental content of the deposited Pd metal layer on alloy materials as a function of unit weight of the surface-modified sample.
- Brunauer, Emmett and Teller (BET) for evaluation of physisorption properties of the unmodified and surface modified materials.
- Sieverts-type apparatus to study the maximum hydrogen absorption uptake as well as hydrogenation kinetics of Pd-modified and unmodified alloy materials.

3.1. INTRODUCTION

Fast kinetics and improved hydrogen sorption properties of AB_2-type and AB_5-type alloys depends on the elemental composition, porosity and surface area, surface morphology and phase composition/crystal structure. Therefore, alteration of these factors may influence the performance of the alloy during hydrogenation either positively or negatively. Thus, an array of characterisation methods was conducted to determine the effect of the above-mentioned factors on the properties of AB_2-type and AB_5-type alloys. X-ray diffraction spectroscopy can be used to track any structural and phase composition alterations taking place in a material through the interaction of monochromatic X-rays with the alloy materials. Another useful characterisation technique is scanning electron microscopy, which can provide us with elemental and composition changes; external morphology and orientation of materials. Particle size distribution can be determined from images resulting from this type of microscopy. Scanning electron microscopy works hand-in-hand with energy dispersive spectroscopy. The role of energy dispersive spectroscopy is to quantitatively determine elemental composition of the substrate materials. While energy dispersive spectroscopy deals with quantitative analysis of materials, atomic absorption spectroscopy provides qualitative measurements of elements in a material of interest. Physisorption properties (surface area, pore volume and pore size) of sample materials can be obtained using Brunauer, Emmett and Teller instrument. To fluently study the hydrogenation behaviour of solid-state hydrogen absorbing materials (AB_2-type and AB_5-type alloys), Sieverts-type apparatus is used to provide information on maximum hydrogen absorption capacity as well as kinetic and thermodynamic properties of such materials. More details, including operations, on all these six techniques are discussed in this chapter.

3.2. X-ray diffraction spectroscopy (XRD)

X-ray diffraction is a rapid analytical technique primarily used for phase identification of a crystalline material and can provide information on unit cell dimensions. XRD occurs when the atomic planes of a crystal cause an incident beam of X-rays to interfere with one another as they leave the crystal [1]. Furthermore, XRD is based on constructive interference of monochromatic X-rays and a crystalline sample, in which the X-rays are generated by a cathode ray tube, filtered to produce monochromatic radiation, collimated to concentrate and directed toward the sample. The interaction of the incident rays with the sample produces constructive interference (and a diffracted ray) when conditions satisfy Bragg's Law ($n\lambda=2d\sin\theta$, where the variable *d* is the distance between atomic layers in a crystal and the variable lambda λ is the wavelength of the incident X-ray beam; n is an integer) [2]. This law was developed in 1913 to explain why the cleavage faces of crystals appear to reflect X-ray beams at certain angles of incidence (theta, θ). It relates the wavelength of electromagnetic radiation to the diffraction angle and the lattice spacing in a crystalline sample [3]. It was further shown that the X- ray waves reveal the atomic structure of crystals and then diffraction occurs only when Bragg's Law is satisfied condition for constructive interference (X-rays 1 & 2) from planes with spacing d [2, 3]. The diffracted X-rays are then detected, processed and counted in the XRD instrument. By scanning the sample through a range of 2θ angles, all possible diffraction directions of the lattice should be attained due to the random orientation of the powdered material [1].

For the purpose of this study, XRD was used to evaluate the crystal/atomic structure and the identification of phases of alloy materials used. Structural changes that may arise upon element substitution and Pd deposition were also monitored using XRD.

In the XRD analysis, dry surface-modified and unmodified alloy samples were mounted in plastic sample holders and the surface was flattened to promote maximum x-rays exposure. Experimental parameters for the XRD analysis are given as follows:

X-ray Diffractometer: Bruker AXS D8 Advance

Detector:	Sodium Iodide
Monochromator:	Graphite
Generator current (mA):	40
Electron Intensity (keV):	40
X-ray source:	Cu-K; α_1= 1.540598 Å, α_2= 1.544426 Å,
	α_1/α_2= 0.497
Scan range (2θ °):	5-100
Scan rate (°/min):	0.05

The XRD patterns of Pd-modified alloys were processed using Powder Cell software to assess formation new phases or disappearance of parent alloy phases. Moreover, Scherrer formula was employed to validate the crystallite sizes of different alloy materials. Scherrer formula is given as $\tau = (\kappa\lambda) \,/\, \beta\cos(\theta)$,

Where τ is the crystallite size nm, λ is the wave length (=0.154 nm for Cu-Kα), β is the full width at half-maximum (FWHM) (in radians), k is a constant (0.94 to spherical crystallites) and θ is the diffraction angle.

3.3. Scanning electron microscopy (SEM)

SEM is a technique used for morphological analysis by producing a largely magnified image using electrons instead of light to form an image. It uses a focused beam of high-energy electrons to generate a variety of signals at the surface of solid specimens as a result of electron-sample interactions. The signals reveal information about the sample including external morphology (texture), chemical composition, crystalline structure and orientation of materials making up the sample [4]. SEM instrument comprises of two main parts: an electron column, and an electron detector. The electron beam is generated in the electron column by an electron cathode, which is then collimated by electromagnetic condenser lenses, focused by an objective lens and finally restored across the sample surface by the scanning

coils. The specimen emits the secondary electrons and backscattered electrons at the irradiated spot of the primary electron beam and they are collected by the detector and formed the specimen image in the microscope [5]. In principle, accelerated electrons in a SEM instrument carry significant amounts of kinetic energy and this energy is dissipated as a variety of signals produced by electron-sample interactions when the incident electrons are decelerated in the solid sample. The signals produced include secondary electrons, primary backscattered electrons, X-rays and Auger electrons. It was also indicated that visible light and heat signal are produced by electron-sample interactions [6].

In this study, high-resolution scanning electron microscopy (HRSEM) was used in the study of AB_2 and AB_5-type alloy particle size/shape; alloy particle size distribution; Pd particle dispersion on the surface of the AB_2 and AB_5-type alloy particles; Pd particle size/shape; and Pd particle size distribution. Particle size distribution histograms were constructed by measuring the particle sizes observed on SEM images of all the unmodified and Pd-modified alloy materials.

The alloy powders of interest were supported on double-sided conductive carbon tape and mounted onto aluminium sample stubs. Carbon sputtering was required wherever fluorination was performed to make the corresponding materials electron-conductive (Agar Turbo Carbon Coater; 8 seconds; 2.0 kV; 150 mA). Cross-sections of the surface-modified materials were prepared by dispersing alloy particles in a cold-mounting resin (Struers Epofix). Air was removed from the mixture using a vacuum installation (Struers Epovac). The mixture was allowed to cure overnight and was mechanically polished using 1200-grit (3.0 μm) silicon carbide paper and a polishing wheel (Struers Knuth Rotor). The sample was subsequently ion-etched (Ion Tech Ltd.; 4.0 mA; 4.0 kV; 15°; 4.0 bar Ar) and carbon coated (Agar Turbo Carbon Coater; 8 seconds; 2.0 kV; 150 mA). Ion-etching was used to remove mechanically-induced surface roughness, as a result of the polishing process, which may result in image degradation, thereby enhancing topographical contrast [7]. Carbon coating (resistivity - 3500 $\mu\Omega.cm^{-1}$ at 20°C) enhanced the electrical conductivity of the sample surface which was primarily insulating as a result of the cold-mounting resin, thereby improving topographical contrast, stabilizing the surface structure, and preventing electrostatic charging.

The description and experimental parameters of a microscope used in this study are given below:

SEM - Hitachi X-650 EM; working distance = 15 mm; accelerating voltage = 25 kV; emission current = 75-80 μA (University of the Western Cape). The electron gun of the microscope was also used as the electron source for EDS elemental studies of the surface-modified and unmodified materials.

3.4. Energy dispersive spectroscopy (EDS)

The Energy Dispersive X-ray Spectroscopy (EDS or EDX) is an analytical tool used for elemental composition of small objects or surfaces of a sample. The EDS setup has four primary components; the excitation source (electron beam or x-ray beam); X-ray detector; pulse processor and analyzer. These components work together from electron beam excitation used in mictroscopes to X-ray emission, which is converted X-ray energy into voltage signals using detector. Therefore, this information is sent to a pulse processor, which measures the signals and passes them onto an analyzer for data display and analysis [8]. The EDS relies on the investigation of an interaction of some source of X-ray excitation and a sample. The sample bombarded with a focused beam of electrons emits the X-ray spectrum. The EDS makes use of this spectrum to obtain a localized chemical analysis. It was shown that each element has a unique atomic structure allowing unique set of peaks on its X-ray spectrum [4]. Qualitative analysis of elemental composition in EDS involves the identification of the lines in the spectrum and is fairly straightforward owing to the simplicity of X-ray spectra. The basic principle in EDS is when an atom in an inner shell is excited by the incident beam, creating an electron hole and the electron from an outer, higher-energy shell then fills the hole. The electrons in the excited state may be released in the form of an X-ray and the number and energy of the X-rays emitted from a specimen can be measured by an energy-dispersive spectrometer [9].

In this study, EDS analysis was conducted for determination of elemental composition of the substrate materials and compare with the targeted composition. In addition, EDS was used in the quantitative determination of the surface loading of

deposited metal (Palladium), as a function of the preparation history of the sample materials.

Samples were dispersed on double-sided conductive carbon tape, which in turn was adhered to aluminium sample stubs. Analysis of the surface metal loading was conducted using an EDAX Genesis spectrometer (baseline - 1500 counts-per-second, time - 100 live seconds) coupled to a Hitachi X-650 EM electron microscope (working distance - 15 mm; accelerating voltage - 25 kV; emission current - 60 μA; amperage time – 100 μs).

3.5. Atomic absorption spectroscopy (AAS)

AAS is a spectro-analytical technique that involves qualitative and quantitative analyses of elemental content of sample materials by using absorption of mono-energetic radiation by gaseous free atoms [10]. The detection limits of the AAS technique are in the low ppm domain depending on the analyte element of interest. The principle of the technique is based on the Beer-Lamberts law (i.e. $A = \varepsilon \ell C$), which relates the absorption of light by a sample material to its chemical properties. The law states a logarithmic dependence of the elemental concentration (C) to the absorbance of the sample (A), the path length that the characteristic light travels through the sample (ℓ), and the absorption coefficient or molar absorptivity (ε) of the sample [11]. In AAS solvated metals are aspirated by a pneumatic nebulizer into either a flame, plasma, or a heated element (e.g. graphite furnace), typically at 3-6 $mL.min^{-1}$. The solvent is vaporised, the particles volatilized, and the gaseous molecules are dissociated into a free atom aerosol [10]. A beam of light with a characteristic wavelength is then passed through the aerosol. Atoms corresponding to the atomic composition of the light source (i.e. hollow cathode lamp) are excited and will absorb light of the characteristic wavelength. The amount of light, and the difference in the light intensity before and after passing through the atomized metal, is monitored by a photomultiplier tube. The difference in the light intensity is then related to the absorbance of the sample material. By careful construction of a calibration curve using standard solutions the absorbance of the sample material can be related to the concentration of the metal of interest in the sample solution.

In this study, AAS was used in the determination of the total elemental content of the deposited Pd metal layer on alloy materials as a function of unit weight of the surface-modified sample. Prior to analyses, the sample solutions were prepared by acid digestion of 1.0g of the surface-modified materials in 50 mL *aqua regia* solution (1 part HNO_3 per 3 parts HCl) at 50°C for 30 minutes and 300 rpm. The *aqua regia* solution formed the highly reactive NOCl species which completely decomposed all components of the sample materials [12]. The digestion was conducted under reflux conditions by inclusion of a condenser to minimise loss of the analyte metal. The solutions were allowed to cool to room temperature, were gravity-filtered, and made up to 100 mL using ultrapure water.

Calibration standard solutions were all freshly prepared in ultrapure water. A minimum of five standards were prepared with the range depending on the sensitivity of the instrument towards the analyte. The concentration of the sample solutions were determined by interpolation from the calibration curves. To confirm the accuracy of the collected analytical data the calibration standard solutions were re-measured after every fifth analysis of the sample solutions and once again after the completion of analysis of all the sample solutions. A blank solution (i.e. *aqua regia* and ultrapure water) was measured directly after the calibration standards to rule out contributions from the solvent and in that way ensure the stability of the analytical baseline. Five measurements were collected for each sample solution to ensure precision in the average absorbance reported.

3.6. Brunauer, Emmett and Teller (BET)

BET method is widely used in solid surface science to explain the physical adsorption of gas molecules on a solid surface. It serves as the basis for an important analysis technique for estimation of the specific surface area of a material [13]. The concept of the BET theory is an extension of the Langmuir theory, which is a theory for monolayer molecular adsorption, to multilayer adsorption with the following hypotheses: (a) gas molecules physically adsorb on a solid in layers infinitely; (b) there is no interaction between each adsorption layer; and (c) the Langmuir theory can be applied to each layer [14]. In BET system, the sample in a

solid is placed in an evacuated sample holder at constant temperature and filled with helium to flush contaminating gases from the sample surface and pores. The helium is then purged from the system and followed by cooling evacuated samples to -196 ^{O}C in a liquid N_2 bath while the sample holder is filled with high-purity N_2 gas. The system monitors the N_2 pressure within the sample holder over time and then pressure is rapidly reduced to reach an equilibrium state. In this case, the quantity of gas adsorbed onto the surface is equivalent to the quantity of gas removed from the gas phase. The adsorption isotherm is obtained by plotting the quantity of N_2 adsorbed versus the equilibrium pressure [13, 14].

This technique was used in this work to evaluate physisorption properties (surface area, pore volume and pore size) of the unmodified and surface modified AB_2 and AB_5 metal hydride-forming materials. BET curves were also used to classify the alloy materials as either type 1 or type 2 isotherm group, based on shapes of the Nitrogen uptake curves.

The specific surface area of the unmodified and surface-modified materials was determined using a porosity and surface area analyser (Micromeritics Tristar). The surface area analyser consisted of a mercury manometer; gas-tight burette, thermostat; liquid N_2-cooled Dewar flask, and a high-vacuum rotary pump. High pressures and cryogenic temperatures were used to increase the adsorption rate onto solid surfaces [15].

3.7. Volumetric method/Sievert's method

Volumetric technique or Sievert's method is the most versatile and direct method for measurement of hydrogen storage capacity in MH materials. Hydrogen absorb or desorb from the sample material is deduced by measuring pressure changes in a known, reference volume held at a fixed temperature, remote from the sample. Hydrogen storage over a wide range of sample temperatures and pressures can be measured by employing a wide range of pressure transducers and appropriate gas handling materials [16]. The Sieverts' apparatus is a gas manifold with a series of tubes and valves connecting the sample reactor to one or more gas reservoirs of

known volume, and pressure transducers for measuring reservoir pressure. Because the volumetric technique measures concentration indirectly through temperature-pressure-volume correlations, the volumes and temperatures of the reservoirs and sample holder (system) must be known in advance [16]. A typical measurement consists of a series of steps: (1) sample chamber and bring the sample to desired temperature. (2) Close the valve between the sample and reservoir and introduce gas into the reservoir to bring it to the pressure of interest, (3) open the valve between the sample and reservoir, and observe reservoir pressure change [17]. The system volumes in sieverts instrument are carefully pre-calibrated, the reservoir and sample holder are maintained at constant (but not necessarily equal) temperatures using an external temperature controller. By fixing volume and temperature, reservoir and sample holder pressures can be measured using pressure transducers to provide isothermal pressure-concentration data. The H_2 sorption kinetics release can be measured by monitoring the change in reservoir pressure versus time. Sieverts technique can also be used to determine pressure–composition isotherm by repeating the measurement at different pressures at a fixed temperature [17].

In this study, Sieverts-type apparatus were used to study the maximum hydrogen absorption uptake as well as hydrogenation kinetics of Pd-modified and unmodified alloy materials. The construction of hydriding kinetic curves was conducted using a Sieverts-type volumetric installation (South African Institute for Advanced Material Chemistry, SAIAMC). The installation conducted precise volumetric measurements of quantities of hydrogen absorbed by hydrogen sorption materials. The procedure consists of determining the quantity of hydrogen absorbed by the material at systematically varied equilibrium pressures at a fixed temperature, and after thermal activation in vacuum. The installation consists of gas distribution, control, and measurement systems. The pressure within the system was monitored using 30 bar absolute pressure transducer. 1.00 g of alloy powder was loaded into the reactor housing and activated by heating to 300 ˚C in a muffle furnace in vacuum better than 1.0×10^{-5} mbar for 90 minutes, followed by hydrogenation (99.999% H_2) at room temperature and initial pressure of 30 bar.

Subsequently, the experimental results obtained from Sievert-type apparatus were processed by application of formal kinetic analysis, using the Avrami-Erofeev Equation [18]:

$$\left(\frac{H}{AB5}\right) = \left(\frac{H}{AB5}\right)_{\max} - \left\{1 - \exp\left(-\left(\frac{t}{t_0}\right)^n\right)\right\} \quad 3.1$$

Where (H/AB_5) is the actual hydrogen concentration in the alloy; $(H/AB_5)_{max}$ is the maximum hydrogen concentration in the alloy; t is time; t_0 is the characteristic time of hydrogen absorption (reciprocal rate constant k); and the index of power, n, is interpreted as a value indirectly connected to the reaction mechanism.

3.8. CONCLUSION

In summary, six characterisation techniques were reviewed in this chapter with detailed discussions for their different applications. The chapter further discussed the principle behind characterisation techniques which are selected for the current study in order to understand different factors including elemental composition, porosity and surface area, surface morphology, phase composition/crystal structure and hydrogen absorption associated with unmodified and Pd-modified AB_2-type and AB_5-type alloys. The XRD was detailed to help with the confirmation major and minor phases present in each alloy material; and their crystal properties. This technique was adopted in this work to evaluate the crystal/atomic structure and the identification of phases of alloy materials used. Structural changes that may arise upon element substitution and Pd deposition were also monitored using XRD. Surface morphology was highlighted to be a vital factor in hydrogenation behaviour of alloy materials. In this regard, SEM technique was identified as a suitable surface technique to give the insight of particle size distribution of particles occupying alloy materials. In parallel to SEM analyses, EDS and AAS techniques can be also employed to quantitatively and qualitatively determine the elemental composition for each material. From the literature, it is learned that physisorption properties (surface area, pore volume and pore size) are of paramount important for adsorption behaviour of any alloy material, hence, BET was reviewed and showed to be suitable technique for physisorption properties investigation. Based on simplicity and supply of high purity hydrogen by Sieverts-type apparatus, it was selected to be a powerful technique in this work in order to study the hydrogenation kinetics and capacity of unmodified and Pd-modified alloy materials.

3.9. REFERENCES

[1] M. Chen, X. Wang, and L. S. Wen, “X-ray photoelectron spectroscopy and auger electron spectroscopy studies of Al-doped ZnO films,” *Appl. Surf. Sci.*, vol. 158, pp. 134–140, 2000.

[2] N. Iwashita, H. Fujimoto, and M. Inagaki, “Specification for a standard procedure of X-ray diffraction measurements on carbon materials,” *Carbon N. Y.*, vol. 42, pp. 701–714, 2004.

[3] L. Ebdon, E. H. Evans, and A. Fisher, *An introduction to analytical atomic spectrometry*. Elsevier Ltd, 2017.

[4] A. Khursheed, “Scanning electron microscope,” *US Pat.*, vol. 7, p. 294, 2007.

[5] J. I. Goldstein, D. E. Newbusy, and J. R. Michael, *Scanning electron microscopy and X-ray microanalysis*. Springer, 2017.

[6] K. C. A. Smith and C. W. Oatley, “The scanning electron microscope and its fields of application,” *Br. J. Appl. Phys.*, vol. 6, pp. 391–399, 1995.

[7] A. W. Robards and A. J. Wilson, *Procedures in Electron Microcopy*. John Wiley & Sons Ltd.: Chichester, 1993.

[8] P. Willich, A. P. von Rosenstiel, and N. Drost, "Quantitative Electron Probe Microanalysis," *Progress in materials analysis*, vol. 1, pp. 211-216, 2013.

[9] D. Vaughan, *Energy-dispersive X-ray microanalysis: an introduction*. Kevex Instruments Publication, 1989.

[10] J. W. Robinson, “Atomic absorption spectroscopy,” *Anal. Chem.*, vol. 32, p. 17A–29A, 1960.

[11] L. H. J. Lajunen, “Spectrochemical Analysis by Atomic Absorption and Emission,” *R. Soc. Chem.*, vol. 2, pp. 45–48, 1992.

[12] J. R. Dean, *Atomic Absorption and Plasma Spectroscopy*. John Wiley Sons, 1997.

[13] S. Brunauer, P. H. Emmett, and E. Teller, “Adsorption of gases in multimolecular layers,” *J. Am. Chem. Soc.*, vol. 60, pp. 309–319, 1938.

[14] J. J. Fripiat, L. Gatineau, and H. Van Damme, “Multilayer physical adsorption on fractal surfaces,” *Langmuir*, vol. 2, pp. 562–567, 1986.

[15] P. A. Webb, C. Orr, and R. W. Camp, *Analytical Methods in Fine Particle Technology*. Micromeritics Instrument corp, 1997.

[16] T. P. Blach, E. Mac, and A. Gray, “Sieverts apparatus and methodology for accurate determination of hydrogen uptake by light-atom hosts,” *J. Alloys Compd.*, vol. 446, pp. 692–697, 2007.

[17] E. Poirier, R. Chahine, and A. Tessier, “Gravimetric and volumetric approaches adapted for hydrogen measurements with in situ conditioning on small sorbent samples,” *Rev. Sci. Instrum.*, vol. 76, pp. 55–101, 2005.

[18] K. D. Modibane, M. Lototskyy, M. W. Davids, M. Williams, M. J. Hato, and K. M. Molapo, “Influence of co-milling with palladium black on hydrogen sorption performance and poisoning tolerance of surface modified AB_5-type hydrogen storage alloy,” *J. Alloys Compd.*, vol. 750, pp. 523–529, 2018.

CHAPTER 4

EFFECT OF PARTIAL SUBSTITUTION OF NICKEL WITH TIN FOLLOWED BY AUTOCATALYTIC PALLADIUM DEPOSITION ON THE HYDROGEN ABSORPTION KINETICS OF $LANI_5$-TYPE METAL HYDRIDE ALLOY

T. R. Somo[a], M. W. Davids[b], K. D. Modibane[a], M. J. Hato[a], M. V. Lototskyy[*,b]

[a]Department of Chemistry, School of Physical and Mineral Sciences, University of Limpopo (Turfloop), Polokwane, Sovenga 0727, South Africa.

[b]HySA System, South African Institute for Advanced Material Chemistry, University of the Western Cape, Bellville 7535, Cape Town, South Africa

*Corresponding Author.

E-mail address: mlototskyy@uwc.ac.za

SUMMARY

Hydrogen absorption performances of $LaNi_5$ alloy are sensitive to the surface reactions with poisonous gases such as oxygen, readily forming oxides/ hydroxides. This work reports the studies on the hydrogen absorption behaviour of AB_5-type hydrogen storage alloys, formed by $LaNi_{(5-x)}Sn_x$ (X=0.2) followed by electroless Pd deposition. The uncoated and Pd-coated materials were characterised using scanning electron microscopy/energy dispersive spectroscopy (SEM/EDS), atomic absorption spectroscopy (AAS), X-ray diffraction (XRD) and Brunauer-Emmet-Teller (BET). XRD analyses indicated that both $LaNi_5$ and $LaNi4_{.8}Sn_{0.2}$ alloys contain $CaCu_5$ as the major phase while their SEM images together with particle size distribution histograms showed increment of particle size upon Sn incorporation. It was further observed from the BET results that autocatalytic deposition of palladium decreases surface areas but increases the pore areas of the parent materials. Palladium particles on the surface of the materials were detected by AAS and EDS analyses. Furthermore, substitution of a small fraction of Ni by Sn leads to an increase in hydrogen absorption capacity even without activation. Moreover, a decrease in hydrogen absorption rate was observed for $LaNi_{4.8}Sn_{0.2}$ alloy and this was related to an increment of the crystalline unit cell volume, however, the absorption rate was enhanced after activation. Kinetic curves of Pd coated alloys show a significant increase of the absorption kinetics due to the presence of Pd nanoparticles which are known to have higher affinity for hydrogen. The results showed that the partial substitution of Ni by Sn followed by Pd deposition offers potential technology for improvement of AB_5-type alloys as catalysts in metal hydride technology for carbon dioxide conversion.

Keywords: hydrogen storage materials, energy storage materials, AB_5 alloy, palladium deposition

4.1. INTRODUCTION

Hydrogen gas plays an important role in reduction of carbon dioxide to hydrocarbons [1]. However, lack of feasible methods to store hydrogen in a safe and compact way is one of the main drawbacks in hydrogen technology [2]. The simplest way is to store hydrogen in solid absorbents such as metal alloys in which hydrogen bound to these materials to form metal hydrides [3]. Metal hydrides (MH) bring along the advantages such as higher gravimetric (18 mass %) and volumetric density (150 $kg \cdot m^{-3}$); and higher stability compared to hydrogen storage in gaseous or liquid form [4]. The most interesting class of hydride-forming materials is the AB_5-type metal hydride material due to its advantages such as easy activation, moderate plateau pressure and high hydrogen capacity at room temperature [5]. For example, inactivated $LaNi_5H_6$ has a volumetric capacity of $5.5x10^{22}$ atoms/cm^3 and gravimetric capacity of 1.4 wt.% at ambient temperature [4]. However, the difficulties in initial activation and slow hydriding/dehydriding kinetics are among the drawbacks that prohibit the use of the AB_5 materials as hydrogen sorbents in order to work as catalysts in carbon dioxide conversion to hydrocarbons [6]. Moreover, Modibane *et al.* [7] observed that during the hydrogen separation from CO_2/CO containing gas mixtures over the AB_5 materials $(La(Ni,Co,Mn,Al)_5$ substrate), a mixture of hydrocarbons was produced due to the reaction between desorbed hydrogen atoms and CO_2. This observation is a clear indication that the amount of hydrogen absorbed on an alloy material and the rate at which it is desorbed are very important factors to consider during CO_2 conversion over AB_5 alloys. In addition, MH performances during hydrogen absorption are often limited due to formation of surface compounds (oxides and hydroxides, carbonyls, sulphides) [7]. Methods such as spark plasma sintering [8], mechanical alloying [9], melt spinning [10], high hydrogen pressure method [11], hydriding combustion synthesis [12], surface modification (such as autocatalytic deposition of palladium) [13, 14] and alloying with other elements (Substitution of B-component in AB_5) [15] have been widely studied for improvement of hydrogen absorption kinetics of metal hydrides from gas mixture. Modibane *et al*. [16] demonstrated the improvement of poisoning tolerance and hydrogen absorption using palladium black addition on AB_5 alloy followed by electroless Pd deposition. Furthermore, the previously reported high chemical

activity of H atoms released from MH [17] during H_2 separation process enables them to freely interact with traces of oxygen in the feed gas to yield H_2O, and with CO_2 (and, most probably, CO) to yield H_2O + hydrocarbons. The combination of partial substitution of Ni and Pd deposition is extremely active towards dissociative hydrogen chemisorption and permeable for hydrogen atoms, which enable hydrogen to rapidly adsorb onto the bulk material while still maintaining the hydrogenation activity even after exposure to poisonous gaseous environment [18]. In addition, autocatalytic deposition of palladium can also result in improvement of surface catalytic activity, specific surface area layer, activation characteristics as well as protective nature of metal hydrides against poisoning materials [19]. Due to its amorphous nature, the sodium hypophosphite-based electroless plating bath that is used during palladium deposition may also improve the hydrogen capacity of the materials since it is documented that amorphous materials can take and release large amount of hydrogen compared to their polycrystalline counterparts [20]. Phosphorous is impregnated into the Pd layer and promotes the formation of amorphous electroless-deposited metal coatings [20, 21].

Therefore, this study reports on the effects of partial substitution of Ni by Sn in $LaNi_5$ alloy followed by autocatalytic deposition of Pd on hydrogen adsorption kinetics for potential carbon dioxide reduction. Tin is also known to enhance the hydrogen capacity and sorption rate of $LaNi_5$ alloy since it has advanced electron attractive power and bigger active sites than that of nickel, similar results were reported by Sato *et al*. [22]. Combining the merits of Ni(Sn) in $LaNi_{4.8}Sn_{0.2}$ alloy and poisoning tolerance of Pd coated alloy, Pd-coated $LaNi_{4.8}Sn_{0.2}$ alloy was prepared in this contribution through simple arc melting method followed by autocatalytic Pd plating. This work can provide further insights into the properties of metal hydride hydrogen storage material after pre-exposure to air. To our knowledge, the preparation of Pd-$LaNi_{4.8}Sn_{0.2}$ alloy for hydrogen absorption kinetics has not been reported to date and in this work it showed significant activity in hydrogen absorption kinetics after pre-exposure to air as compared to unmodified AB_5 alloy. Success in enhancement of hydrogen absorption kinetics of this alloy may open doors for alternative pathways to carbon dioxide conversion into hydrocarbons since $LaNi_5$ has been reported to decompose into $La(OH)_3$, $LaCO_3OH$, and metallic nickel during CO_2 conversion [23].

4.2. EXPERIMENTAL METHODS

4.2.1. Materials

The AB_5-type ($LaNi_5$ and $LaNi_{4.8}Sn_{0.2}$) hydride-forming alloys were prepared from La (99.9%), Ni (99.95%) and Sn (99.98%) purchased from Sigma Aldrich. The AB_5 hydride forming alloy was prepared by arc-melting on a water-cooled copper crucible in protective argon atmosphere. All prepared ingots were melted three times to provide homogeneity. Subsequently, the prepared metal ingots were pulverised by ball-milling in argon for 10 min. The materials were allowed constant exposure to air throughout the experimental studies.

4.2.2. Surface modification of alloy

Surface modification of the substrate materials was conducted through autocatalytic deposition of Pd in hypophosphite-based bath following a procedure described here [20]. The rationale behind this approach was the combination of the enhanced activation kinetics observed with deposition of Pd catalytic layers and to form materials with excellent hydrogen sorption properties. The autocatalytic deposition of Pd was applied to ~5 g batch of each substrate ($LaNi_5$ and $LaNi_{4.8}Sn_{0.2}$ alloys). Prior to palladium deposition, the materials were first sensitized and activated in a palladium-tin (Pd-Sn) colloidal solution [20] resulting in increased densities of Pd deposition and surface Pd loading on the intermetallide.

4.2.3. Characterisation Techniques

X-ray diffraction (XRD) studies of the alloys were performed using a Bruker Advance powder diffractometer (Madison, USA; 40 mA, 40 keV, λCu-K = 0.15406 nm) at the Materials Research Group, iThemba Labs, in Cape Town, South Africa for phase identification. Scanning electron microscopes/Energy-dispersive spectroscopy (SEM/EDS, Edax Genesis, 100 live seconds) studies were carried out using Leo

1450 microscope (20 kV, secondary electrons), Physics department, University of the Western Cape (UWC) to evaluate the morphology of AB_5-type alloy particle size/shape; Pd particle dispersion on the surface of the AB_5-type alloy particles and Pd particle size/shape. The elemental analysis was determined using a Perkin Elmer AAnalyst 400 atomic absorption spectrometer (AAS) to ascertain the quantity of palladium deposited on the surface of the materials. A Tristar micromeritics instrument was used for low-pressure nitrogen (77 K) adsorption/desorption isotherms, BET surface area and pore volume measurements. Approximately, 0.5 g of alloy was de-gassed by heating to 180 °C under N_2 flow for 24 hours. The BET measurements were used to evaluate the effect of Pd deposition on the surface area and pore volume of the parent AB_5 materials.

The effect of partial substitution of nickel by tin followed by autocatalytic palladium deposition on the kinetics of hydrogen absorption was studied by a comparison of hydrogen absorption before (after pre-exposure to air) and after activation by evacuation and heating at 300 ˚C. Evacuation and heating prevented the possibility of the presence of residual oxygen on the surface of the alloy. Hydrogen absorption was conducted using a Sieverts-type volumetric installation, South African Institute for Advanced Material Chemistry (SAIAMC), UWC. The measurements were carried out at T = 20 ˚C, P_0 ~ 30 bar H_2, for 2 hours. The experimental results were processed by application of formal kinetic analysis, using the Avrami-Erofeev Equation [16]:

$$\left(\frac{H}{AB5}\right) = \left(\frac{H}{AB5}\right)_{\max} - \left\{1 - \exp\left(-\left(\frac{t}{t_0}\right)^n\right)\right\} \qquad 4.1$$

Where (H/AB_5) is the actual hydrogen concentration in the alloy; $(H/AB_5)_{max}$ is the maximum hydrogen concentration in the alloy; t is time; t_0 is the characteristic time of hydrogen absorption (reciprocal rate constant k); and the index of power, n, is interpreted as a value indirectly connected to the reaction mechanism.

4.3. RESULTS AND DISCUSSION

4.3.1. Structural Characterisation

The as-prepared $LaNi_5$ alloy (Figure 4.1(a)) is comprised of a single $CaCu_5$-type phase with lattice periods corresponding well to the literature data for the same material derived from synchrotron XRD measurements [24]. After partial substitution of Sn for Ni in $LaNi_5$ alloy (Figure 4.1(b)) and Table 4.1) a one-phase structure that is composed of major $CaCu_5$-type intermetallic phase with lattice parameters *a* = 5.0652(3) Å and *c* = 4.0326(2) Å is observed. Furthermore, the pattern of Sn-substituted material consists of broadened diffraction peaks as compared to $LaNi_5$ material and the peaks have shifted towards lower 2 theta values while their intensities weakened. All these effects are attributed to inhomogeneity in the B-component (Ni(Sn)) of the parent AB_5-type material [20] and the larger Van der Waals radius (224 pm) of Sn compared to the radius of Ni (200 pm). In addition, the crystallite sizes were calculated from the Scherrer formula (Equation 4.2) and represented in Table 1.

$$\tau = (\kappa\lambda) \,/\, \beta\cos(\theta) \qquad 4.2$$

Where τ is the crystallite size nm, λ is the wave length (=0.154 nm for Cu-Kα), β is the full width at half-maximum (FWHM) (in radians), k is a constant (0.94 to spherical crystallites) and θ is the diffraction angle. Noticeably, the crystallite size decreased from 5.52 nm of $LaNi_5$ to 5.11 nm (Table 4.1) suggesting partial substitution of Ni. The refinement of the XRD data of $LaNi_{4.8}Sn_{0.2}$ alloy showed the increase in unit cell volume and lattice constants. The estimated abundance and lattice period of this phase exhibit a trend of increase with introduction of Sn in the charge (Table 4.1). This observation allows us to suggest that Sn (structure type Cu, *a* = 5.0652(3) Å and c=4.0326(2) Å) substitutes Ni in the Ni-based phase further referred as Ni(Sn). The Sn content in Ni(Sn) estimated from its lattice period by applying Vegard's law [16] (shown in the last column of Table 4.1) was around 0.724 % which shows the formation of a small amount of orthorhombic Ni(Sn) phase, which agrees with the previous report [22]. Interestingly, the unit cell aspect ratio (*c*/*a*) for the AB_5 phase noticeably increased after partial substitution of Ni by Sn from 0.794 to 0.796 (or by 0.25%).

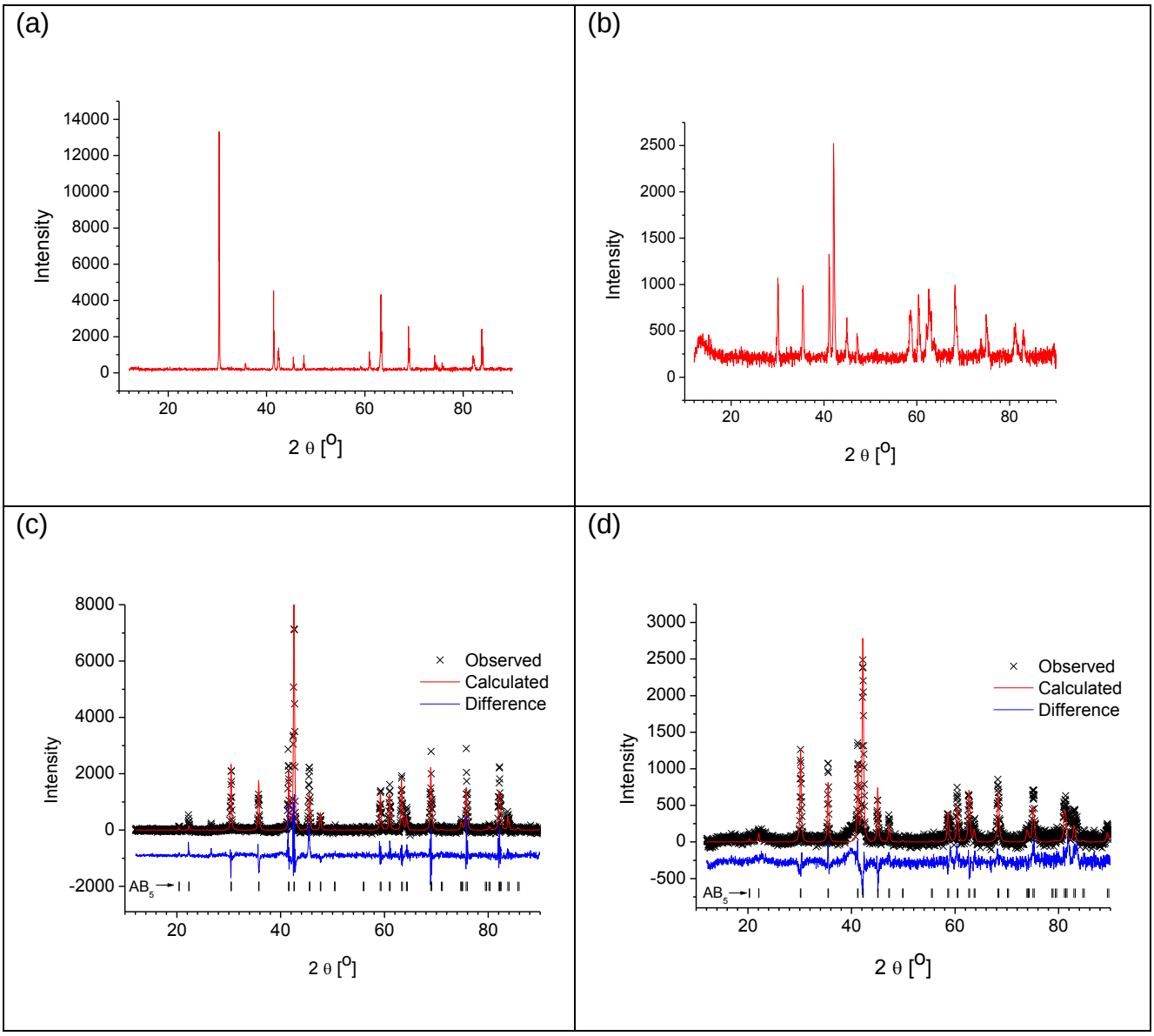

Figure 4.1: X-ray diffractogram of a) $LaNi_5$, b) $LaNi_{4.8}Sn_{0.2}$, c) Pd-$LaNi_5$ and d) Pd-$LaNi_{4.8}Sn_{0.2}$

On the other hand, the XRD patterns of $LaNi_5$ (Figure 4.1(c)) and $LaNi_{4.8}Sn_{0.2}$ (Figure 4.1(d)) material after autocatalytic Pd deposition revealed sharp diffraction peaks which are in resemblance with the diffraction peaks of Pd uncoated alloys. The Pd-$LaNi_5$ and Pd-$LaNi_{4.8}Sn_{0.2}$ alloys crystallised in the hexagonal $CaCu_5$ type structure with lattice parameters *a* = 5.0285(2) Å, *c* = 3.9931(2) Å and a crystallite size of 5.52 nm; and *a* = 5.0583(3) Å, *c* = 4.0229(4) Å and a crystallite size of 5.09 nm, respectively, as presented in Table 4.1. Rietveld refinements were performed with the aim being to detect Pd phase upon Pd deposition. The X-ray Rietveld refinements of Pd-modified materials do not show any palladium phase. The absence of palladium phase may be due to the amorphous nature of the particles

from electroless plating bath or the lack of detectable quantities for XRD analysis. It was seen that after Pd deposition, there was decrease of *c/a* and the unit cell volume for the AB_5 phase. After Pd deposition, the Sn content in Ni(Sn) estimated from its lattice period by applying Vegard's law (Table 4.1) decreased to 0.589 %. Moreover, palladium is not expected to get incorporated in the AB_5 materials either substitutionally or interstitially [20], hence, there are no noticeable changes in either broadness or position of diffraction peaks after surface modification.

Table 4.1: Results of refinement of XRD patterns of AB_5-type alloys.

Sample	Preparation condition		Lattice constants		Unit cell volume	crystallite size	Estimated Sn content in the phase
	Sn	Pd	*a* [Å]	*c* [Å]	*V* [Å^3]	τ[nm]	[at.%]
$LaNi_5$	No	No	5.0285(2)	3.9931(2)	87.442(8)	5.52	-
$LaNi_{4.8}Sn_{0.2}$	Yes	No	5.0652(3)	4.0326(2)	89.601(9)	5.11	0.724(5)
Pd- $LaNi_5$	No	Yes	5.0188(2)	3.9823(2)	86.870(7)	5.52	-
Pd- $LaNi_{4.8}Sn_{0.2}$	Yes	Yes	5.0583(3)	4.0229(4)	89.14(1)	5.09	0.589(1)

4.3.2. Morphological and Elemental Characterisations

The surface morphologies of the $LaNi_{4.8}Sn_{0.2}$ and $LaNi_5$ alloys are shown in Figure 4.2(a-b and c-d). The morphological studies were carried out using High Resolution-SEM which is able to detect nano-sized Pd particles. Figure 4.2(a) and (b) show that $LaNi_5$ alloy powder is comprised of clean, smooth surface with particles varying in size from 1 to 11 µm as depicted by particle size distribution histogram (figure 4.2(c)). Similar results were reported by Cuevas *et al.* [13]. From the histogram, it was observed that the majority of the alloy particles have particle size of ~1 µm. After Sn incorporation, the appearance of large particles ranging at 9-13 µm on the surface of AB_5 alloy is observed (Figure 4.2(d) and (e). When comparing particle size

distribution histograms (figure 4.2(c) and (f)) of the two alloys, it is seen that the particle sizes changed from a range of 1-8 µm to 1-14 µm after Sn substitution.

Table 4. 2: Elemetal composition data of $LaNi_5$ and $LaNi_{4.8}Sn_{0.2}$ alloy.

Materials	Element	EDS data		Target composition
		Net counts	Wt.%	Wt.%
$LaNi_5$	La	7.2	33.96	32.18
	Ni	9	66.04	67.93
	Total	-	100	100
$LaNi_{4.8}Sn_{0.2}$	La	6.6	32.92	31.31
	Ni	8.4	61.22	63.44
	Sn	3.4	5.86	5.35
	Total	-	100	100

In parallel to the SEM studies, EDS analyses were employed for determination of the elemental compositions of AB_5 alloys. The EDS data (Table 4.2) showed a satisfactory alignment with a target alloy composition (represented by last columns). The EDS results for $LaNi_{4.8}Sn_{0.2}$ alloy show some overestimation in Sn content, indicating that slightly more than 0.2 of Sn element was added. Comparison of the fractions of the "B" components of the $LaNi_{4.8}Sn_{0.2}$ alloy indicated that the alloy is a typical non-stoichiometric alloy with Sn and Ni occupying the "B" site to form Ni(Sn).

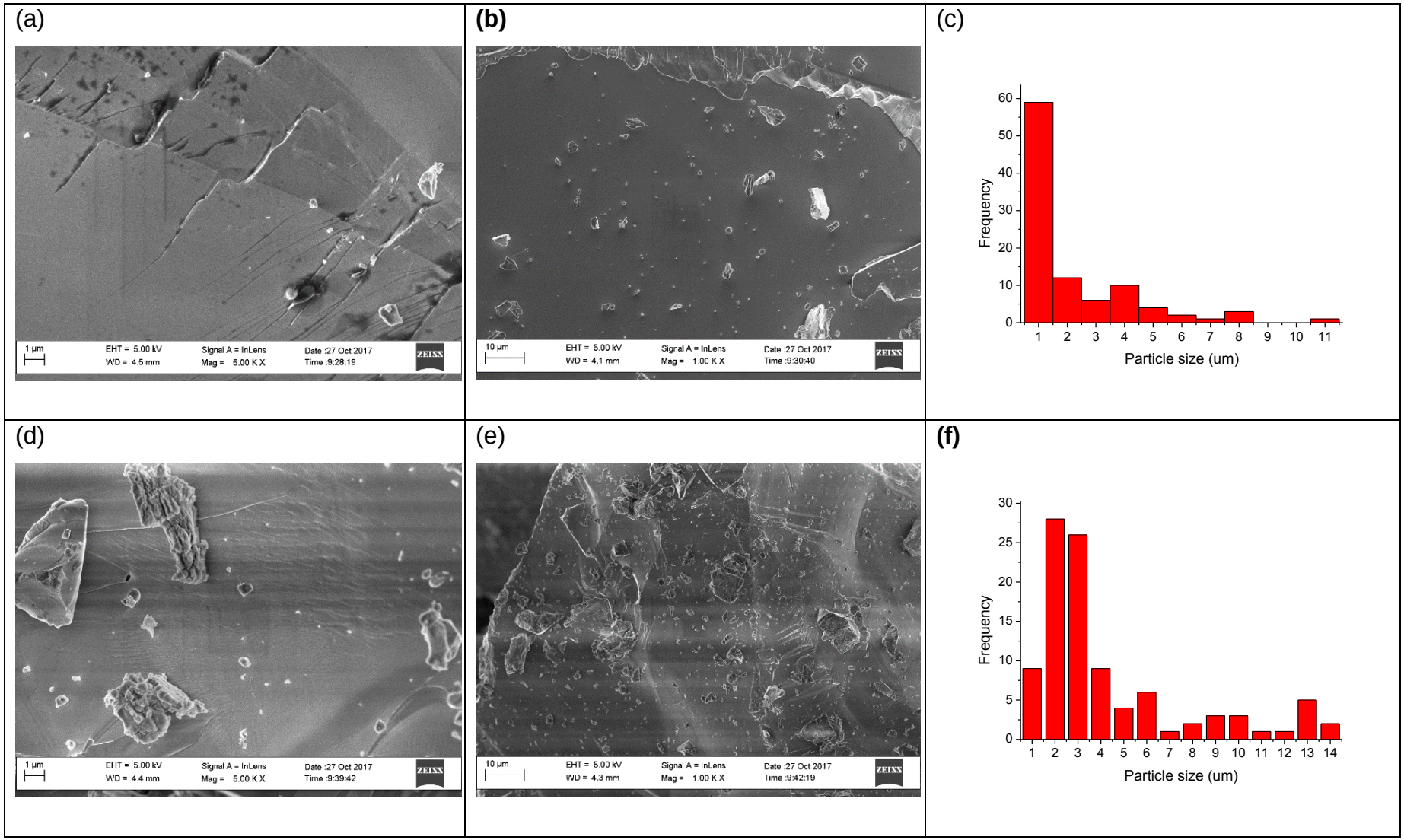

Figure 4.2: SEM micrographs of (a, b) $LaNi_5$ and (c, d) $LaNi_{4.8}Sn_{0.2}$ and their particle size distribtuion histograms ((c) Pd-$LaNi_5$ and (f) Pd-$LaNi_{4.8}Sn_{0.2}$)

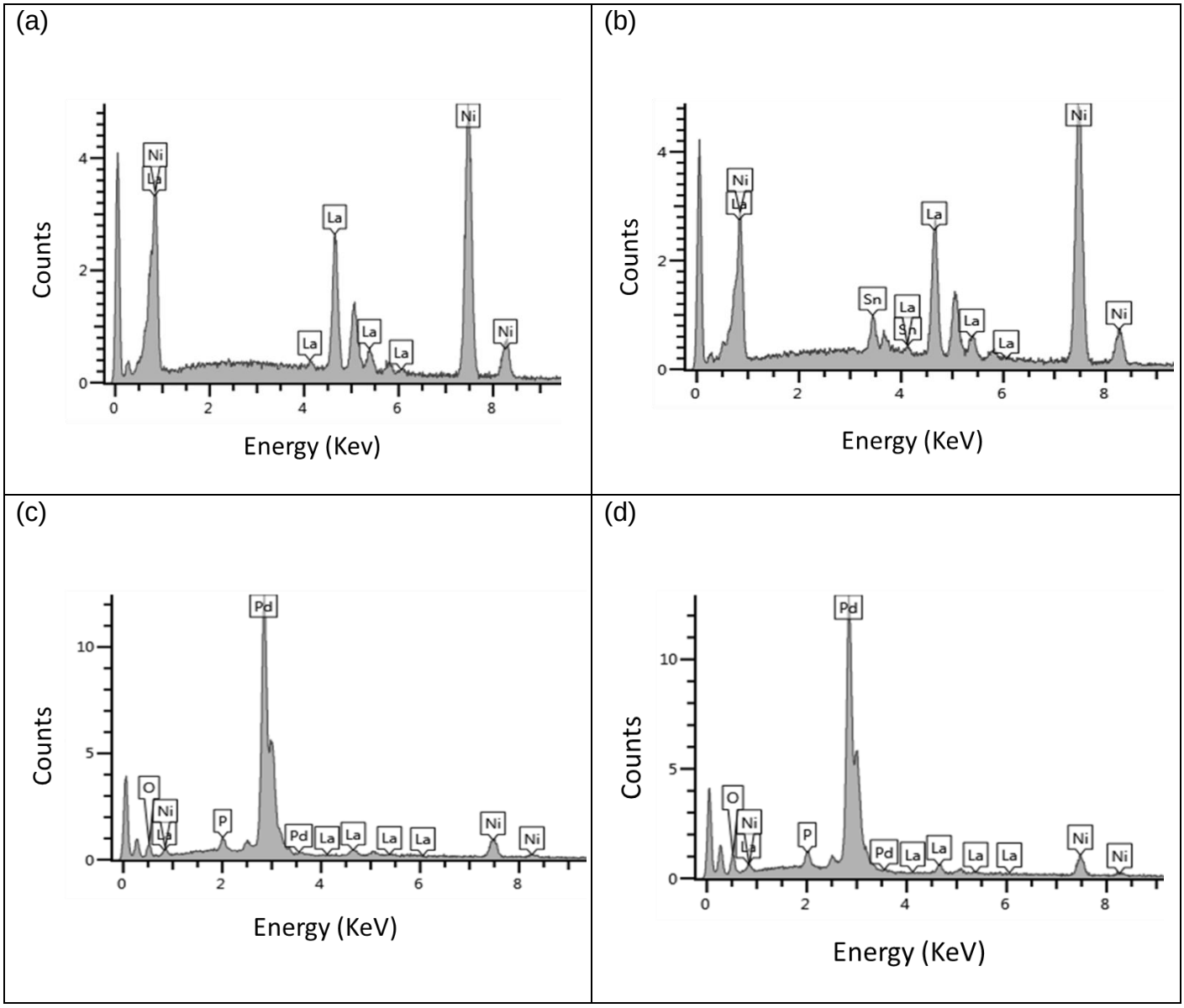

Figure 4.3: EDS plots of a) $LaNi_5$, b) $LaNi_{4.8}Sn_{0.2}$, c) Pd-$LaNi_5$ and d) Pd-$LaNi_{4.8}Sn_{0.2}$

The occurrence of palladium-phosphorus particles on the surfaces of the materials that underwent autocatalytic deposition of Pd was observed on SEM images to be spherical (Figure 4.4(a)-(d)). Palladium coatings on the AB_5-type substrates were found to be discontinuous in nature. Similar observations were observed before by Williams *et al.* [20]. Furthermore, it was observed on the particle size distribution histograms that the Pd-coated $LaNi_5$ alloy consisted of particles ranging in size between 1 and 36 nm with majority having particle size of 4 to 7 nm (Figure 4.4(c)).

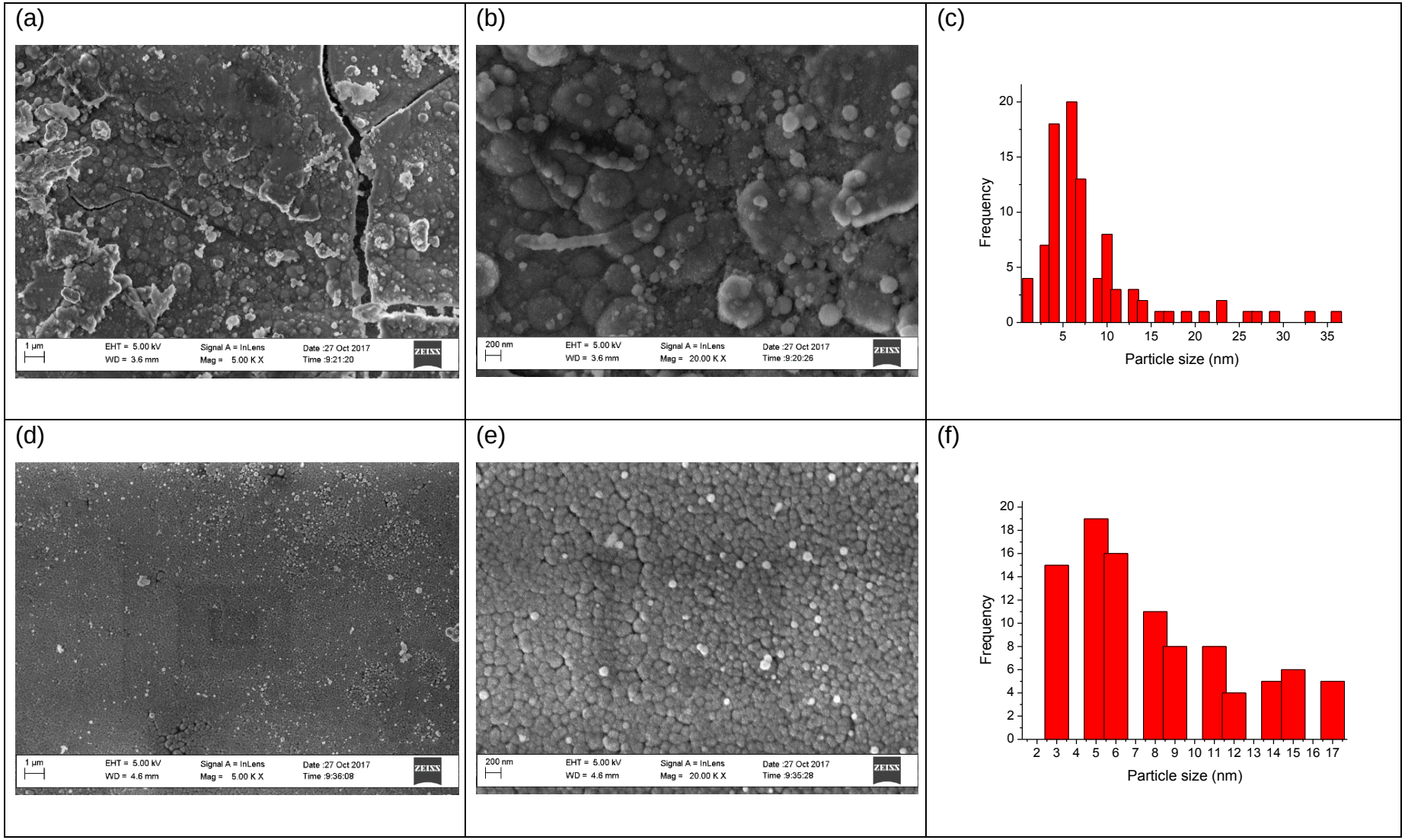

Figure 4.4: SEM micrographs of (a, b) Pd-$LaNi_5$ and (c, d) Pd-$LaNi_{4.8}Sn_{0.2}$ samples and their particle size distribution histograms ((c) Pd-$LaNi_5$ and (f) Pd-$LaNi_{4.8}Sn_{0.2}$).

Pd-coated $LaNi_{4.8}Sn_{0.2}$ alloy is comprised of particles in the range of 3-17 nm (Figure 4.4(f)). On a contrary, Williams *et al*. observed larger and wider size distribution of 135 nm exhibited by Pd particles on the AB_5 alloy [20]. The surface Pd loading of surface modified AB_5 alloys was estimated using EDS (Figure 4.3 (c) and (d)). It was observed in the figures that both alloys showed Pd peak at the same intensity. This was supported by very close amounts of Pd deposited for each alloy recorded by EDS to be 1.35 wt.% for Pd-$LaNi_5$ and 1.44 wt.% for Pd-$LaNi_{4.8}Sn_{0.2}$ alloy. Some traces of phosphorous, which are due to the presence of phosphorous in NaH_2PO_2-based plating bath, were revealed by EDS on the surface of each Pd-coated alloy. In support to EDS analysis, AAS was employed to further ascertain the quantity of palladium deposited on the AB_5 alloys. The total deposited Pd determined using AAS was found to be 0.1044 wt. % for both modified alloys.

4.3.3. Gas absorption studies

4.3.3.1. Nitrogen adsorption-desorption isotherms

BET was used in this study to evaluate the effect of metal substitution (Sn for Ni) and autocatalytic deposition of Pd on the physisorption properties (surface area, pore volume and pore size) of the AB_5 materials (Figure 4.5). The analysis was performed by the flow of the nitrogen on the materials. Figures 4.5(a)-(d) show the nitrogen adsorption and desorption by all materials. None of the four isotherms exhibits hysteresis behaviour. The Nitrogen adsorption and desorption isotherms of the unmodified alloys may be classified as type 1 isotherm group due to the hump-shaped curve occurring at relative pressure of 0.3 while the straightened isotherms of Pd-coated alloys can be categorised as type 2 isotherm group [25]. The intermediate flat region observed with isotherms of Pd-modified materials resembles the monolayer formation. On average, the uncoated alloys absorbed the lowest maximum nitrogen quantity of 0.6 cm^3/g (Table 4.3). They were followed by Pd-coated $LaNi_{4.8}Sn_{0.2}$ alloy, which absorbed 2.558 cm^3/g of nitrogen gas. Pd-coated $LaNi_5$ alloy absorbed the largest nitrogen gas (11.39 cm^3/g). The increased absorption of the gas by the samples after deposition of Pd can be attributed to

larger pore diameters of Pd modified alloys (Table 4.3), allowing rapid uptake of the gas over given time.

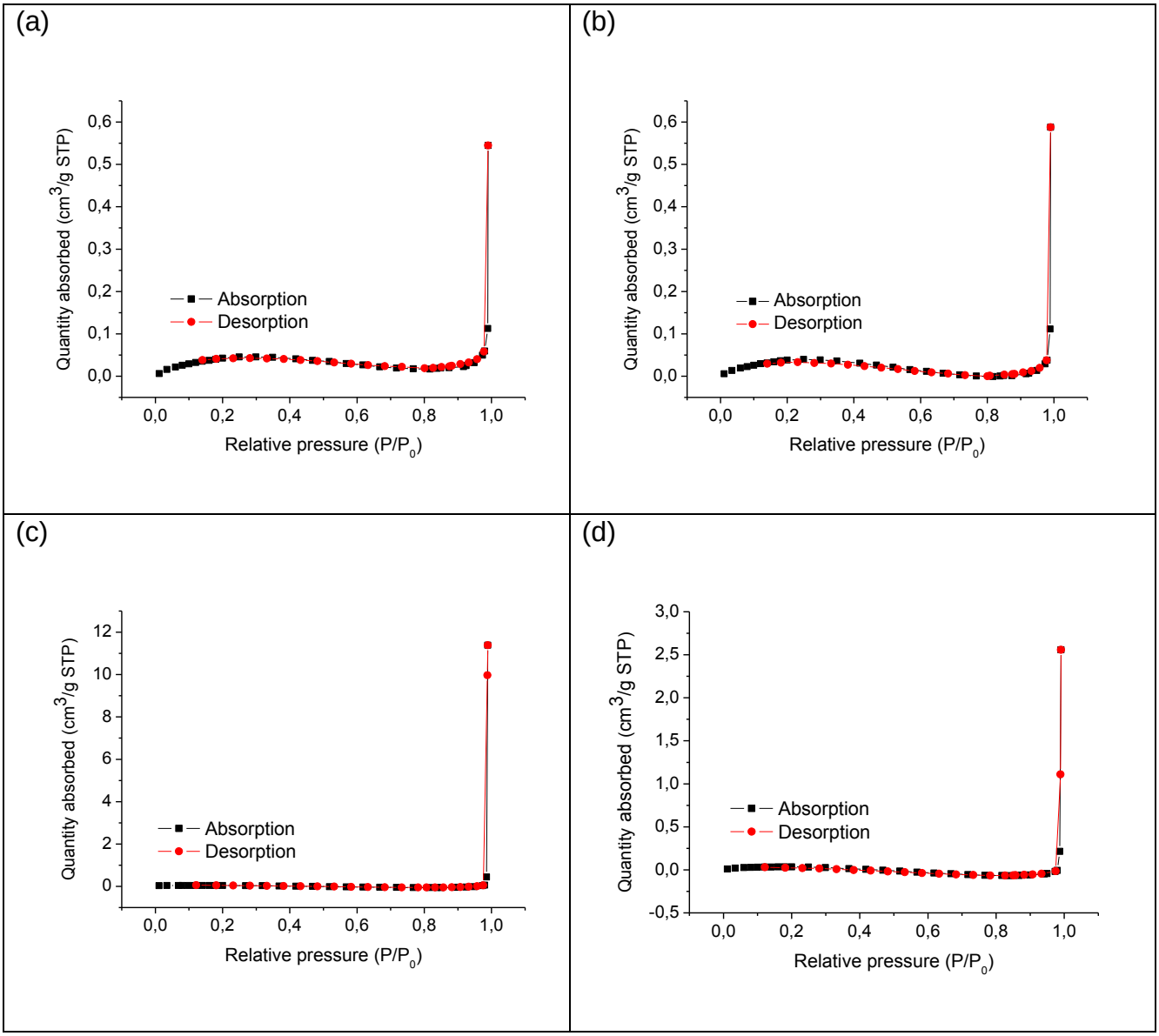

Figure 4.5: Adsorption-desorption isotherm of BET for a) $LaNi_5$, b) $LaNi_{4.8}Sn_{0.2}$, c) Pd-$LaNi_5$ and d) Pd-$LaNi_{4.8}Sn_{0.2}$.

In Table 4.3, it is observed that the BET surface area of $LaNi_5$ is 0.1889 m^2/g, which is close to the reported one of 0.25 m^2/g by Hu *et al* [26]. The surface area of the alloy was reduced to 0.1770 m^2/g after Sn-substitution. The table further indicates that the surface areas of the two unmodified materials were further decreased by autocatalytic deposition of palladium. The observed decrease in surface area after palladium deposition could be attributed to an increase in the metal loading on the

surface of the materials [14]. Furthurmore, palladium deposition resulted in enlargement of pore diameters, pore areas and pore volume (Table 4.3).

Table 4.3: Physical properties of uncoated and Pd-coated alloys.

Sample	BET surface area	Maximum quantity absorbed	Pore diameter	Pore area	Pore volume
	m^2/g	cm^3/g	Å	m^2/g	cm^3/g
$LaNi_5$	0.1889	0.5447	1050	0.0897	0.0024
$LaNi_{4.8}Sn_{0.2}$	0.1770	0.5879	1065	0.1000	0.0027
Pd- $LaNi_5$	0.1472	11.39	1632	1.463	0.0597
Pd- $LaNi_{4.8}Sn_{0.2}$	0.1311	2.558	1843	0.7408	0.0342

4.3.3.2. Hydrogen absorption kinetics

Hydrogen absorption kinetics of non-activated and of activated samples were studied using hydrogen absorption experiments on a Sieverts-type volumetric setup which were tested at 30 bar initial hydrogen pressure and constant temperature of 20 °C. The materials were divided into two groups. The first group included the non-activated unmodified and modified materials and is presented by Figure 4.6. As depicted by the figure, both unmodified alloys exhibited very long incubation periods before hydrogen absorption can take place. This observation can be attributed to the fact that after exposure to air, the materials allowed surface oxidations to take place, readily forming oxides/hydroxides film which prevents hydrogen dissociation and penetration into the interstitial sites [27-29]. The partial substitution of Sn for Ni resulted in an increase in maximum hydrogen storage capacity. The presence of protective surface oxide layers on the surfaces of the alloys is further suggested by sigmoid-shaped kinetic curves of these alloys [30]. Leon *et al.* [30] further advised that the shape of these kinetic curves is a characteristic of a nucleation process. The

index of power, *n*, (obtained using Equation 4.1) for unmodified $LaNi_5$ and $LaNi4_{.8}Sn_{0.2}$ alloys were found to be 0.99 and 0.50, respectively (Table 4.4). This indicates that the hydrogen absorption reaction for $LaNi_5$ alloy is controlled by nucleation and diffusion while for $LaNi4_{.8}Sn_{0.2}$ alloy only the diffusion mechanism is involved according to Forde *et al.* [31]. Therefore, the rate limiting steps for the unmodified alloys are surface processes together with nucleation and diffusion mechanisms.

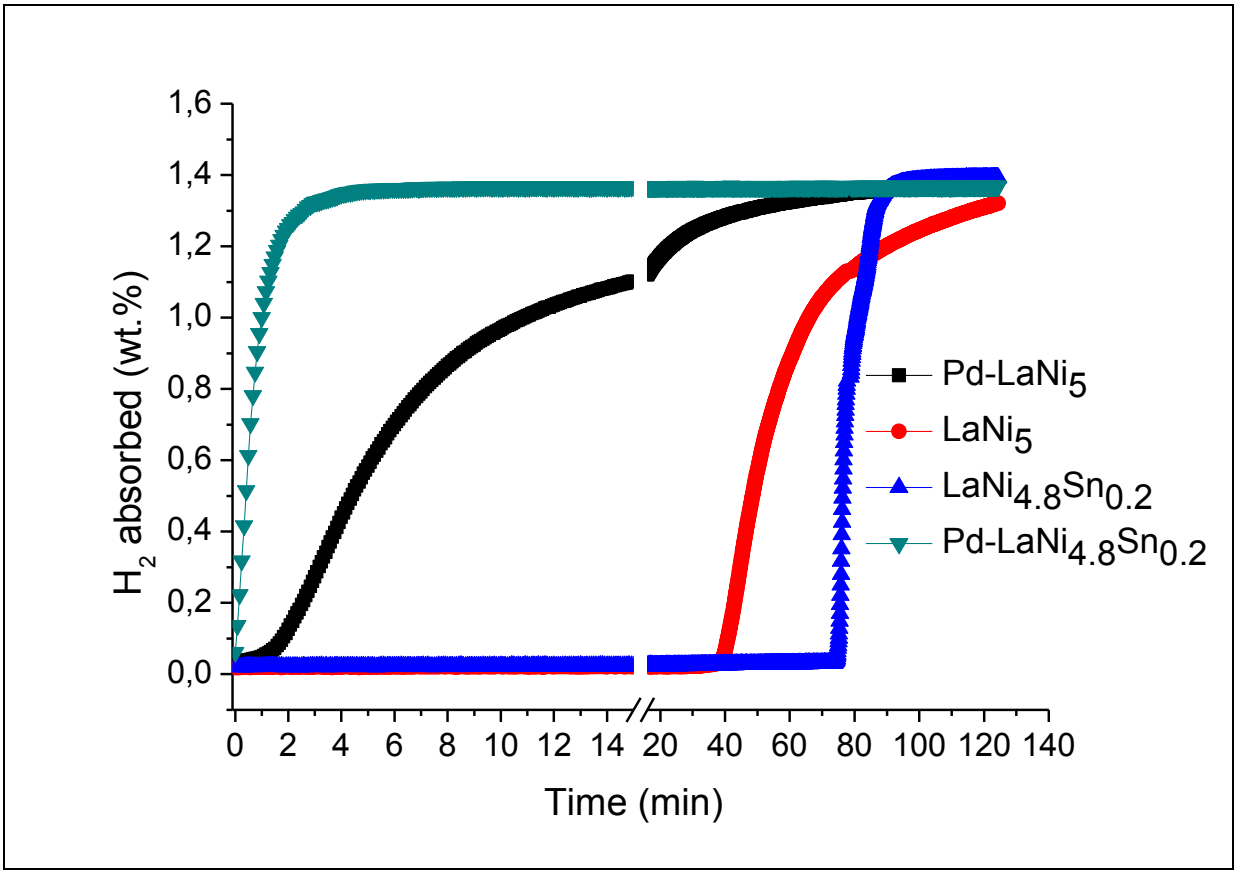

Figure 4.6: Dynamics of hydrogen absorption (T = 20 ˚C, P_{H2} = 30 bar) by uncoated and Pd-coated AB_5 alloys after pre-exposure to air and no preliminary activation (vacuum heating).

On the other hand, Pd-coated $LaNi_5$ alloy exhibited an incubation period of less than 2 minutes before hydrogen absorption can take place but a sigmoidal curve is still maintained by this alloy. Pd-coated $LaNi_{4.8}Sn_{0.2}$ alloy showed superiority over the other three alloys in terms of hydrogen absorption rate, with its kinetic curve revealing no precence of incubation period. This observation shows the importance of combining partial substitution of Sn for Ni and autocatalytic Pd deposition methods. It is well documented that Pd acts as a catalyst for hydrogen molecules

splitting and transfer into the bulk alloy, consequently, and improving initial activation [32]. Moreover, Liu *et al.* [33] reported that alloys with amorphous surfaces absorb hydrogen faster compared to their crystalline counterparts. It was seen that amorphous phosphorus particles from the electroless plating bath facilitated the creation of an interfacial channel between the bulk alloy and the palladium surface [20]; which may have increased the rate of transport of the hydrogen atoms, after dissociation of the hydrogen molecules on the palladium particles, and towards the bulk material. Hydrogen absorption reactions for both Pd-coated alloys are controlled by nucleation and diffusion mechanisms as suggested by their index of power (Table 4.4).

Table 4.4: Fit of the experimental data for hydrogen absorption by non-activated and activated materials using the Avrami-Erofeev equation

Sample	$\left(\frac{H}{AB5}\right)_{\max}$ (wt.%)		Rate constant, k (min^{-1})		Index of power	
	Non-activated	Activated	Non-activated	Activated	Non-activated	Activated
$LaNi_5$	1.29	1.45	0.06	0.21	0.99	0.98
$LaNi_{4.8}Sn_{0.2}$	1.40	1.37	0.24	19.21	0.50	0.58
Pd- $LaNi_5$	1.36	1.47	0.16	7.04	0.62	0.68
Pd- $LaNi_{4.8}Sn_{0.2}$	1.37	1.35	1.32	68.03	0.97	0.50

The second group included materials which were activated prior to measurement of hydrogen absorption for 1 hour under vacuum heating at 300 ˚C), the materials were then cooled to ambient temperature (20 ˚C), followed by H_2 absorption. The H_2 absorption kinetic curves are presented in figure 4.7. The kinetic curve of $LaNi_5$ material shows improvement in both the absorption kinetics and maximum hydrogen uptake capacity with a reduced incubation period, suggesting that the oxide film was removed through vacuum heating. However, the sigmoid shape is still present; suggesting that the oxide film was not completely removed or initial activation of the

alloy is generally poor. The index of power for this particular alloy slightly dropped from 0.99 to 0.98, signifying that nucleation and diffusion mechanisms are still the dominant rate determining steps during hydrogen absorption reaction. The maximum hydrogen absorbed and rate constant of $LaNi_5$ alloy were enhanced from 1.29 wt.% to 1.45 wt.% and from 0.06 to 0.21 min^{-1}, respectively (Table 4.4). The kinetic curves of $LaNi_{4.8}Sn_{0.2}$, Pd-$LaNi_5$ and Pd-$LaNi_{4.8}Sn_{0.2}$ alloys exhibited similar trend with no or little incubation period in comparison with the first non-activated group due to a complete removal of oxide film leading to an oxide-free metal surface as observed by Shan *et al.* [34]. Table 4 depicts that the power index of Pd-coated $LaNi_{4.8}Sn_{0.2}$ alloy is the only one that changed significantly after activation from 0.97 to 0.50. This observation implicates that once the alloy is activated, nucleation mechanism is no longer playing a role as rate determining step during hydrogen absorption process. The supremacy of Pd-coated $LaNi_{4.8}Sn_{0.2}$ alloy over the other alloys is still depicted by its kinetic curve, reaching maximum hydrogen capacity within 0.2 minutes with a highest rate constant of 68,03 min^{-1} (Table 4.4).

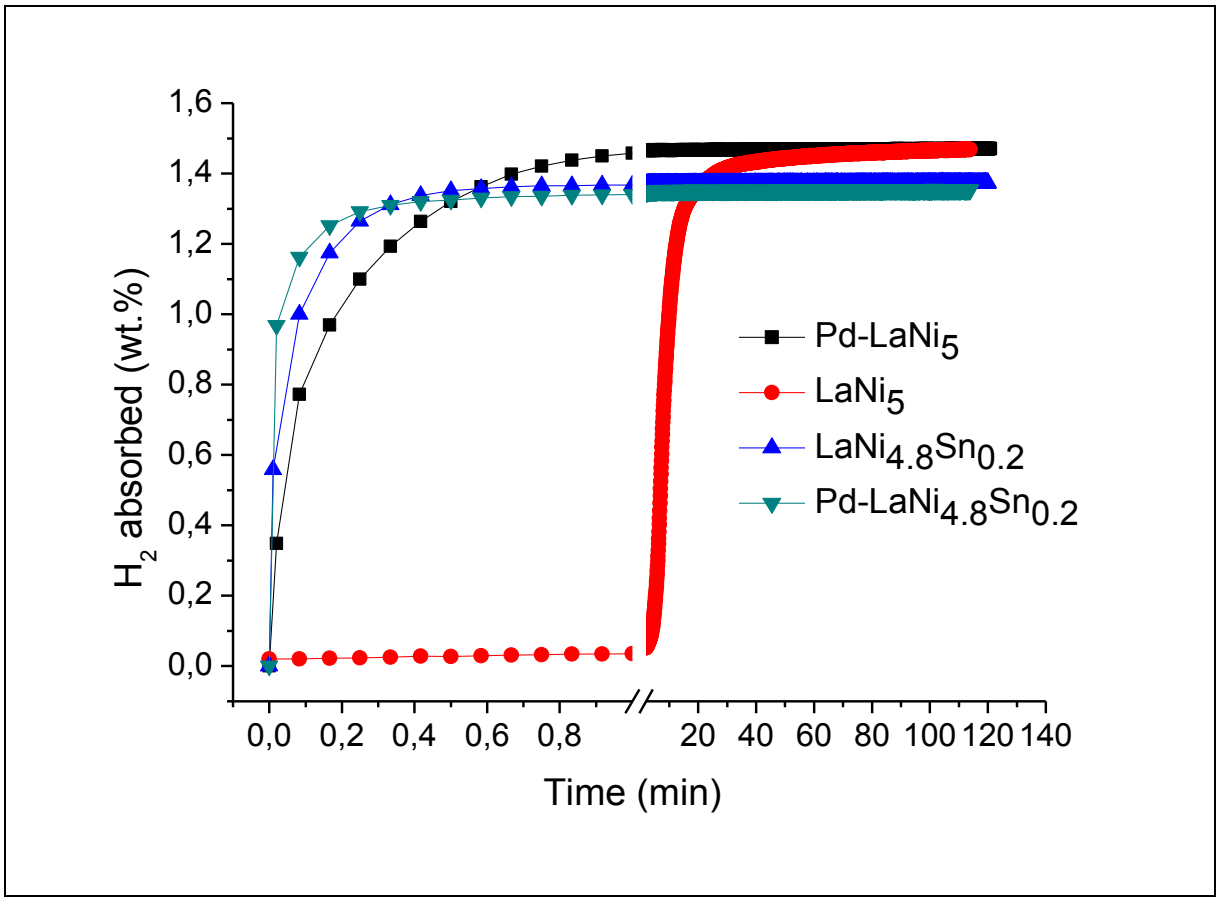

Figure 4.7: Dynamics of hydrogen absorption (T = 20 ˚C, P_{H2} = 30 bar) by uncoated and Pd-coated AB_5 alloys after preliminary activation (vacuum heating at 300 ˚C).

4.4. CONCLUSIONS

The experimental study herein presented the effect of combining Sn-substitution and electroless Pd deposition on the hydrogen absorption kinetics of $LaNi_5$ alloy. The study shows that Sn-substitution alone does not significantly improve the poisoning tolerance of the parent material as shown by sigmoid-shaped kinetic curve of the non-activated $LaNi_{4.8}Sn_{0.2}$ alloy and long incubation period. Interestingly, the alloy benefited from Sn-substitution since a slight enhancement of maximum hydrogen storage capacity by 0.11 wt.% after exposure to air was observed. This small change in hydrogen storage capacity can be attributed to an increase in pore diameter and lattice constant observed from BET and XRD results, respectively. All materials (non-activated and activated) that underwent autocatalytic deposition of palladium showed excellent H_2 absorption kinetics. It is therefore deduced that Pd layer on the surface of the materials is able to prevent the formation of oxides, promoting fast absorption of hydrogen by reducing the incubation period. Furthermore, the impregnation of phosphorus-containing electroless plating bath, which is amorphous in nature, may have also played a role in enhancing the hydriding kinetics by creating an interfacial channel between the bulk alloy and the palladium surface. The findings of our study gave us courage to conclude that Pd-coated $LaNi_{4.8}Sn_{0.2}$ alloy meets some of the requirements (fast hydrogen absorbing material with large hydrogen uptake capacity; poisoning-tolerant and decomposition-resistant material) to be applied in CO_2 conversion.

4.5. REFERENCES

[1] S. Kato, S. K. Matam, and M. Rohwerder, “The Origin of the Catalytic Activity of a Metal Hydride in CO_2 Reduction,” *Angew. Chemie Int. Ed.*, vol. 55, pp. 1–6, 2016.

[2] G. Gahleitner, “Hydrogen from renewable electricity : An international review of power-to-gas pilot plants for stationary applications,” *Int. J. Hydrogen Energy*, vol. 38, pp. 2039–2061, 2012.

[3] M. Ceramics, V. V Skorokhod, and V. P. Klimenko, “Reversable hydriding of $LaNi_{5-x}Al_x$−Pd composite in the presence of carbon monoxide,” *Powder Metall. Met. Ceram.*, vol. 39, pp. 575–583, 2001.

[4] L. Schlapbach and A. Züttel, “Hydrogen-storage materials for mobile applications,” *Nature*, vol. 414, pp. 353–358, 2001.

[5] Y. Chen, C. A. C. Sequeira, X. Song, R. Neto, and Q. Wang, “Polytypism of La–Ni phases in multicomponent AB_5 type hydride electrode alloys,” *Int. J. Hydrogen Energy*, vol. 27, pp. 63–68, 2002.

[6] D. Z. Y. Zhang, B. Li, H. Ren, X. Li, T. Qi, “Enhanced Hydrogen Storage Kinetics of Nanocrystalline and Amorphous Mg_2Ni-type Alloy by Melt Spinning,” *Materials (Basel).*, vol. 4, pp. 274–287, 2011.

[7] K. D. Modibane, M. Williams, and M. Lototskyy, “Poisoning-tolerant metal hydride materials and their application for hydrogen separation from CO_2/CO containing gas mixtures,” *Int. J. Hydrogen Energy*, vol. 38, pp. 9800–9810, 2013.

[8] J. Liu, X. P. Song, and G. L. Chen, “Hydrogen storage performance of Mg-based composites prepared by spark plasma sintering,” *J. Alloys Compd.*, vol. 486, pp. 338–342, 2009.

[9] L. Zaluski, A. Zaluska, J. O. Strrm-olsen, and R. Schulz, “Catalytic effect of Pd on hydrogen absorption in mechanically alloyed Mg_2Ni , $LaNi_5$ and FeTi,” *J. Alloys Compd.*, vol. 217, pp. 295–300, 1995.

[10] Y. Zhang, W. Zhang, J. G. Z. Yuan, and W. B. Y. Qi, “A Comparison Study of Hydrogen Storage Thermodynamics and Kinetics of $YMg_{11}Ni$ Alloy Prepared by Melt Spinning and Ball Milling,” *Acta Metall. Sin.*, vol. 30, pp. 1040–1048, 2017.

[11] D. Kyoi, T. Sakai, N. Kitamura, A. Ueda, and S. Tanase, “Synthesis of FCC Mg–Ta hydrides using GPa hydrogen pressure method and their hydrogen-desorption properties,” *J. Alloys Compd.*, vol. 463, pp. 306–310, 2008.

[12] H. Gu, Y. Zhu, and L. Li, “Hydrogen storage properties of Mg–Ni–Cu prepared by hydriding combustion synthesis and mechanical milling,” *Int. J. Hydrogen Energy*, vol. 34, pp. 2654–2660, 2009.

[13] F. Cuevas and M. Hirscher, “The hydrogen desorption kinetics of Pd-coated $LaNi_5$-type films,” *J. Alloys Compd.*, vol. 313, pp. 269–275, 2000.

[14] A. Alshaibani, “Effect of chemically reduced palladium supported catalyst on sunflower oil hydrogenation conversion and selectivity,” *Arab. J. Chem.*, vol. 10, pp. S1188–S1192, 2017.

[15] Y. Zhang, S. Xu, and D. Zhao, “Hydrogen storage kinetics of nanocrystalline and amorphous Cu−Nd-added Mg_2Ni-type alloys,” *Trans. Nonferrous Met. Soc. China*, vol. 24, pp. 3524–3533, 2014.

[16] K. D. Modibane, M. Lototskyy, M. W. Davids, M. Williams, M. J. Hato, and K. M. Molapo, “Influence of co-milling with palladium black on hydrogen sorption performance and poisoning tolerance of surface modified AB_5-type hydrogen storage alloy,” *J. Alloys Compd.*, vol. 750, pp. 523–529, 2018.

[17] X. Su, J. Xu, and Y. Huang, “Catalytic carbon dioxide hydrogenation to methane : A review of recent studies,” *J. Energy Chem.*, vol. 25, pp. 553–565, 2016.

[18] K. L. Yeung, S. C. Christiansen, and A. Varma, “Palladium composite membranes by electroless plating technique Relationships between plating kinetics, film microstructure and membrane performance,” *J. Memb. Sci.*, vol. 159, pp. 107–122, 1999.

[19] M. Lototskyy, K. D. Modibane, M. Williams, Y. Klochko, V. Linkov, and B. G. Pollet, “Application of surface-modified metal hydrides for hydrogen separation from gas mixtures containing carbon dioxide and monoxide,” *J. Alloys Compd.*, vol. 580, pp. S382–S385, 2013.

[20] R. V Denys, M. V. Lototskyy, V. M. Linkov, and M. Williams, “Palladium mixed-metal surface-modified AB_5-type intermetallides enhance hydrogen sorption kinetics,” *S. Afr. J. Sci.*, vol. 106, pp. 1–6, 2010.

[21] D. B. Willey, D. Pederzolli, and I. R. Harris, “Low temperature hydrogenation properties of platinum group metal treated, nickel metal hydride electrode alloy,” *J. Alloys Compd.*, vol. 332, pp. 806–809, 2002.

[22] Y. Ishibashi, M. Terashima, and R. Yamakawa, “H_2 reactivity on the surface of LaNi4.7Sn0.3,” *J. Alloys Compd.*, vol. 402, pp. 219–223, 2005.

[23] L. M. Kustov and A. L. Tarasov, “Hydrogenation of carbon dioxide: a comparison of different types of active catalysts,” *Ital. Oral Surg.*, vol. 24, pp. 349–350, 2014.

[24] J. Anthuvan, A. Pandurangan, and C. Senthil, “Nickel/carbon core/shell nanotubes: Lanthanum nickel alloy catalyzed synthesis, characterization and studies on their ferromagnetic and lithium-ion storage properties,” *Mater. Res. Bull.*, vol. 60, pp. 621–627, 2014.

[25] N. A. Ghani, “Modification of Activated Carbon from Biomass Nypa and Amine Functional Groups as Carbon Dioxide Adsorbent,” *J. Phys. Sci.*, vol. 28, pp. 227–240, 2017.

[26] W. Hu, Y. Kiros, and D. Noreus, “AB_5-type hydrogen storage alloys as catalysts in hydrogen-diffusion electrodes for novel H_2/Hydride/Perovskite/O_2 alkaline fuel cells,” *J. Phys. Chem. B*, vol. 108, p. 18530, 2004.

[27] H. Uchida, “Surface processes of H_2 on rare earth based hydrogen storage alloys with various surface modifications,” *Int. J. Hydrogen Energy*, vol. 24, pp. 861–869, 1999.

[28] X. Shan, J. H. Payer, and W. D. Jennings, “Mechanism of increased

performance and durability of Pd-treated metal hydriding alloys," *Int. J. Hydrogen Energy*, vol. 34, pp. 363–369, 2009.

[29] S. Yamanaka, M. Sato, S. Yamanaka, Y. Sato, and H. Ogawa, "Influence of Interstitial Impurity on Hydrogen Solubility in Zirconium," *J. Nucl. Sci. Technol.*, vol. 3131, pp. 135–143, 2012.

[30] A. Leon, "Hydrogenation characteristics of air-exposed magnesium films," *J. Alloys Compd.*, vol. 345, pp. 158–166, 2002.

[31] T. Forde, J. P. Maehlen, V. A. Yartys, M. V Lototsky, and H. Uchida, "Influence of intrinsic hydrogenation/dehydrogenation kinetics on the dynamic behaviour of metal hydrides: A semi-empirical model and its verification," *Int. J. Hydrogen Energy*, vol. 32, pp. 1041–1049, 2007.

[32] V. B. Parambhath, R. Nagar, and S. Ramaprabhu, "Effect of Nitrogen Doping on Hydrogen Storage Capacity of Palladium Decorated Graphene," *Langmuir*, vol. 28, p. 7826−7833, 2012.

[33] F.-J. Liu, "F-treatment effect on the initial activation characteristics of Mg-La-Ni amorphous alloys," *J. Alloys Compd.*, vol. 231, pp. 696–701, 1995.

[34] L. Al, M. Ni, X. Shan, J. H. Payer, and J. S. Wainright, "Increased performance of hydrogen storage by Pd-treated," *J. Alloys Compd.*, vol. 426, pp. 400–407, 2006.

CHAPTER 5

IMPROVED HYDROGENATION KINETICS OF $TiMn_{1.52}$ ALLOY COATED WITH PALLADIUM THROUGH ELECTROLESS DEPOSITION FOR POTENTIAL CO_2 CONVERSION

T. R. Somo[a], M. W. Davids[b], M. V. Lototskyy[*,b], M. J. Hato[a], K. D. Modibane[*,a],

[a]Department of Chemistry, School of Physical and Mineral Sciences, University of Limpopo (Turfloop), Polokwane, Sovenga 0727, South Africa.

[b]HySA System, South African Institute for Advanced Material Chemistry, University of the Western Cape, Bellville 7535, Cape Town, South Africa

*Corresponding Author.

E-mail address: mlototskyy@uwc.ac.za (M.V. Lototskyy); kwena.modibane@ul.ac.za (K.D. Modibane).

SUMMARY

Deterioration of hydrogen charging performances resulting from the surface chemical action of electrophilic gases, such as CO_2 limits the use of $TiMn_{1.52}$ alloy for practical application in CO_2 conversion into hydrocarbons. Hence in this study, we report the effect of autocatalytic Pd deposition on the morphology, structure and hydrogenation kinetics of $TiMn_{1.52}$ alloy as a potential metal hydride (MH) catalyst in CO_2 conversion reactions. It has been shown that the catalytic activities of MHs may be used in hydrogenation of CO_2 to hydrocarbons. The selected alloy has been demonstrated to be effectively surface modified by Pd deposition to improve hydrogenation kinetics as one of the requirements for catalytic properties of MHs in CO_2 conversion applications. The uncoated and Pd-coated materials were characterised using scanning electron microscopy/energy dispersive spectroscopy (SEM/EDS) and X-ray diffraction (XRD). XRD analyses indicated that $TiMn_{1.52}$ alloy contain C14-type Laves phase without any second phase while the SEM images together with particle size distribution histogram showed a smooth non-porous surface with irregular-shaped particles ranging in size from 1 to 8 µm. The XRD pattern of Pd-coated alloy also revealed that C14-type Laves phase was still maintained upon Pd deposition. This was further supported by similar calculated crystallite size of 29 nm for both materials. Palladium particles on the surface of the materials were confirmed by EDS analyses. Furthermore, Sieverts-type apparatus was used to study the kinetics of the alloys after pre-exposure to air and after vacuum heating at 300 ˚C. The Pd-coated AB_2 alloy exhibited good coating quality as confirmed by EDS with enhanced hydrogen absorption kinetics after pre-exposure to air without activation. The improvement of MH aborption kinetics is an indication that the material may be an effective MH catalyst in CO_2 conversion to hydrocarbons. Without activation, improved hydrogen absorption kinetics of Pd-coated alloy was observed as compared to uncoated alloy and it was attributed to improved surface tolerance or hydrogen spillover mechanism due to Pd-coatings. Pd deposition reduced the incubation period of the material from 5 to less than 2 minutes. Vacuum heating at 300 ˚C resulted with the removal of surface barriers and showed improved hydrogen absorption performances for both coated and uncoated alloys.

Keywords: hydrogen storage materials, AB_2 alloys, $TiMn_{1.52}$ alloy, palladium deposition

5.1. INTRODUCTION

Solid-state hydrogen storage through metal alloys seem to be a reliable and safe way to absorb hydrogen as a result of easy access of hydrogen offered by these materials [1]. Metal hydrides, which are formed by absorption of hydrogen by metal alloys, can be used in many practical applications including battery electrodes, hydrogen-based fuel cells for transportation, hydrogen compression and purification, heat pumping, thermal storage and as catalyst precursors in carbon dioxide conversion to hydrocarbons [2]. The catalytic activity of metal hydrides for hydrogenation of CO_2 was discovered in recent years and several reviews as well as studies have been published already [3-6]. For example, Ando *et al*. [7] observed that the hydrogenation of carbon dioxide to methane can be catalysed over an intermetallic compound of $LaNi_5H_6$ at 250–350 ˚C. Conversely, the studies indicated that small amounts of CO_2 are converted over these catalysts at ambient conditions because most alloys are active for hydrogenation of carbon oxides at temperatures above 100 ˚C [7]. This is caused by poor hydrogen absorption/desorption by metal alloys with an oxidised surface, which possess high activation barrier for dissociation of hydrogen atoms especially at low temperatures [5]. As a result, properties such as poisoning-tolerance and hydrogenation kinetics need to be enhanced for better catalytic activity of metal hydrides. Ti-Mn based AB_2-type Laves phase alloys are an attractive class of metal hydrides due to their better activation property and low cost [8]. Because of its light weight, large hydrogen absorption capacity of more than 1.0 H/M and moderate equilibrium plateau pressure (reported to be 0.7 MPa) under near ambient temperatures as compared to other Ti-Mn binary alloys [9], $TiMn_{1.52}$ alloy is one of the most promising hydride-forming materials for hydrogen storage and subsequently hydrogenation of CO_2. Nevertheless, this alloy has also experienced deterioration of hydrogen charging performances resulting from the surface chemical action of electrophilic gases, such as CO_2; and as such activation prior to hydrogen absorption is required [8, 10]. In order to improve its hydrogenation behaviour, alteration of $TiMn_{1.52}$ alloy through addition or partial substitution of elemental additives for Ti, Mn or both Ti and Mn has been extensively studied [11]. An example includes the study carried out by Liu *et al*. [8], where Ti was partially substituted with Zr while Cr, V, Ni, Fe and Cu metals were partially used in place of Mn to form $(Ti_{0.85}Zr_{0.15})_{1.05}Mn_{1.2}Cr_{0.6}V_{0.1}M_{0.1}$ alloy (where M=Ni, Fe, Cu). The substituted alloy showed a great improvement in cycling life but it showed poor hydrogenation

behaviour without activation due to its poor poisoning-resistance, resulting in slow hydriding kinetics. Other improvements of the hydrogenation behaviour have been previously reported through surface protecting techniques such as microencapsulation, coating with metal oxides and fluorination treatment [12]. All these techniques have high and low affinity for hydrogen and poisonous gases, respectively, but their limitations are not avoidable. For instance, the microencapsulation technique, which involves coating of the bulk alloy with 10 wt.% of Ni or Cu, utilises large amounts of coating metal that is not responsible for hydrogen storage. It is also not economically favoured and produces heavy metal alloys [12]. On the other hand, surface modification through deposition of PGMs, particularly palladium which has strong affinity for hydrogen, has been reported to possess relatively favourable and efficient improvement towards hydrogenation properties of alloy materials [13, 14]. In this investigation, autocatalytic palladium deposition was identified for surface-modification of $TiMn_{1.52}$ alloy and its effect on hydrogen sorption kinetics after exposure to air was then studied using Sieverts-type apparatus. To the best of our knowledge, such studies on hydrogenation kinetics of Pd-coated $TiMn_{1.52}$ alloy do not appear to have been reported as yet.

5.2. EXPERIMENTAL METHODS

5.2.1. Materials

The AB_2-type ($TiMn_{1.52}$) hydride-forming alloy was prepared from Ti (99.9%) and Mn (99.9%) purchased from Sigma Aldrich. The AB_2 hydride forming alloy was prepared by arc-melting on a water-cooled copper crucible in protective argon atmosphere. All prepared ingots were melted three times to provide homogeneity. Subsequently, the prepared metal ingots were pulverised by ball-milling in argon for 10 min. The material was allowed constant exposure to air throughout the experimental studies.

5.2.2. Surface modification of alloy

Surface modification of the $TiMn_{1.52}$ alloy was conducted through autocatalytic deposition of Pd in hypophosphite-based autocatalytic plating bath following a procedure described here [15]. The main purpose of surface coating with Pd was to improve the poisoning-tolerance of the material as well as to form a material with excellent hydrogen sorption properties. The autocatalytic deposition of Pd was applied to ~5 g batch of $TiMn_{1.52}$ alloy. Prior to palladium deposition, the materials were first sensitized and activated in a palladium-tin (Pd-Sn) colloidal solution [15] resulting in increased densities of Pd deposition and surface Pd loading on the intermetallide.

5.2.3. Characterisation techniques

X-ray diffraction (XRD) studies of the alloys were performed using a Bruker Advance powder diffractometer (Madison, USA; 40 mA, 40 keV, λCu-K = 0.15406 nm) at the Materials Research Group, iThemba Labs, in Cape Town, South Africa for phase identification.

Scanning electron microscopes/Energy-dispersive spectroscopy (SEM/EDS, Edax Genesis, 100 live seconds) studies were carried out using Leo 1450 microscope (20 kV, secondary electrons), Physics department, University of the Western Cape (UWC) to evaluate the morphology of AB_2-type alloy particle size/shape; Pd particle dispersion on the surface of the AB_2-type alloy particles and Pd particle size/shape.

The effect of autocatalytic palladium deposition on hydrogenation kinetics of $TiMn_{1.52}$ alloy was evaluated by a comparison of hydrogen absorption after pre-exposure to air and hydrogen absorption after vacuum heating at 300 ˚C. Vacuum heating prevented the formation of oxide layers on the surface of the alloy. Hydrogen absorption was conducted using a Sieverts-type volumetric installation, South African Institute for Advanced Material Chemistry (SAIAMC), UWC. The measurements were carried out at T = 20 ˚C, P_0 ~ 30 bar H_2, for 2 hours.

5.3. RESULTS AND DISCUSSION

5.3.1. Structural characterisation

Figure 5.1 shows the XRD patterns of Pd-coated and uncoated $TiMn_{1.52}$ alloys. The XRD analysis indicated that $TiMn_{1.52}$ alloy exhibit amorphous structure and C14-type Laves phase without any second phase. The amorphous nature and C14-type Laves phase of the same alloy were previously reported by Hu *at al*. [16] and Ramya *et al*. [11], respectively. The most interesting feature about amorphous hydrogen storage materials is that they have favourable hydrogen absorption/desorption kinetics, exhibiting easy flow of hydrogen atoms [17]. When the alloy is coated with Pd, two sharp diffraction peaks of much higher intensities than those of $TiMn_{1.52}$ alloy appear at 2θ = 30.56˚ and 2θ = 31.83˚. The peaks are attributed to (021) and (040) reflections of phosphorus structure, respectively [18]. The phosphorus was impregnated into the Pd layer during plating NaH_2PO_2-derived Pd layer. In addition, another two peaks appeared at 2θ = 62.49˚ and 2θ = 64.82˚. Crystallite sizes of the two alloys were calculated using Scherrer's equation (Equation 5.2) [19], where the peak at 2θ = 40.05˚ was used as a representative peak.

$$\tau = (\kappa\lambda) \,/\, \beta\cos(\theta) \qquad 5.2$$

Both the uncoated and Pd-coated alloys were found to have same crystallite size of 29 nm, suggesting that there was no admixing/incorporation between palladium nanoparticles and the bulk $TiMn_{1.52}$ alloy.

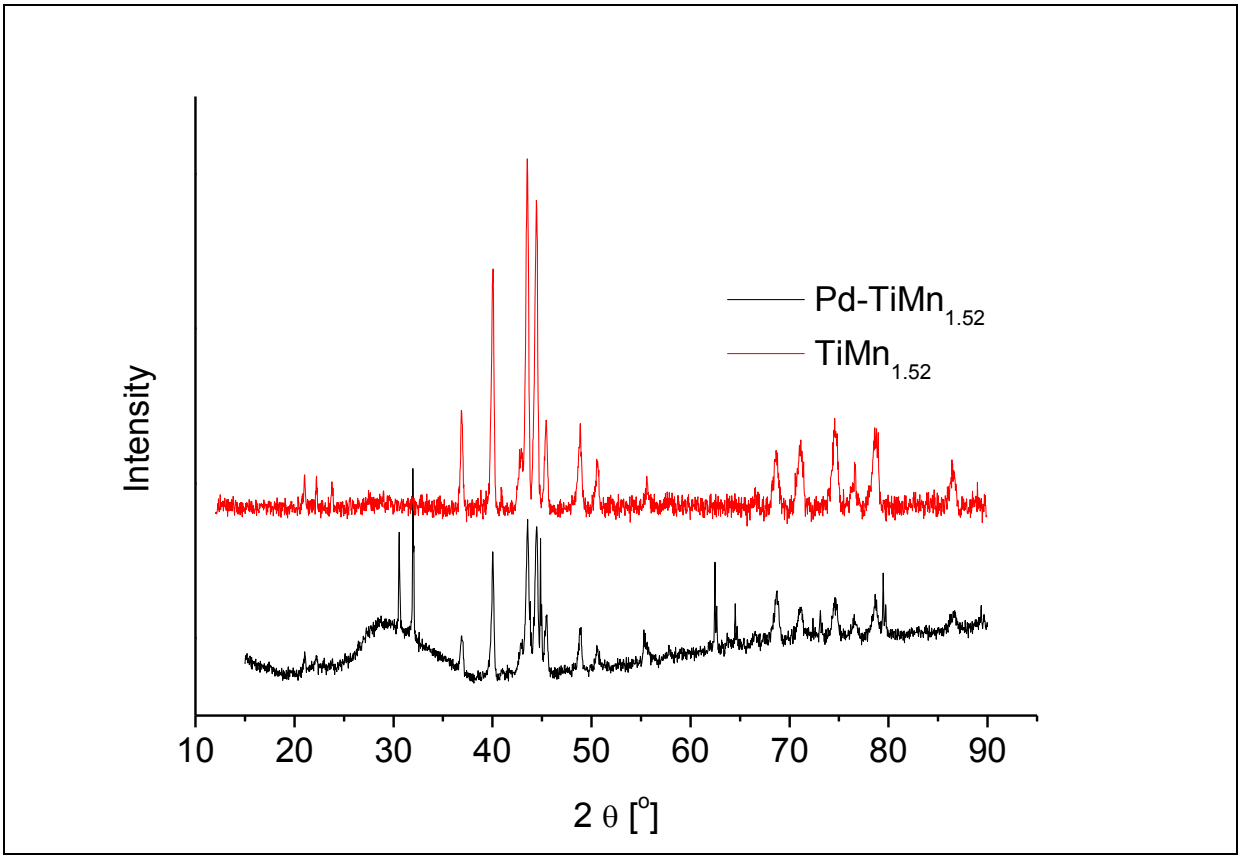

Figure 5.1: X-ray diffractograms of $TiMn_{1.52}$ and Pd-$TiMn_{1.52}$.

5.3.2. Morphological and elemental characterisations

Figure 5.2 presents SEM images of $TiMn_{1.52}$ before and after surface coating by autocatalytic palladium deposition. The uncoated alloy exhibited a relatively smooth surface, which is occupied by irregular-shaped particles varying in size from 1 to 8 µm. particle size distribution histogram of the material indicated that majority of the particles have a size of 1 µm. The alloy may be classified as a non-porous material. For the sample coated with Pd, a discontinuous layer of near-spherical Pd particles was observed. Moreover, the layer seemed to be very dense and uniform. Particle size distribution histogram (Figure 5.2 (f)) estimated that this alloy has particles ranging in size from 50 to 475 nm while majority of the particles have particle size of 200 nm.

Table 5.1: Table 1: Elemental composition data of $TiMn_{1.52}$ alloy.

Material	Element	EDS data		Target composition
		Net counts	Wt.%	Wt.%
$TiMn_{1.52}$	Ti	10.25	37.00	36.44
	Mn	9.7	63.00	63.56
	Total	-	100	100

EDS analyses (Figure 5.3) were employed in parallel to the SEM studies in order to determine the elemental compositions of the alloys. Table 5.1 shows that EDS data correspond very well with the targeted composition of $TiMn_{1.52}$ alloy, indicating a successful admixing of Ti and Mn metals (ratio of 1:1.52) through arc melting process.

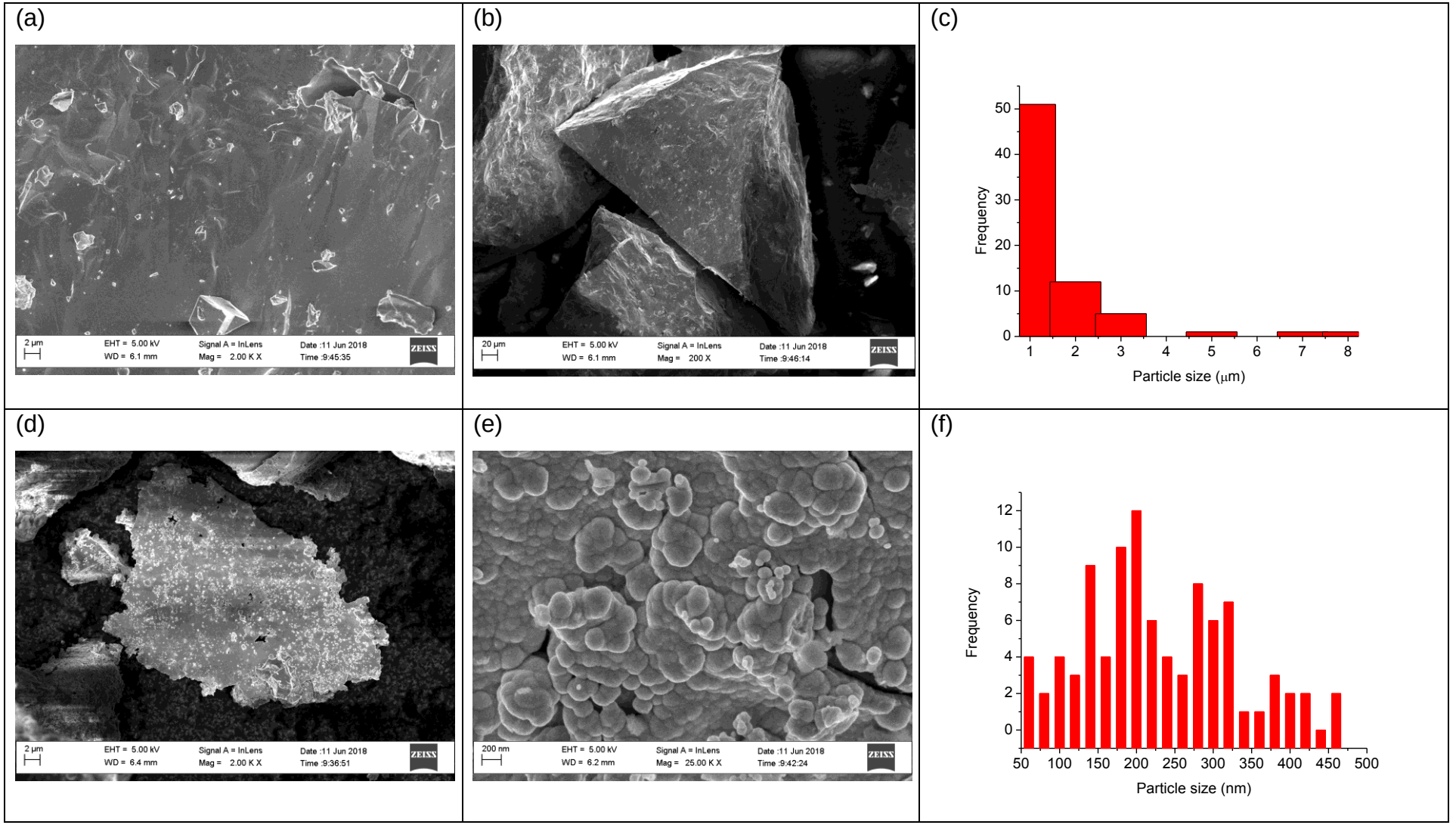

Figure 5.2: SEM micrographs of (a, b) $TiMn_{1.52}$ and (d, e) Pd-$TiMn_{1.52}$ and their particle size distribution histograms ((c) $TiMn_{1.52}$ and (f) Pd-$TiMn_{1.52}$).

The EDS of Pd-coated alloy (Figure 5.3 (b)) reveal that the impurities are phosphorus, carbon and tin at a level of 0.70, 2.31 and 4.54 wt.%, respectively. The presence of these impurities may have resulted from palladium-tin (Pd-Sn) colloidal solution during sensitisation and activation of AB_2 alloys as well as from NaH_2PO_2-based plating bath during autocatalytic deposition of palladium. When comparing the EDS graphs (Figure 5.3 (a, b)) of the two alloys, we observe that the net counts of Ti and Mn decreased from 10.25 and 9.7 to 0.9 and 1.5 respectively. This observation may be attributed to a successful palladium loading, covering most part of the alloy surface with a net count of 4.8 witnessed from the EDS data.

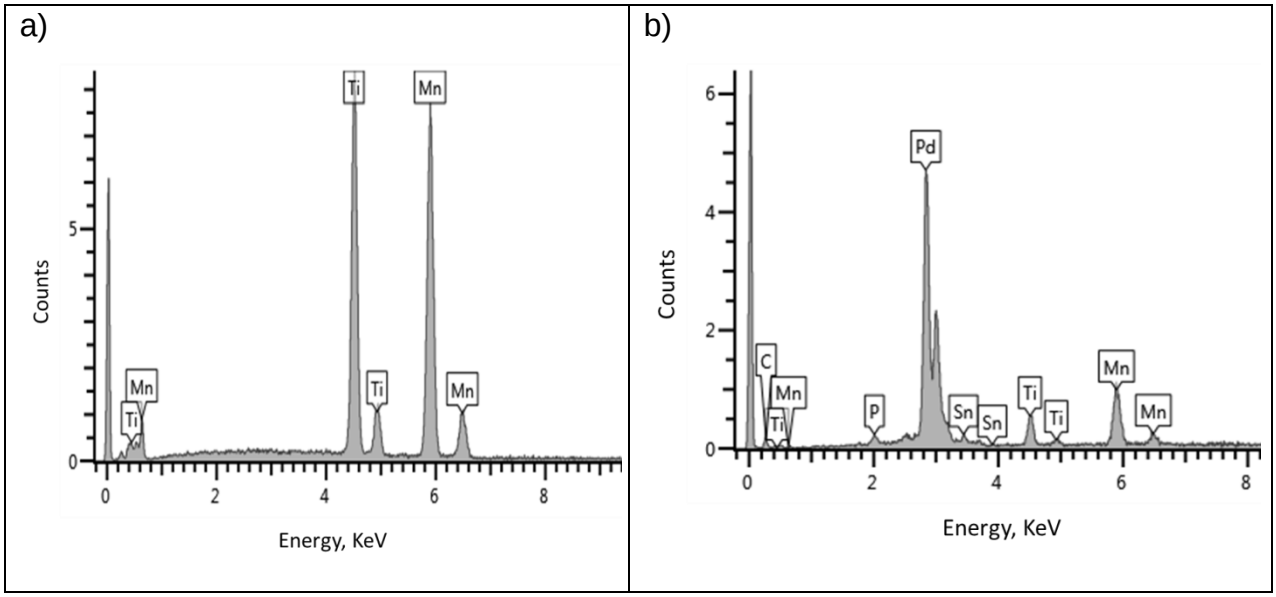

Figure 5.3: EDS plots of (a) $TiMn_{1.52}$ and (b) $TiMn_{1.52}$.

5.3.3. Hydrogen absorption kinetics

Studies of the hydrogenation performances of uncoated and Pd-coated $TiMn_{1.52}$ alloy were conducted after pre-exposure to air and after pre-activation by vacuum heating. The hydrogenation kinetic curves obtained after pre-exposure to air are presented in Figure 5.4. In addition, Table 5.2 present the results obtained through fitting of the experimental data on Avrami-Erofeev model. Fitting of the experimental data on Avrami-Erofeev model is described here [15]. Without vacuum activation, uncoated $TiMn_{1.52}$ alloy exhibit slow hydrogen absorption, accompanied by long incubation period of ~5 minutes. This is attributed to the presence of poisonous oxides film on

the surface, which causes difficulties in transportation of atomic hydrogen into the bulk alloy. Index of power of 1.37 (Table 5.2) signifies that hydrogen absorption for unmodified $TiMn_{1.52}$ alloy without activation is controlled by nucleation and growth mechanisms.

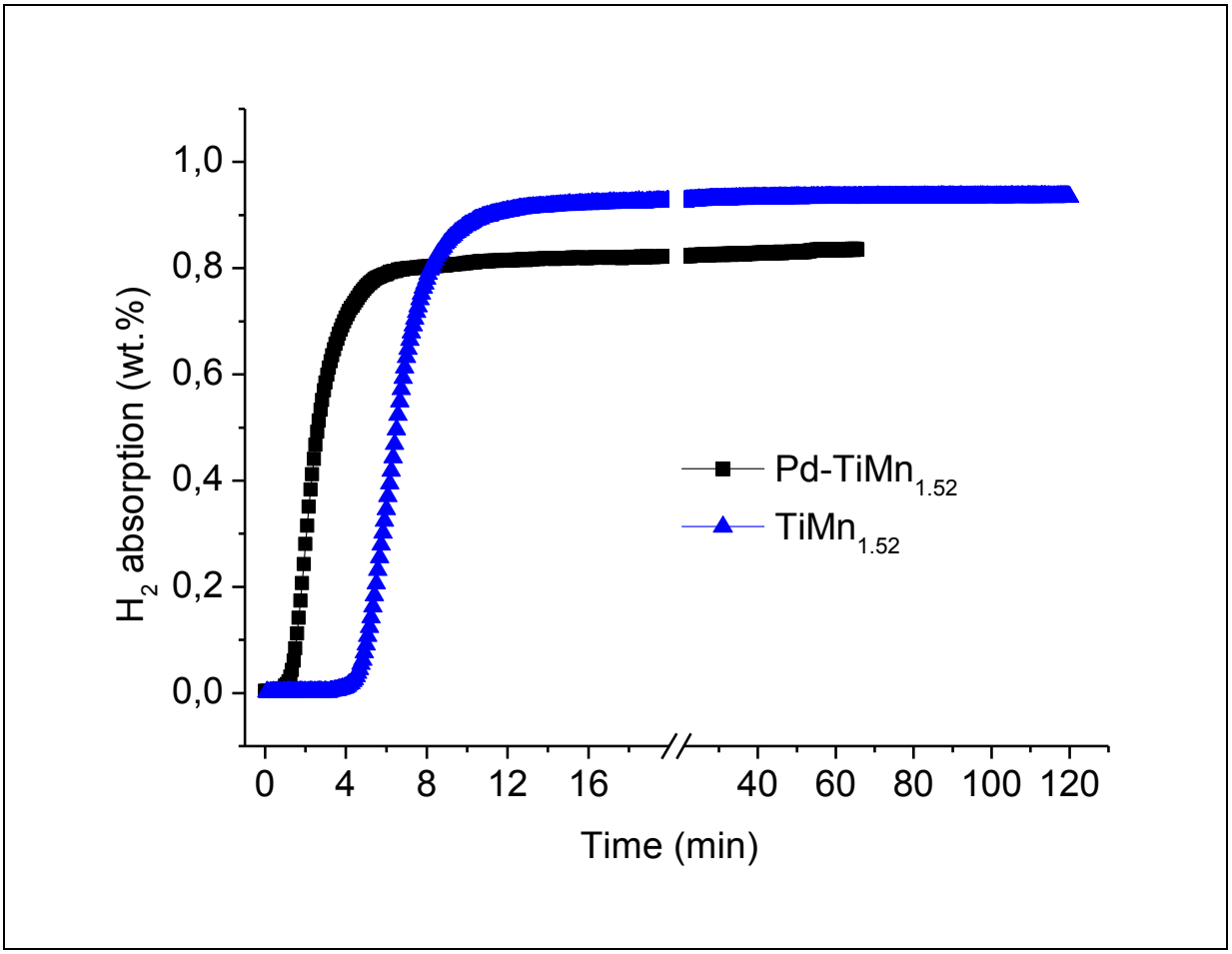

Figure 5.4: Dynamics of hydrogen absorption (T = 20 ˚C, P_{H2} = 30 bar) by uncoated and Pd-coated AB_2 alloys after pre-exposure to air and without preliminary activation (vacuum heating).

The hydrogenation kinetic curves obtained after preliminary activation are presented in Figure 5.5. After activation in vacuum by heating at 300 ˚C, the hydrogenation kinetics of $TiMn_{1.52}$ alloy significantly improved and this was supported by sudden increase of rate constant from 0.438 to 13.2 min^{-1} (Table 5.2). This is due to the fact that vacuum heating results in removal of any oxide layers, producing a fast hydrogen-absorbing surface. However, the maximum hydrogen absorption capacity for the activated uncoated alloy was found to be lower than that for the non-activated uncoated alloy, as depicted in Table 5.2. Subsequently, the maximum hydrogen

absorption capacity continued to drop after eletroless Pd coating. Similar trend was observed by Davids *et al*. [20] when loading Pd on TiFe alloy surface.

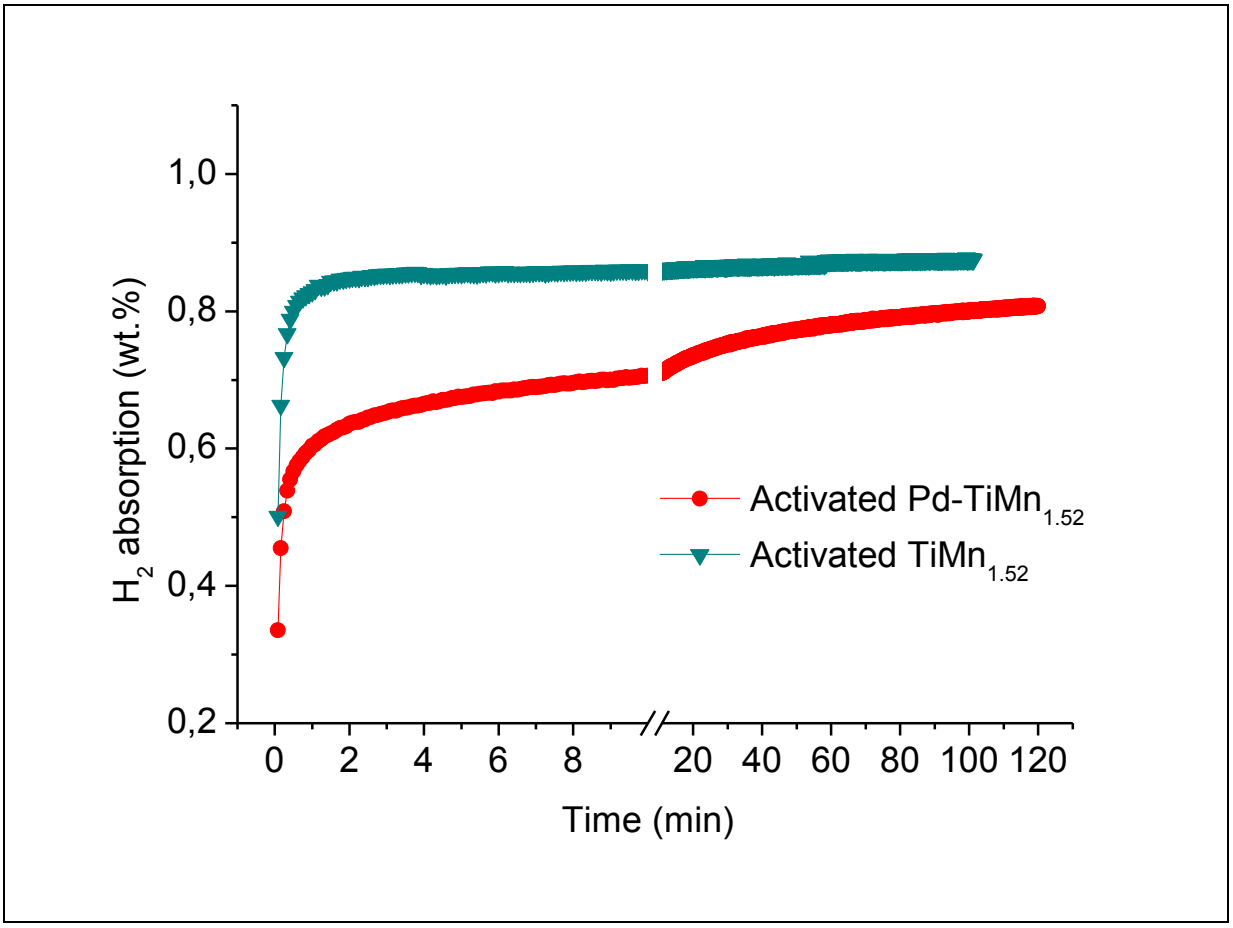

Figure 5.5: Dynamics of hydrogen absorption (T = 20 ˚C, P_{H2} = 30 bar) by uncoated and Pd-coated AB_2 alloys after preliminary activation (vacuum heating).

Loss in hydrogen absorption capacity after Pd coating may be attributed to large metal (Pd) loading on the surface of $TiMn_{1.52}$ alloy. Doyle *et al.* [21] recommended that in order to avoid losses in hydrogenation behaviour, the total weight of PGMs during surface modification of metal hydride-forming alloy through PGMs should be in trace amounts (≤0.1wt%). In our case, EDS analysis revealed more than 0.1 wt% of Pd particles on the surface of $TiMn_{1.52}$ alloy, hence a decrease in maximum hydrogen absorption capacity was observed upon Pd deposition. In addition, the presence of impurities such as Sn and C on the surface of Pd-coated alloy might have hindered complete hydrogen absorption by the material. Although a decrease in hydrogen capacity was observed, there was an improvement in hydrogenation kinetics, carried out without activation by vacuum heating, upon Pd-coating. The enhancement can be attributed to the partial removal of surface oxide films upon

autocatalytic deposition of palladium, as well as to the catalytic activity of Pd(P) nanoparticles facilitating splitting of hydrogen molecules into hydrogen atoms. The incubation period is shorter for the alloy coated with Pd.

Table 5.2: Fit of the experimental data for hydrogen absorption by non-activated and activated materials using the Avrami-Erofeev equation.

Material	$\left(\frac{H}{AB5}\right)_{\max}$ (wt.%)		Rate constant, k (min^{-1})		Index of power, n	
	Non-activated	Activated	Non-activated	Activated	Non-activated	Activated
$TiMn_{1.52}$	0.933	0.869	0.438	13.2	1.37	0.50
Pd-$TiMn_{1.52}$	0.827	0.779	0.771	1.05	0.925	0.50

After vacuum heating, the surface coated alloy exhibited faster and reproducible hydrogen absorption performances without the presence of incubation period as compared to surface coated alloy without vacuum heating. Its hydrogenation kinetics is slower than for activated unmodified $TiMn_{1.52}$ alloy. This is supported by higher rate constant of activated unmodified alloy (k = 13.2 min^{-1}) as compared to that of activated modified alloy (k = 1.05 min^{-1}). Activated, uncoated alloy together with inactivated and activated Pd-coated alloys all exhibited an index of power of between 0.5 and 1. Therefore, their interaction with hydrogen is controlled by nucleation mechanism.

5.4. CONCLUSIONS

This chapter presents the effect of autocatalytic deposition of palladium on the structure, morphology as well as the hydrogenation kinetics of $TiMn_{1.52}$ alloy. The study demonstrates that surface modification of $TiMn_{1.52}$ alloy through Pd deposition results in the formation of discontinuous layer of Pd nanoparticles on the surface of the alloy, causing relatively improved activation performances and hydrogen absorption kinetics even after its exposure to air. The effect was attributed to improved H_2 dissociation on Pd nanoparticles. The maximum hydrogen absorption capacity of the material decreased upon Pd deposition, and this was associated with a large metal loading on the surface.

5.5. REFERENCES

[1] B. Sakintuna, F. Lamari-darkrim, and M. Hirscher, “Metal hydride materials for solid hydrogen storage: A review,” *Int. J. Hydrogen Energy*, vol. 32, pp. 1121–1140, 2007.

[2] F. Laurencelle, Z. Dehouche, and F. Morin, “Experiments on a Metal Hydride based Hydrogen Compressor,” *Int. J. Hydrogen Energy*, vol. 30, pp. 879–892, 2005.

[3] L. Li, D. Mao, and J. Yu, “Highly selective hydrogenation of CO_2 to methanol over CuO-ZnO-ZrO_2 catalysts prepared by a surfactant-assisted coprecipitation method,” *J. Power Sources*, vol. 279, pp. 394–404, 2015.

[4] S. Kato, S. K. Matam, and M. Rohwerder, “The Origin of the Catalytic Activity of a Metal Hydride in CO_2 Reduction,” *Angew. Chemie Int. Ed.*, vol. 55, pp. 1–6, 2016.

[5] L. M. Kustov and A. L. Tarasov, “Hydrogenation of carbon dioxide: a comparison of different types of active catalysts,” *Ital. Oral Surg.*, vol. 24, pp. 349–350, 2014.

[6] G. Ibram and N. Materials, “Conversion of carbon dioxide into methanol - A potential liquid fuel: Fundamental challenges and opportunities (a review),” *Renew. Sustain. Energy Rev.*, vol. 31, pp. 221–257, 2014.

[7] H. Ando, M. Fujiwara, and M. Tanaka, “Catalytic hydrogenation of carbon dioxide over $LaNi_5$ activated during the reaction,” *J. Mol. Catal. A*, vol. 144, pp. 117–122, 1999.

[8] P. Liu, X. Xie, and T. Liu, “Hydrogen storage properties of $(Ti_{0.85}Zr_{0.15})_{1.05}Mn_{1.2}Cr_{0.6}V_{0.1}M_{0.1}$ (M=Ni, Fe, Cu) alloys easily activated at room temperature,” *Prog. Nat. Sci. Mater. Int.*, vol. 27, pp. 652–657, 2017.

[9] J. Zhu, L. Dai, Y. Yu, J. Cao, and L. Wang, “A direct electrochemical route from oxides to $TiMn_2$ hydrogen storage alloy,” *Chinese J. Chem. Eng.*, vol. 23, pp. 1865–1870, 2015.

[10] P. Vermeulen, R. A. H. Niessen, and P. H. L. Notten, “Hydrogen storage in metastable $Mg_yTi_{(1-y)}$ thin films,” *Electrochem. commun.*, vol. 8, pp. 27–32, 2006.

[11] K. Ramya, N. Rajalakshmi, and B. Sivasankar, “Electrochemical studies on the effect of nickel substitution in $TiMn_2$ alloys,” *J. Alloys Compd.*, vol. 352, pp. 315–324, 2003.

[12] D. B. Willey, I. R. Harris, and A. S. Pratt, “The improvement of the hydrogenation properties of nickel-metal hydride battery alloy by surface modification with platinum group metals (PGMs),” *J. Alloys Compd.*, vol. 295, pp. 613–620, 1999.

[13] W. Davids, M. V Lototskyy, and V. Linkov, “Chemical surface modification for the improvement of the hydrogenation kinetics and poisoning resistance of TiFe,” *J. Alloys Compd.*, vol. 509S, pp. S770– S774, 2011.

[14] M. Ceramics, V. V Skorokhod, and V. P. Klimenko, “Reversable hydriding of $LaNi_{5-x}Al_x$−Pd composite in the presence of carbon monoxide,” *Powder Metall. Met. Ceram.*, vol. 39, pp. 575–583, 2001.

[15] R. V Denys, M. V. Lototskyy, V. M. Linkov, and M. Williams, “Palladium mixed-metal surface-modified AB_5-type intermetallides enhance hydrogen sorption kinetics,” *S. Afr. J. Sci.*, vol. 106, pp. 1–6, 2010.

[16] Y. Q. Hu, H. F. Zhang, and Z. Q. Hu, “Preparation and hydriding/dehydriding properties of mechanically milled Mg–30 wt% $TiMn_{1.5}$ composite,” *J. Alloys Compd.*, vol. 354, pp. 296–302, 2003.

[17] C. Iwakura, S. Nohara, and H. Inoue, “Hydriding and dehydriding characteristics of an amorphous Mg_2Ni–Ni composite,” *J. Alloys Compd.*, vol. 285, pp. 246–249, Jun. 1999.

[18] P. K. Sarswat, S. SarKar, and M. L. Free, “Structural and Electrical irregularities caused by selected dopants in black-phosphorus,” *J. solid state Sci. Technol.*, vol. 5, pp. Q1–Q7, 2016.

[19] A. M. Sheikh, E. L. Silva, and M. Y. Abellah, “Pd-based Catalysts for Ethanol

Oxidation in Alkaline Electrolyte," *Am. J. Min. Metall.*, vol. 2, pp. 64–69, 2014.

[20] W. Davids, M. V Lototskyy, and M. Williams, "Surface modification of TiFe hydrogen storage alloy by metal-organic chemical vapour deposition of palladium," *Int. J. Hydrogen Energy*, vol. 36, pp. 9743–9750, 2011.

[21] I. Mark, L. Doyle, and D. Benjamin, "Hydrogen storage materials," *United states Pat.*, vol. 6, p. 165, 2000.

CHAPTER 6

GENERAL DISCUSSION, CONCLUSIONS AND RECOMMENDATIONS

6.1. CONCLUSIONS

The ultimate main objective of this study was to develop a class of hydride-forming alloys that are surface-modified through autocatalytic deposition of palladium that meet requirements for practical application of these materials in catalytic hydrogenation of carbon dioxide into hydrocarbons. These requirements included easy activation; rapid hydrogen uptake rates; stable operation under conditions of mild temperature and pressure and sorption stability in the presence of gaseous impurities. These targets were achievable through catalytic loading of Pd nanoparticles onto the surface of the hydride-forming alloy materials, motivated by unique interactions between Pd and hydrogen as well as high affinity of hydrogen possessed by Pd. The hypothesis of this study was whether surface-modified AB_5 ($LaNi_5$) and AB_2 ($TiMn_{1.52}$) type alloys should exhibit improved hydrogenation kinetics as well as outstanding poisoning-tolerance compared to their unmodified counterparts at room temperature before and after activation through vacuum heating. Moreover, for $LaNi_5$ alloy, it was hypothesised in this study that partial substitution of Ni with elements having big active sites than Ni to form an alloy that can results in larger maximum hydrogen absorption capacity with enhanced kinetics upon activation.

In addressing these hypotheses the following sub-objectives were investigated:

1. The effect of partial substitution of nickel by tin followed by autocatalytic palladium deposition on the hydrogen absorption kinetics of $LaNi_5$-type metal hydride alloy.
2. Improved hydrogenation kinetics of $TiMn_{1.52}$ alloy coated with palladium through autocatalytic deposition for potential CO_2 conversion.

A comprehensive literature review combined in chapter 2, which contains a set of physico-chemical properties governing the applicability of the sample materials as hydrogen sorbents, helped in identifying these alloys. AB_5-type alloys were identified as potential CO_2 conversion catalyst precursors of interest due to their reversible

interactions with hydrogen under mild conditions of pressure and temperature; minimal energy expenditure; simplicity in operation; high hydrogen selectivity, and release of high-pressure high-purity hydrogen at elevated temperature. On the other hand, the potential use of $TiMn_{1.52}$ material for catalytic application was motivated by low cost, reasonable plateau pressure and pressure-composition-temperature performances, confirmed by a comprehensive literature review. Inadequate rates of hydrogen uptake caused by presence of poisonous gases such as CO and CO_2 limit the application of AB_2- and AB_5-type alloys in catalytic conversion of CO_2 into hydrocarbons. In addition, literature reveals that because of poor poisoning-tolerance, these materials function well during CO_2 conversion only at temperatures over 250 ˚C. Palladium can act as surface protective layer on the surface of an alloy to prevent the prevention of oxide layers due to its high and ferocious affinity towards hydrogen, the ability to dissociate hydrogen molecules with no or very little activation energy required, and their wide applicability in hydrogen exchange reactions. Autocatalytic deposition of palladium was considered and used as a plating technique in this study as a result of its ability to deposit most PGM's, ability to plate metal surface layers on materials with irregular shape, ability to control the surface chemistry of the modified material on a molecular or atomic domain, and deposition of homogeneous coatings. Characterisation techniques, which were reviewed in detail in chapter 3, included SEM/EDS, XRD, BET, AAS and Sieverts-type apparatus.

Results of characterisation of unmodified and surface-modified sample materials were collected and are summarised as follows:

1. The study was initiated by an investigation of partial substitution of Sn for Ni in $LaNi_5$ alloy. Just a small amount (0.2 of Ni) was replaced to get $LaNi_{4.8}Sn_{0.2}$ alloy and the reason behind small substitution is related to the fact that too much of Sn would results in a much heavier alloy material, which is not recommended for catalytic applications including CO_2 conversion process. Both Sn-substituted and non-substituted alloys consisted of similar $CaCu_5$-type intermetallic phase but the pattern of Sn-substituted material consists of broadened diffraction peaks as compared to $LaNi_5$ material and the peaks have shifted towards lower 2 theta values while their intensities weakened. All these effects are attributed to inhomogeneity in the B-component (Ni(Sn)) of

the parent AB_5-type material and the larger Van der Waals radius (224 pm) of Sn compared to the radius of Ni (200 pm). The unit cell aspect ratio (c/a) for the AB_5 phase noticeably increased after partial substitution of Ni by Sn from 0.794 to 0.796 (or by 0.25%).

The Nitrogen adsorption and desorption isotherms of the unmodified alloys may be classified as type 1 isotherm group due to the hump-shaped curve occurring at relative pressure of 0.3. Upon Sn substitution, the surface area of the alloy was reduced from 0.1889 m^2/g to 0.1770 m^2/g while pore diameters, pore areas and pore volume were all increased.

Hydrogen absorption kinetics of non-activated and of activated samples were studied using hydrogen absorption experiments on a Sieverts-type volumetric setup which were tested at 30 bar initial hydrogen pressure and constant temperature of 20 $^{\circ}C$. Without activation and after pre-exposure to air, both unmodified alloys exhibited very long incubation periods (35.4 minutes and 78.26 minutes for $LaNi_5$ and $LaNi_{4.8}Sn_{0.2}$ alloy, respectively) before hydrogen absorption can take place. This observation can be attributed to the fact that after exposure to air, the materials allowed surface oxidations to take place, readily forming oxides/hydroxides film which prevents hydrogen dissociation and penetration into the interstitial sites. Interestingly, the kinetic parameter, k, increased from 1.29 to 1.40 min^{-1} upon Sn substitution, indicating improvement of hydrogenation rate. Furthermore, the partial substitution of Sn for Ni resulted in an increase in maximum hydrogen storage capacity.

After vacuum heating at 300 $^{\circ}C$ prior to hydrogen uptake, the kinetic curve of $LaNi_5$ material shows improvement in both the absorption kinetics (from 0.06 to 0.21 min^{-1}) and maximum hydrogen uptake capacity (from 1.29 wt.% to 1.45 wt.%) with a reduced incubation period, suggesting that the oxide film was removed through vacuum heating. The kinetic curve of $LaNi_{4.8}Sn_{0.2}$ alloy exhibited no or little incubation period in comparison with the non-substituted AB_5 alloy as a result of a complete removal of oxide film leading to an oxide-free metal surface. It was therefore concluded that Sn substitution is of paramount importance for enhancement of hydrogenation kinetics and maximum hydrogen uptake capacity, however, it still exhibit poor poisoning-tolerance due to lack of protective layer to prevent oxide layer formation.

2. Surface modification through autocatalytic deposition of palladium on AB_5-type alloys was successfully applied as the aim to form a poisoning-tolerant surface layer that would enhance the hydrogenation performance of the bulk alloy. Importantly, XRD evaluation confirmed that the $CaCu_5$-type phase observed in the parent alloys was maintained upon Pd deposition while the Pd phase was not detected due to small amount of Pd deposited (0.1044 wt. % for both modified alloys according to AAS analyses). The Pd layers deposited on the surfaces of AB_5-type alloys in NaH_2PO_2-based Pd autocatalytic plating bath were amorphous. The amorphosity of the NaH_2PO_2-derived Pd layer was a result of the impregnation of P atoms into the Pd layer. The Nitrogen adsorption and desorption isotherms of the Pd-modified alloys were classified as type 2 isotherm group as a result of straightened isotherms. Due to larger pore diameters of Pd modified alloys compared to those of unmodified alloys, large and rapid uptake of nitrogen gas over time was observed for alloys that are coated with Pd.

   Studies of the hydrogenation performances and kinetics of the surface modified alloys, before and after vacuum heating prior to hydrogen uptake, demonstrated significantly enhanced hydrogen absorption rates compared to the parent materials. The enhanced kinetics was a result of the removal of the surface oxide layer with surface-modification and the catalysis of the hydrogen dissociation process by the Pd catalytic layers. Showed a great working relationship between Sn substitution and autocatalytic Pd deposition as the combination of the two processes improved the kinetic parameter, rate constant k, from 0.21 min^{-1} associated with $LaNi_5$ material to 68.03 min^{-1} at 20 ˚C and initial hydrogen pressure of 30 bar. This is attributed to combining the merits of Ni(Sn) in $LaNi_{4.8}Sn_{0.2}$ alloy, which bring new, large active sites to allow rapid uptake of hydrogen, and poisoning tolerance of Pd nanoparticles.
3. Another study based on AB_2-type alloy, $TiMn_{1.52}$ material, was undertaken with the aim to compare the performance of Pd nanoparticles on different alloys (i.e. AB_5-type and AB_2-type alloy). The XRD analysis indicated that $TiMn_{1.52}$ alloy exhibit amorphous structure and C14-type Laves phase without any second phase. The most interesting feature about amorphous hydrogen storage materials is that they have favourable hydrogen absorption/desorption kinetics, exhibiting easy flow of hydrogen atoms. When the alloy is coated

with Pd, two sharp diffraction peaks of much higher intensities than those of $TiMn_{1.52}$ alloy appear at $2\theta = 30.56^{o}$ and $2\theta = 31.83^{o}$. The peaks are attributed to (021) and (040) reflections of phosphorus structure, respectively. The phosphorus was impregnated into the Pd layer during plating NaH_2PO_2-derived Pd layer. Both the unmodified and Pd-modified alloys were found to have same crystallite size of 29 nm, suggesting that there was no admixing/incorporation between palladium nanoparticles and the bulk $TiMn_{1.52}$ alloy.

Studies of the hydrogenation performances of uncoated and Pd-coated $TiMn_{1.52}$ alloy were conducted after pre-exposure to air and after pre-activation by vacuum heating. Without vacuum activation, uncoated $TiMn_{1.52}$ alloy exhibit slow hydrogen absorption, accompanied by long incubation period of ~5 minutes. This is attributed to the presence of poisonous oxides film on the surface, which causes difficulties in transportation of atomic hydrogen into the bulk alloy. Interestingly, the incubation period was decreased to less than 2 minutes while rate constant increased from 0.438 min^{-1} to 0.771 min^{-1} upon Pd deposition as a result of no or little oxides on the surface of Pd-modified alloy.

In comparison, positive results on poisoning tolerance and hydriding kinetics of both AB_2 and AB_5 alloys were obtained upon autocatalytic deposition of Pd. Therefore, it could be concluded that the selected metal alloy materials can be employed as catalyst precursors in Sabatier reaction, which involves reduction of CO_2 into hydrocarbons.

6.2. RECOMMENDATIONS

Based on the analyses and conclusions of the study, a number of recommendations regarding future research directions of investigation were made:

1. Formation of oxide layers caused by impurities such as carbon monoxide and sulphur compounds has the effect of poisoning the alloy surface. Exposure of parent $LaNi_5$ material to air results in poor hydrogen storage capacity and kinetics. The Sn substituted alloys can be used in improving hydrogenation kinetics and uptake due to higher equilibrium pressure of $LaNi_{4.8}Sn_{0.2}$ alloy.

Effect of substituting larger or smaller amounts of Sn than 0.2 on hydriding kinetics and absorption capacity should be tested.

2. Efforts should be made to extend the laboratory-scale surface modification technology, discussed in this work, to further the up-scaling pilot studies of hydrogen storage using up to 10 kg batch of alloy. This can be done by loading the materials into a tumble mixer. The tumble mixer in the up-scaling of the surface modification procedure provides good mixing resulting in uniform surface coating.
3. $LaNi_{4.8}Sn_{0.2}$ alloy sample exhibit poor poisoning-resistance at room temperature but the introduction on Pd nanoparticles through autocatalytic deposition prevented the formation of oxide layers and facilitated rapid hydrogen dissociation. Hence Sn substitution and Pd deposition complimented each other to improve hydrogenation performance of the parent $LaNi_5$ material; and as a result, investigation of the catalytic properties of the surface-modified $LaNi_{4.8}Sn_{0.2}$ material for applications in catalytic reduction/hydrogenation of CO_2 should be investigated.

4. The CO_2 conversion catalytic set-up should be in the consideration of installing mass spectroscopy in the set-up for analysis of composition gas mixture and monitoring the purity of hydrocarbons formed upon reaction between CO_2 and hydrogen.
5. The fourier-transform infrared spectroscopy (FTIR), which provides information about vibrational absorption of the molecule revealing the functional groups present in the molecule, should be incorporated as well to evaluate the influence of gas impurities which interferes with the surface on the MH materials during hydrogen desorption.
6. Hydrogenation kinetics of AB_2-type alloy; $TiMn_{1.52}$ was successfully improved through autocatalytic palladium deposition technique, but not as significantly as it was seen with AB_5-based alloys. Therefore, combining Pd deposition and other surface improvement technologies such as fluorination should be in practice. Also, the reducing agent (NaH_2PO_2-based plating bath) used in this study during deposition of Pd may be altered and other reducing agents such as N_2H_4-based plating bath should be tested.

APPENDIX 1

3rd International Hydrogen Technologies Congress (IHTEC-2018), March 15-18, 2018, Alanya/Antalya, Turkey

Fabrication of graphene oxide/metal organic framework nanocomposite with improved electrocatalytic activity for hydrogen evolution reaction

Emmanuel I. Iwuoha[2], Mogwasha Daphney Makhafola[1], Kabelo Edmond Ramohlola[1], Thabang Ronny Somo[1], Gobeng Release Monama[1], Mpitloane Joseph Hato[1], Kerileng M. Molapo[2], Kwena Desmond Modibane[1,*]

[1]University of Limpopo, Private Bag X1106, Sovenga, 0727, South Africa,
[2]University of the Western Cape, Private Bag X17, Bellville, 7535, South Africa

[*]E-mail addresses:kwena.modibane@ul.ac.za

Abstract
In this study, a composite of graphene oxide (GO) and HKUST-1 type of metal organic framework (MOF) was synthesized by impregnation method, and its application as electrocatalyst for hydrogen production via hydroge evolution reaction (HER) was studied. X-ray diffraction (XRD), Fourier Transform Infrared spectroscopy (FTIR), Scanning electron microscopy (SEM) and Transmission electron microscopy (TEM) were used to characterize GO, MOF, and GO/MOF catalysts. The XRD and FTIR results of the composite showed the phases and characteristic bands for both parent materials as indicative of the composite. The SEM and TEM images revealed the presence of octahedral structure of MOF in the GO sheet-like structure. The performance of the proposed electrolytic system for electrochemical HER was studied by cyclic voltammetry and Tafel plots. The results showed that the addition of GO/MOF in the electrolytic system reveals better catalytic characteristics such as highest catalytic activity and lowest onset potential.

Keywords: Hydrogen evolution reaction, Metal organic framework, Graphene oxide

I. Introduction
In developing countries, energy supplies are mainly based on combustion of fossil fuels accompanied by a number of environmental problems such as green house emission. In order to overcome those challenges, renewable energies are needed, since the supply of non-renewable energy sources is finite. Owing to its excellent properties (i.e. light weight and high energy density), hydrogen has been designated as the best energy carrier. However, there are significant challenges hindering the large scale applications and commercialization of hydrogen fuel especially in mobile transportation. These problems include the lack of safe handling and effective methods for hydrogen production and storage (Salehabadi, Salavati-Niasari and Gholami, 2017). With this being noted, electrochemical reduction of water is considered as one of the promising route for hydrogen production due to its simplicity and economical way to produce hydrogen with large and quantity high purity. Even though in the electrochemical studies platinum (Pt) is known as an excellent electrode for hydrogen generation, it is limited by its high cost and low abundance (Satyapal *et al*., 2007). MOFs have shown to be very promising HER electrocatalysts mainly due their extremely large surface area, high porosity, adjustable pore sizes as well as defined hydrogen occupation sites (Ramohlola *et al*., 2017). Unfortunately, these MOF materials have been reported to exhibit several weak points such as the relative low stability in solution and conductivity hampering their realistic applications. Combining MOF materials with other substrates has been proposed in order to mitigate the above-mentioned drawbacks (Zhou *et al*., 2013). Graphene oxide (GO) with rich functional groups is very suitable to construct graphene-based hybrid composites (Zhou *et al*., 2015). Petit and Bandosz (2015) have reported the formation of GO/MOF composites using hydrothermal method, where the synergetic effect between MOF units and GO layers was responsible for enhanced adsorption amounts compared to the parent material. To the best of our knowledge, there are no studies reported on HER using composite of GO/MOF prepared by impregnation procedure. Hence in this study, a composite of MOF with GO (GO/MOF) was prepared through impregnation method and applied for electrochemical hydrogen generation.

II. Experimental Set-up and Procedure
GO/MOF composite (Scheme 1) was prepared through impregnation method of directly mixing of GO and MOF. Briefly, 0.1 g of as-synthesized MOF sample was dehydrated at 150 °C for 1 hour. It was then suspended in 10 mL DMF. In a separate beaker, 0,1 g of graphene oxide was dispersed in 1,4 mL DMF, and then the two mixtures were mixed together and stirred magnetically for 24 hours at 50 °C. Electrochemical measurements were carried out using EPSILON electrochemical workstation. The data was collected using a conventional three-electrode set-up with gold electrode (3 mm diameter, 0.071 cm^2 area) as a working electrode, Pt wire as a counter electrode and Ag/AgCl wire as a reference electrode. Repetitive scanning of the solutions of MOF, GO and MOF composite (~$2.0x10^{-3}$ $mol.L^{-1}$) was measured from -1.0 to 1 V at the scan rate of 0.02 - 0.10 Vs^{-1}. Electrochemical experiments were performed in 10 ml of 0.1 M TBAP/DMSO electrolytic system. HER studies were done using different concentrations of 0.03 - 0.45 M H_2SO_4 as H_2 source in 0.1 M TBAP/DMSO system and ~$2.0x10^{-4}$ $mol.L^{-1}$ of MOF, GO and MOF composite composite as electrocatalysts.

APPENDIX 2

Modibane, Kwena <kwena.modibane@ul.ac.za>

IntechOpen - Minor Review Requested - MOFs

Dolores Kuzelj <kuzelj@intechopen.com> Mon, May 28, 2018 at 2:17 PM
To: Kwena Desmond Modibane <kwena.modibane@ul.ac.za>

Dear Dr. Modibane,

I am pleased to inform you that your chapter titled "Graphene oxide/Metal Organic Frameworks (CuPc/MOF) Nanocomposite with Improved Electrocatalytic Efficiency for Hydrogen Production and Storage," submitted to the book under the working title "MOFs," has been reviewed. The Editor has accepted your full chapter but requested that you implement some minor changes outlined in the review comments.

In the attachment you will find recommendations/suggestions for changes from the Editor(s) that would improve the overall quality of your chapter.

Current Step: Upload Revision
Upload your revised chapter on your Author Panel incorporating the review comments within the next 3 days.

Next Step:
Language Copyediting and Typeset Proof. Once your revision is uploaded, your paper will undergo specialized proofreading and editing to improve grammar, spelling, style, and accuracy at no additional charge, while our Technical Editors prepare your chapter for online publication.

Upcoming Promotion!
I would also like to take this opportunity to inform you of an upcoming promotion. When your full chapter is accepted for publication you can pre-order your book and get one print copy for free on the first order you place. All contributing authors can benefit from this exclusive promotion available only through your Author Panel.

If you have any additional questions or concerns, do not hesitate to contact me.

Cordially,

Dolores Kuzelj
Author Service Manager

IntechOpen
The Shard, 32 London Bridge Street, London SE1 9SG, United Kingdom
+38551688994
www.intechopen.com